Tropical Pacific Climate Variability under Solar Geoengineering: Impacts on ENSO Extremes

Abdul Malik[1,2,3], Peer J. Nowack[1,~~3,~~4,5,6], Joanna D. Haigh[1,~~3~~4], Long ~~Cao~~[5] Cao[7], Luqman ~~Atique~~[5] Atique[7], Yves Plancherel[1]

[1]Grantham Institute – Climate Change and the Environment, Imperial College London, London, United Kingdom
[2]Oeschger Centre for Climate Change Research, and Institute of Geography, University of Bern, Bern, Switzerland
[3]~~Department~~[3]4700 King Abdullah University of Science and Technology, Thuwal 23955-6900, Kingdom of Saudi Arabia
[4]Department of Physics, Blackett Laboratory, Imperial College London, United Kingdom
[4]~~Data~~[5]Data Science Institute, Imperial College London, United Kingdom
[5]~~School~~[6]School of Environmental Sciences, University of East Anglia, Norwich, United Kingdom
[7]School of Earth Sciences, Zhejiang University, Hangzhou, China

Correspondence to: Abdul Malik (~~a~~abdul.malik@~~imperial.ac.uk~~kaust.edu.sa)

Abstract

Many modelling studies suggest that the El Niño Southern Oscillation (ENSO), in interaction with the tropical Pacific background climate, will change ~~under~~with rising atmospheric greenhouse gas concentrations. Solar geoengineering (reducing the solar flux from outer space) has been proposed as a means to counteract anthropogenic ~~greenhouse-induced changes in~~ climate~~. Effectiveness~~ change. However, the effectiveness of solar geoengineering concerning a variety of aspects of Earth's climate is uncertain. Robust results are particularly ~~difficult~~challenging to obtain for ENSO because existing geoengineering simulations are too short (typically ~50 ~~years~~ yrs) to detect statistically significant changes in the highly variable tropical Pacific background climate. We here present results from a 1000-year ~~sunshade~~long solar geoengineering simulation, G1, carried out with the coupled atmosphere-ocean general circulation model HadCM3L. In agreement with previous studies, reducing the ~~shortwave~~ solar ~~flux~~ irradiance (4 %) to offset global mean surface warming in the model more than compensates the warming in the tropical Pacific that develops in the 4×CO_2 scenario~~: we observe~~. We see an overcooling of 0.3°C ~~(5 %)~~ and a 0.23-mm day^{-1} (5 %) reduction in mean rainfall over tropical Pacific relative to preindustrial conditions in the G1 simulation~~. This is due~~, owing to the different latitudinal distributions of the shortwave (solar) and longwave (CO_2) forcings. The location of the Intertropical Convergence Zone (ITCZ) ~~located north of equator~~ in the tropical Pacific, which moved 7.5° southwards under 4×CO_2, is ~~also~~ restored to its preindustrial ~~location~~position. However, other aspects of the tropical Pacific mean climate are not reset as effectively. Relative to preindustrial conditions, in G1 the time-averaged zonal wind stress, zonal sea surface temperature (SST) gradient, and meridional SST gradient are each statistically significantly reduced by around 10 %, ~~11 %, and 9 %, respectively,~~ and the Pacific Walker Circulation (PWC) is consistently weakened~~.~~, resulting in conditions conducive to increased frequency of El Niño events. The overall amplitude of ENSO strengthens by ~~5-8 %,~~9-10 % in G1, but there is a 65 % reduction in the asymmetry between

Formatted: Justified, Line spacing: single
Formatted: Superscript
Formatted: Superscript
Formatted: Justified
Formatted: Justified
Formatted: Justified
Formatted: Justified, Line spacing: single

cold and warm events: cold events intensify more than warm events. ~~Importantly~~Notably, the frequency of extreme El Niño and La Niña events increases by ~~44~~ca. 60 % and ~~32~~30 %, respectively, while the total number of El Niño events increases by ~~12 %. Paradoxically~~around 10 %. All of these changes are statistically significant either at 95 or 99 % confidence level. Somewhat paradoxically, while the number of total and extreme events ~~increase~~increases, the ~~most~~ extreme El Niño events ~~also~~ become weaker relative to the preindustrial state while the extreme La Niña events become even stronger. That is, such extreme El Niño events in G1 become less ~~extreme~~intense than ~~in~~under preindustrial conditions, but ~~extreme El Niño events become~~ also more frequent. In contrast, extreme La Niña events become stronger in G1~~. This~~, which is in agreement with the general overcooling of the tropical Pacific in G1 relative to preindustrial conditions~~, which depict a shift towards generally more La Niña-like conditions.~~ .

1 Introduction and Background

Since the industrial revolution~~ the increasing concentrations~~, anthropogenic emissions of Greenhouse Gases (GHGs) ~~are mainly responsible for higher global~~ have led to globally increasing surface temperatures (Stocker 2013). Higher temperatures, in turn, and more generally a rapidly changing climate, can have adverse effects on humans, plants, and animals through changes in various ecosystems, rising sea levels, melting glaciers, and could significantly impact the frequency and intensity of extreme weather events (Moore et al., 2015).

Various strategies, principally a reduction ~~in~~of GHG emissions ~~of GHGs~~ and ~~enhancing the~~enhancements of carbon dioxide sinks (Pachauri et al~~.~~., 2014), have been proposed to mitigate anthropogenic climate change. Another group of strategies ~~involving~~involves the intentional modification of ~~Earth’s~~Earth's radiation balance on a global scale, known as solar geoengineering~~ or climate engineering, have been proposed to overcome the negative consequences of human-induced GHGs~~ (Crutzen 2006; Wigley 2006; Curry et al., 2014). For any serious consideration of such geoengineering strategies, it is essential to understand their potential perils as well as benefits~~ and perils. The principal~~. One route to study the potential impacts of geoengineering on various components of ~~Earth’s~~Earth's climate system (e.g., atmosphere, ocean, cryosphere, etc.) is through employing state-of-the-art coupled atmosphere-ocean general circulation models (AOGCMs).

In this context, Kravitz et al. (2011) proposed the ~~Geo-engineering~~Geoengineering Model Intercomparison Project (GeoMIP~~)~~), which ~~originally~~initially consisted of a set of four experiments (viz. G1, G2, G3, and G4). These experiments are designed to ~~understand~~investigate the effects of geoengineering on the regional and global climate ~~by balancing~~when it is implemented to offset the annual mean global radiative forcing at the top of the ~~Earth’s~~Earth's atmosphere~~, approximately offsetting global mean surface warming~~ introduced by GHGs. These experiments are collectively called Solar Radiation Management (SRM) or solar geoengineering (Kravitz et al., 2013a). In the G1 experiment, atmospheric CO_2 is instantaneously quadrupled, but the global ~~GHGs~~GHG-induced longwave radiative effects are offset by a simultaneous reduction in the shortwave Total Solar Irradiance, TSI, (Kravitz et al., 2011). In terms of radiative forcing, the quadrupling of CO_2 is similar to the year 2100 in the RCP8.5 emission scenario (Representative Concentration Pathway with a radiative forcing of 8.5 W m^{-2} by the year 2100; ~~-~~Schmidt et al., 2012). In this paper, we focus on the G1 experiment to investigate how effectively solar geoengineering could mitigate the effects of ~~large~~substantial changes in atmospheric CO_2 on the tropical Pacific climate~~?~~.

The El Niño Southern Oscillation (ENSO) is an important coupled ocean-atmosphere mode of interannual variability in the tropical Pacific (Park et al., 2009; Vecchi and Wittenberg 2010~~)~~), which affects both regional and global climate (see Ropelewski and Halpert 1987; Bove et al~~,~~., 1998; Malik et al., 2017). ENSO oscillates between a warm, El Niño, and a cold, La Niña, phase every 2-7~~-years~~year (Santoso et al., 2017). As diagnosed from Sea Surface Temperature (SST) indices in state-of-the-art AOGCMs, there ~~is~~was no intermodel consensus about change in frequency of ENSO events and amplitude in a warming climate (Vega-Westhoff and Sriver 2017; Yang et al., 2018~~). However,~~) until Cai et al. (2018) used SST indices based on Principal Component Analysis (PCA). However, before that, Cai et al. (2014 and 2015b) also showed evidence of a doubling of El Niño and La Niña events in the Coupled Model Intercomparison Project (CMIP) phases 3 (A2 scenario) and 5 (RCP8.5) by investigating a performance-based subset of models using rainfall-based ENSO indices instead of SST-based indices. Similarly, Wang et al. (2017) also ~~observed~~reported a doubling of extreme El Niño events, relative to the preindustrial level, in the RCP2.6 transient scenario a century after stabilization of global mean temperature.~~ While models agree that the frequency will increase, the response of the amplitude of ENSO is less clear.~~ Chen et al. (2017), analyzing 20 CMIP5 models (RCP8.5), found both strengthening (in 6 models) and weakening (in 8 models) of ENSO amplitude. However, Cai et al. (2018) later found robust evidence of a consistent increase in El Niño amplitude in the subset of CMIP5 climate models, which were capable of reproducing both eastern and central Pacific ENSO modes. In summary, changes in ENSO characteristics such as amplitude~~,~~ and ENSO extremes are projected in a warming climate (e.g., Cai et al., 2014~~ and~~, 2015b, 2018; Kim et al., 2014; Wang et al., 2018).~~ In the present work we investigate the potential of solar geoengineering to mitigate changes in the amplitude and in the frequency of extreme ENSO events, essentially asking if decreasing the downwelling shortwave radiative flux can balance the GHGs-induced longwave effects on ENSO.~~

Increasing GHGs have distinct effects on the tropical Pacific mean climate. In CMIP3 and CMIP5 simulations, the equatorial tropical Pacific consistently shows ~~an El Niño-like~~a significant mean~~-~~ warming response to increased GHG forcing (van Oldenborgh et al., 2005; Collins et al., 2010; Vecchi and Wittenberg ~~et al.,~~ 2010; Huang and Ying ~~et al.,~~ 2015; Luo et al., 2015).~~ Models also~~ CMIP 3 and CMIP5 models generally show more warming on than off~~-the-~~-equatorial tropical Pacific (Liu et al., 2005; Collins et al., 2010; Cai et al., 2015a). Consistent with these warming patterns, studies typically found a weakening of zonal SST gradient (ZSSTG), Pacific Walker Circulation (PWC~~), zonal SST gradient (ZSSTG~~), zonal wind stress, and a shoaling of the equatorial tropical Pacific thermocline (see van Oldenborgh et al., 2005; Latif et al., 2009; Park et al., 2009; Yeh et al., 2009; Collins et al., 2010; Kim et

Formatted: Normal, Indent: Left: 0 cm al., 2014; Cai et al., 2015a; Zhou et al., 2015; Coats and Karnauskas 2017; Vega-Westhoff and Sriver~~ 2017; Wang et al.,~~ 2017). Changes in the mean state of the tropical Pacific can bring about variations in ENSO properties such as amplitude, frequency, and spatial pattern (Collins et al., 2010; Vecchi and Wittenberg 2010; Cai et al., 2015a).

~~Since increasing GHG forcing affects circulation patterns related to tropical Pacific and the mean state of tropical Pacific Ocean,~~We note that a ~~detailed investigation is required to know if the region returns to preindustrial conditions in the solar geoengineering scenario.~~previous study by Guo et al. (2018) found no statistically significant change in the intensity of Walker Circulation ~~relative to~~ in GeoMIP models when comparing preindustrial ~~conditions in~~ simulations to the G1 experiment~~ in GeoMIP models, and~~. Similarly, Gabriel and Robock (2015)~~ similarly~~ found no statistically significant change in frequency and amplitude of ENSO events under both global warming and geoengineering scenarios in ~~the~~ 6 GeoMIP models that captured ENSO variability best. However, ~~this could be attributed to the short~~ these authors themselves highlighted the length ~~(50 years)~~ of ~~the GeoMIP~~their simulations ~~used in the analyses, meaning~~(~50 years) as a key constraint for their studies. They suggested that ~~longer~~long term simulations ~~are needed~~(>50 years) would be required to detect ~~any~~ possible ~~subtle~~ENSO changes~~ in a statistically significant manner~~. Guo et al. (2018) concluded that 60 or more years of model simulations are required to detect changes in the PWC, while Vecchi et al. (2006) and Vecchi and Soden (2007) argue that 130~~ years~~ yrs are ~~required~~necessary to ~~detect~~identify any robust change in the PWC (Gabriel and Robock 2015). ~~According to~~Similarly, Stevenson et al. (2010~~),~~) estimated that 250 years are ~~required~~needed to detect changes in ENSO variability with a statistical significance of 90 %. ~~Long~~Here we aim to address this gap in the literature and establish a baseline for future studies through the analysis of long-term ~~geoengineering~~(1000 year) simulations ~~are clearly necessary to detect changes in extreme weather events and modes of internal~~of a single climate ~~variability.~~model.

Formatted: Font: Times New Roman, 12 pt, English (U.S.)

~~We here examine the impacts of geoengineering on tropical Pacific mean climate and ENSO variability in 1000-year simulations of HadCM3L (Cox et al., 2000), the same model used by Cao et al. (2016) and Cai et. al. (2014). Cai et. al. (2014) had performed 33 perturbed physics experiments with HadCM3L and found that the frequency of El Niño events increases under global warming scenario, consistent with other 9 CMIP3 and 11 CMIP5 simulations. Using HadCM3L, we investigate the extent to which decreasing the downward shortwave radiative flux by solar geoengineering can mitigate or minimize the changes in frequency of extreme ENSO events and amplitude that are triggered by increasing greenhouse forcing. We acknowledge that some of our results are necessarily model-dependent, but by using a much longer simulations than used previously, our results provide statistical robustness for the given model system. Specifically, we ask~~Here, we employ three 1000-year long climate model simulations (preindustrial forcing, abrupt-4xCO_2 forcing, and G1) to estimate the efficacy of solar geoengineering in resetting the tropical Pacific circulation. Specifically, we investigate: (1) if solar geoengineering can mitigate the changes in mean tropical Pacific climate found in previous GHG warming studies, and even bring it back to the preindustrial conditions~~,~~; (2) if ENSO frequency and amplitude are different under G1 conditions than under preindustrial simulations~~,~~; and (3) if the G1 experiment reduces the ~~doubling~~increase in the frequency of extreme ENSO events, as ~~observed~~shown by Cai et al. (2014, 2015b and ~~2015b)~~2018), under increased GHG forcing, relative to the preindustrial state. For this purpose, we are primarily interested in the more subtle differences in climate between G1 and preindustrial conditions, but also consider the profound changes under 4xCO_2 where, by design, the global mean surface temperature is much higher, and thus many other climate aspects vastly differ from the other two scenarios.

Formatted: Font: Times New Roman, 12 pt, English (U.S.)

Section 2 describes the climate model HadCM3L, the data and the statistical methods used to detect changes in tropical Pacific and ENSO variability. The same section also evaluates the capability of HadCM3L to model ENSO. Section 3 evaluates the response of a list of metrics used to understand how the mean state and ENSO variability are affected in ~~the~~ different experiments (preindustrial, 4xCO_2, G1). Section 4 elaborates on the mechanism of ENSO variability under GHG forcing and solar geoengineering for the given model system. Finally ~~Sect. 4~~, Section 5 presents the discussion and ~~conclusion~~conclusions.

2 Data and methods

Formatted: Justified

2.1 Climate model

HadCM3L (Cox et al., 2000) has a horizontal resolution of 2.5° latitude × 3.75° ~~× 2.5~~°longitude (~T42) with 19 (L19) atmospheric and 20 (L20) ocean levels. ~~Land~~HadCM3L stems from the family of HadCM3 climate models; the only difference is lower ocean resolution (HadCM3: 1.25° × 1.25°; Valdes et al., 2017). In HadCM3L, land surface processes are simulated by the MOSES-2 module (Essery and Clark 2003; Cao et al., 2016). HadCM3L does not include an interactive atmospheric chemistry scheme and thus does not consider ~~the potential~~ effects of ozone changes on ENSO ~~amplitudes~~amplitude and surface warming under 4xCO_2 (e.g., Nowack et al., 2015; 2017, 2018) or G1 (e.g., Nowack et al., 2016). Instead, we use ~~a~~ preindustrial background ozone climatology, prescribed on pressure levels. In section 2.4, we evaluate the ability of HadCM3L to model ENSO. We acknowledge that some of our results will necessarily be model-dependent, and underline the need for similar studies with other climate models. Still, by using much longer simulations than used previously, our results provide statistical robustness for the given model system.

Formatted: Not Superscript/ Subscript

Formatted: Subscript

Formatted: Font: Calibri, 11 pt

~~HadCM3L is capable of reproducing present-day ENSO periodicity, teleconnection patterns, and amplitude (Collins et al., 2001). There is a non-linear relationship between tropical Pacific SST and rainfall (Ham 2017) which can be diagnosed by Niño3 region (5°N-5°S; 150°W-90°W) rainfall skewness. During extreme El Niño events, the northern part of tropical Pacific Intertropical Convergence Zone (ITCZ) moves equatorward, causing significant increases in rainfall (> 5 mm day^-1^) over the eastern equatorial Pacific that biases (skews) the statistical distribution of rainfall in the Niño3 region. Thus, for studying extreme ENSO events the model should be capable of simulating Niño3 rainfall above 5 mm day^-1^ and Niño3 rainfall skewness of greater than 1 (see our Sect. 3.2.2, and Cai et al., 2014 and 2015b). With a Niño3 rainfall skewness of 2.06 for the preindustrial control, HadCM3L fulfills this criterion.~~

2.2 Simulations and observational data

Here, we use HadCM3L simulations carried out by Cao et al. (2016). To achieve a quasi-equilibrium preindustrial climate state, the model was spun up for 3000 years with constant CO_2 concentrations (280 ~~ppm~~ppmv; parts per million by volume) and TSI (1365 W m^{-2}). Then, three 1000-~~yr~~year long experiments were carried out, starting from this preindustrial climate state. These experiments are: (1) the preindustrial control (piControl) experiment with constant values of CO_2 (280 ~~ppm~~ppmv) and TSI (1365W m^{-2}~~),~~); (2) a quadrupled CO_2 (4×CO_2) experiment in which CO_2 is suddenly increased to 1120 ~~ppm,~~ppmv; and (3) ~~a sun-shade~~sunshade geoengineering (G1) experiment where the radiative effects of the instantaneously quadrupled CO_2 are offset by simultaneously reducing TSI (by 4 %). All experiments follow the GeoMIP protocol (see Kravitz et al., 2011); the only difference being that simulations were run for 1000 years (see Cao et al., 2016~~).~~) instead of 50 years as in GeoMIP.

~~Next to the simulations, we also use observational datasets: we employ the~~The monthly SST dataset from HadISST (1° latitude × 1° longitude; Rayner et al., 2003) and the rainfall data from the Global Precipitation Climatology Project (GPCP; Adler et al., 2003) version 2.3 (2.5° latitude × 2.5° longitude) over the period 1979-2017 are used to ~~obtain~~provide observational constraints and to identify the rainfall threshold to be used for defining extreme El Niño events ~~in climate model simulations.~~ . Further, we use ERA5 reanalysis data (Copernicus Climate Change Service (C3S), 2017) covering years 1979-2019 to evaluate the capability of HadCM3L to simulate ENSO variability. ERA5 has a horizontal resolution of 0.25° latitude × 0.25° longitude. Specifically, we use monthly mean surface latent heat flux (lh), sensible heat flux (sh), net shortwave radiation flux (sw), net longwave radiation flux (lw), ocean temperature, and zonal and meridional components of wind stress.

2.3 Definitions and statistical tests

We analyze changes in the tropical Pacific (25° N-25° S; 90° E-60° W) mean climate. We present ~~mean~~ climatologies for SSTs, rainfall, Intertropical Convergence Zone (ITCZ~~,~~), vertical velocity averaged between 500 and 100 hPa (~~Omega 500~~Omega500-100), PWC, zonal wind stress, zonal and meridional SST ~~ggradients~~gradients (ZSSTG and MSSTG, respectively), and thermocline depth. ~~The difference of~~We calculate mean ~~climatology of~~climatological differences for all these variables simulated under 4×CO_2~~,~~ and G1 ~~is calculated~~ relative to ~~the~~ piControl~~. The~~ and assess their statistical significance ~~of climatological mean values and their difference with piControl is tested~~ using non-parametric Wilcoxon ~~Signed~~ signed-rank and Wilcoxon rank~~-~~-sum tests (Hollander and Wolfe 1999; Gibbons and Chakraborti 2011~~), respectively.~~). All analyses are performed on re-gridded (2° longitude × 2.5° latitude) HadCM3L output ~~from~~for model years 11 to 1000~~.~~ unless otherwise stated. The first 10 years are skipped to remove the ~~initally large~~initially significant atmospheric transient effects stemming from instantaneously increasing CO_2 (see Kravitz et al., 2013b; Hong et al., 2017). Since ENSO events peak in boreal winter (December-January-February; DJF; Cai et al., 2014~~,~~; Gabriel and Robock 2015; Santoso et al., 2017~~)~~), the entire analysis is performed for DJF, unless otherwise stated. Accordingly, we also analyze mean state changes in the tropical Pacific during boreal winter.

Both rainfall and SST-based ENSO indices are used in the present study. Niño3 (5° N-5° S; 150° W-90° W~~),~~) and Niño4 (5° N-5° S; 160° E-150° ~~W), and Niño3.4 (5° N-5° S; 170° W-120°~~ W) indices are defined by averaging SST over corresponding ENSO regions. Normalized ENSO anomalies (i.e~~.~~., the ENSO indices) are calculated relative to piControl mean and standard deviation (s.d.) and are quadratically detrended before analysis. The Niño3 index is chosen for studying the characteristics of extreme El Niño events~~,~~ since during an extreme El Niño event, following the highest SSTs, convective activity moves towards the eastern Pacific, and the ITCZ moves over the Niño3 region resulting in ~~anomalous~~ rainfall higher than 5mm day^{-1} (Cai et al., 2014). ~~Similarly~~Similar to Cai et al. 2014, events with Niño3 rainfall greater than 5 mm day^{-1} are considered extreme El Niño events, whereas events with Niño3 SST index greater than 0.5 s.d. and Niño3 rainfall less than 5 mm day^{-1} are defined as moderate~~.~~ events unless otherwise stated. The Niño4 index is chosen for studying the characteristics of extreme La Niña events~~,~~ since maximum cold temperatures occur in this region (Cai et al., 2015a, 2015b). La Niña extreme (Niño4 < -1.75 s.d.), moderate (-1 > Niño4 > -1.75), and weak (-0.5 > Niño4 > -1) events are defined following Cai et al. (2015b). These definitions classify the 1988 and 1998 La Niñas in observations as extreme events (see Cai et al., 2015b~~)~~)), and HadCM3L can reproduce such extreme anomalies (see Sect. 3.2~~.3~~), which allows us to study changes in their number and magnitude.

To understand the mechanisms responsible for ~~our model system.~~ changes in ENSO variability, we have calculated ENSO feedbacks (e.g., Bjerkness (BJ) and heat flux (hf) feedbacks) and ocean stratification. BJ feedback is an equatorial zonal wind stress dynamic response to equatorial SST anomalies. It is positive feedback that maintains the ZSSTG (Lloyd et al., 2011). Here, we calculate the BJ feedback by point-wise linear regression (Bellenger et al., 2014) of the zonal wind stress anomalies over the entire equatorial Pacific (5° N-5° S; 120° E-80° W; Kim et al., 2011; Ferret et al., 2019) onto the eastern equatorial Pacific (5° N-5° S; 180° W-80° W; Kim et al., 2011; Ferret et al., 2019) SST anomalies. We then define the BJ feedback as the mean regression coefficient (Bellenger et al., 2014) over the eastern equatorial Pacific region. The hf feedback is a regression coefficient calculated by point-wise linearly regressing the net surface heat flux (sum of sw, lw, lh, and sh) anomalies into the ocean onto the SST anomalies over the eastern equatorial Pacific (5° N-5° S; 180° W-80° W; Kim and Jin 2011a). This regression coefficient is also termed as a thermal damping coefficient (Kim and Jin 2011a). It is a negative feedback in which an initial positive SST anomaly causes a reduced surface net heat flux into the ocean, thus lessening the initial SST anomaly (Lloyd et al., 2011). Ocean stratification is defined as the difference in the volumetric average of ocean temperatures over the upper 67 m, and the temperature of a single ocean layer at 95 m, both spatially averaged over the region, 5° N-5° S; 150° E-140° W, where strong zonal wind stress anomalies also occur (see Fig. 4a and Fig. S1; Cai et al., 2018).

Following Cai et al. (2014), the statistical significance of the change in the frequency of ENSO events is tested using a bootstrap method with 10,000 realizations~~. The~~ for the piControl ~~time series is sampled 10,000 times, allowing for resampling~~data. We then find the s.d. of events ~~in~~over these 10,000 realizations. If the difference of events ~~between~~of piControl with 4xCO_2 and G1 is larger than 2 s.d~~.~~., the change in frequency is considered statistically significant. The same method is used for testing the statistical significance of a change in ENSO amplitude, ZSSTG, ~~meridional SST gradient (~~MSSTG~~), and~~, ENSO amplitude asymmetry~~.~~, ENSO feedbacks, and ocean stratification. All ~~comparisons of~~changes in 4×CO_2 and G1 are ~~made~~described relative to piControl.

Formatted: Font: Times New Roman, 12 pt, English (U.S.)

2.4 ENSO representation in HadCM3L

Before employing HadCM3L for studying ENSO variability under 4×CO_2, and G1, we evaluate its piControl simulation against present-day observational data. There is a non-linear relationship between tropical Pacific SST and rainfall (Ham 2017), which can be diagnosed by Niño3 region rainfall skewness (Cai et al., 2014). Skewness is a measure of asymmetry around the mean of the distribution (see eq. S1). Positive skewness means that in given data distribution, the tail of the distribution is spread out towards high positive values, and vice versa (Ghandi et al., 2016). The skewness criterion is used to exclude climate models simulating overly wet or dry conditions over the Niño3 region (Cai et al., 2017). During extreme El Niño events, the ITCZ moves equatorward, causing significant increases in rainfall (> 5 mm day^{-1}) over the eastern equatorial Pacific that skews the statistical distribution of rainfall in the Niño3 region. Thus, for studying extreme ENSO events, the model should be capable of simulating Niño3 rainfall above 5 mm day^{-1} and Niño3 rainfall skewness of greater than 1 over the entire simulated period (see our Sect. 3.2.2, and Cai et al., 2014 and 2015b). With a Niño3 rainfall skewness of 2.06 for piControl, HadCM3L fulfils this criterion.

In addition, we evaluate the ENSO modelled by HadCM3L following a principal component (PC) approach suggested by Cai et al. (2018). Considering distinct eastern and central Pacific ENSO regimes based on Empirical Orthogonal Function (EOF) analysis, they found that climate models capable of reproducing present-day ENSO diversity show a robust increase in eastern Pacific ENSO amplitude in a greenhouse warming scenario. Specifically, the approach assumes that any ENSO event can be represented by performing EOF analysis on monthly SST anomalies and combining the first two principal patterns (Cai et al., 2018). The first two PCs time series, PC1 and PC2, show a non-linear relationship in observational datasets (Fig. S1m). Climate models that do not show such a non-linear relationship cannot satisfactorily reproduce ENSO diversity, and hence are not sufficiently skilful for studying ENSO properties (Cai et al., 2018). Here, we perform EOF analysis on quadratically detrended monthly SST and wind stress anomalies of ERA5 and piControl over a consistent period of 41-year. We evaluate HadCM3L's ability to simulate two distinct ENSO regimes and the non-linear relationship between the first two PCs, i.e., $PC2(t) = \alpha[PC1(t)]^2 + \beta[PC1(t)]^2 + \gamma$ (Fig. S1). From ERA5, $\alpha = -0.36$ (statistically significant at 99 % confidence level, hereafter "cl") whereas in piControl $\alpha = -0.31$ (99 % cl), which is same as the mean $\alpha = -0.31$ value calculated by Cai et al. (2018) averaged over five reanalysis datasets. The 1st and 2nd EOF patterns of monthly SST and wind stress anomalies of piControl (Fig. S1 b, e) are comparable with that of ERA5 (Fig. S1 a, d). EOF1 of piControl shows slightly stronger warm anomalies in the eastern equatorial Pacific, whereas negative anomalies over the western Pacific are slightly weaker compared to ERA5. In EOF1, the stronger wind stress anomalies occur to the west of the Niño3 region, which is a characteristic feature during the eastern Pacific El Niño events (see Kim and Jin 2011a). Compared to ERA5, the spatial pattern of warm eastern Pacific anomalies is slightly stretched westwards, and wind stress anomalies are relatively stronger over the equator and South Pacific Convergence Zone (SPCZ). The 2nd EOF, in both ERA5 and piControl, shows warm SST anomalies over the equatorial central Pacific Niño4 region. The variance distributions for ERA5 and HadCM3L match well for EOF1 (ERA5: 82 %, piContol: 90 %) whereas a large difference exist for EOF2 (ERA5: 18 %, piControl: 10 %).

The PCA is also useful for evaluating how well HadCM3L represents certain types of ENSO events. Eastern and central Pacific ENSO events can be described by an E-Index (PC1-PC2)/√2), which emphasizes maximum warm anomalies in the eastern Pacific region, and a C-Index (PC1+PC2)/√2) respectively, which focuses on maximum warm anomalies in the central Pacific (Cai et al., 2018). Here, we show the eastern Pacific (EP) Pattern (Fig. S1 g, h) and central Pacific (CP) pattern (Fig. S1 j, k) by linear regression of mean DJF E- and C-Index, respectively, onto mean DJF SST and wind stress anomalies. We find that model's EP and CP patterns agree reasonably well with that of ERA5. HadCM3L underestimates the E-index skewness (1.16) whereas overestimates the C-Index skewness (-0.89) compared to ERA5 (2.08 and -0.58 respectively) averaged over DJF. HadCM3L's performance averaged over the entire simulated period of piControl is also consistent with ERA5 (Fig. S1; α: -0.32, EOF1: 64 %, EOF2, 8%, E-index skewness: 1.30, C-index skewness: -0.42). In general, in HadCM3L, the contrast between the E- and C-index skewness over the entire simulated period is sufficient enough to differentiate relatively strong warm (cold) events in the eastern (central) equatorial Pacific compared to the central (eastern) equatorial Pacific. Finally, we also evaluated the hf and BJ feedbacks which, for piControl, are very similar to those of ERA5 (Table S5-6).

We conclude that HadCM3L has a reasonable skill for studying long-term ENSO variability and its response to solar geoengineering. However, we also highlight the need for and hope to motivate future modelling studies that will help identify model dependencies in the ENSO response.

3 Results

3.1 Changes in the tropical Pacific mean state

In this section, we ~~analyse~~analyze several ~~important~~significant changes in the tropical Pacific mean state under 4xCO_2 and G1~~ relative to the preindustrial simulation~~. In particular, we look into meridional and zonal SST changes, corresponding surface wind responses, and ~~also~~ coupled ~~changes~~variations in the thermocline depth. ~~We also show~~Our analysis reveals that this leads to significant ~~differences~~changes in the precipitation climatology among the simulations. Finally, we find consistent ~~differences in the Walker Circulation, as for example evident from changes in the vertical velocities in the tropical West Pacific upwelling~~

~~region.~~effects on the PWC. All these ~~differences~~results are important not just as general climatic features but ~~are additionally~~also because they are mechanistically linked to changes in ENSO extremes discussed in detail in Sect. 3.2.

3.1.1 Sea surface temperature

~~The tropical~~Tropical Pacific SSTs are spatially asymmetric along the equator. The western equatorial Pacific (warm pool) is warmer on average than the eastern equatorial Pacific (cold tongue) (Vecchi and Wittenberg 2010). ~~In HadCM3L, the~~ The piControl simulation ~~depicts this~~(Fig. 1a) reproduces the SST asymmetry between the western and eastern equatorial Pacific well (cf. Fig~~.~~ 1a in Vecchi and Wittenberg 2010). Under 4×CO_2 ~~this~~, the SST zonal asymmetry is significantly reduced (Fig. 1b), and the entire equatorial tropical Pacific ~~resembles a persistent El Niño-like~~shows a warming state (e.g., Meehl and Washington 1996; Boer et al., 2004~~) on top of a general background level of warming.~~). The solar dimming in G1 largely offsets the warming ~~observed~~seen under 4×CO_2 and brings the tropical Pacific mean SSTs close to the preindustrial state (Fig. 1c). The ~~South Pacific Convergence Zone (~~SPCZ~~),~~, where the highest SSTs of the warm pool occur (Cai et al., 2015a; ~~red~~blue line in Fig. 1a), moves towards the equator under 4xCO_2 (~~red~~blue line, Fig. 1b), but returns to approximately its preindustrial position in G1 (Fig. 1c).

The tropical Pacific is 3.90 °C warmer ~~than piControl~~ in 4×CO_2 but 0.30 °C colder in G1, with ~~the difference~~both differences being significant at the 99 % ~~confidence level (hereafter "~~cl~~",~~ (see Fig. 1d-e, Table S1). The Pacific cold tongue warms more rapidly than the Pacific Warm Pool under 4×CO_2. In contrast, in G1, a ~~more rapid~~stronger cooling occurs in the Pacific Warm Pool and the SPCZ than in the cold tongue region. The Pacific Warm Pool is ~0.4-0.6 °C colder in G1 ~~than in piControl~~, whereas the ~~East~~east Pacific cools less (~-0.2 °C in the Niño3 region~~).~~), indicating a change in SST asymmetry under G1.

Our SST results under 4xCO_2 qualitatively agree with previous studies (Liu et al., 2005; van Oldenborgh et al., 2005; Collins et al., 2010; Vecchi and Wittenberg et al., 2010; Cai et al., 2015a; Huang and Ying et al., 2015; Luo et al., 2015; Kohyama et al., 2017; Nowack et al., 2017~~) that indicated an El Niño like mean state response to increased GHG concentration scenarios in the tropical Pacific.~~). Overcooling of the tropics (and as such, the tropical Pacific) is ~~also~~ a robust signal in G1 simulations, even short ones, simply due to the different meridional distribution of shortwave and longwave forcing (Govindasamy and Caldeira 2000; Lunt et al., 2008; Kravitz et al., 2013b; Curry et al., 2014; Nowack et al., 2016). The results presented here based on a long simulation not only ~~confirm~~corroborate previously published ~~results~~findings but also statistically demonstrate that under G1, the ~~warm pool~~Warm Pool and SPCZ ~~cools~~cool faster than the cold tongue.

3.1.2 Precipitation

In the tropical Pacific, there are three dominant bands of rainfall activity: one in the western Pacific Warm Pool, one in the SPCZ, and the last one ~~is part of~~along the ITCZ situated ~~over~~at around 8° N and 150° W-90° W. ~~The~~Further, the eastern equatorial Pacific is relatively dry compared with these three rainy bands~~. In~~ (cf. Fig. 2a Sun et al. 2020). Under piControl, HadCM3L simulates ~~well~~ these spatial rainfall ~~spatial~~ patterns well, with maxima of ~6-8, ~12-14, and ~8-10 mm day^{-1} over the Pacific Warm Pool, the SPCZ, and the ~~northern part of the~~ ITCZ, respectively (Fig. 2a). Under 4×CO_2, the spatial rainfall ~~spatial~~ pattern changes significantly. The ITCZ moves equatorward, and the SPCZ becomes zonally oriented (~~green~~blue line, Fig. 2b). The rainfall asymmetry between the western and eastern equatorial Pacific decreases under 4×CO_2. ~~Precipitations migrate~~Precipitation migrates from the ~~western~~west Pacific to the Niño3 region, with maximum rainfall at ~145° W. The reduced zonal asymmetry in the rainfall between western and eastern Pacific is effectively restored to the preindustrial state in G1 (Fig. 2c).

A statistically significant (99 % cl) overall precipitation increase of 0.21 mm day^{-1} (+5 %) is ~~observed~~seen over the tropical Pacific under 4×CO_2 (Fig. 2d). In contrast, the mean rainfall in G1 decreases by 0.23 mm day^{-1} (-5 %; Fig. 2e), consistent with the simulated ~~decrease of~~reduction in temperature (-0.30 °C) over the tropical Pacific. However, there is a strong regional structure: under 4×CO_2, rainfall decreases to a maximum of ~3 mm day^{-1} over parts of the Pacific Warm Pool and off-equatorial regions, whereas a significant increase of ~15-18 mm day^{-1} ~~is observed~~develops over the Niño3 region. ~~In~~ An overall increase in mean rainfall under the GHG warming scenario has also been reported in many previous studies (e.g., Watanabe et al., 2012; Chung et al., 2014; Power et al., 2013; Nowack et al., 2016). Under G1, rainfall decreases over the Pacific Warm Pool, SPCZ, and ITCZ regions~~, whereas~~. In contrast, rainfall increases significantly over most parts of central and eastern equatorial Pacific, with a maximum (~ 1.5-2 mm day^{-1}) ~~centered at ~150° W (Fig. 2e).~~centred at ~150° W (Fig. 2e). Kravitz et al. (2013b) reported a decrease of 0.2 mm day^{-1} over the tropical regions. Under G1, the magnitude of the lapse rate decreases, resulting in increased atmospheric stability and hence suppressed convection, which leads to an overall reduction of rainfall over the tropics (Bala et al., 2008; Kravitz et al., 2013b).

Formatted: Font: Times New Roman, 12 pt, English (U.S.)

The position of the ITCZ over the tropical Pacific (25° N-25° S; 90° E-60° W) is calculated by finding the latitude of maximum rainfall (~~green~~blue lines, Fig. 2a-~~c). In piControl, the~~e). The median position of this maximum ITCZ (from 154° W-82° W) ~~north of the equator~~ is 7.5° N, 0°, and 7.5° N under piControl, 4×CO_2, and G1, respectively. ~~Under 4×CO2, the ITCZ moves 7.5° southward (Fig. S1).~~ Thus, under 4×CO_2, the ITCZ mean position ~~moves~~shifts over the equator and is positioned within the Niño3 region. G1 restores the ITCZ and SPCZ to their preindustrial orientations ~~but~~. Still, differences in the magnitude of rainfall persist over these regions, as well as over the Pacific Warm Pool (Fig. 2a, c, e). That is, while the ~~problem of reduced~~relative additional rainfall asymmetry between the western and eastern Pacific in 4×CO_2 is ~~largely~~mostly resolved in G1, the tropical Pacific is overall wetter under 4×CO_2 but drier in G1.

3.1.3 Zonal wind stress

Changes in zonal wind stress are directly dependent on and ~~interacting~~interact with ENSO amplitude (Guilyardi 2006), ENSO period (Zelle et al., 2005; Capotondi et al., 2006), and ZSSTG (Hu and Fedorov 2016). A positive feedback loop between zonal wind stress, SST, and thermocline depth influences the ~~development~~evolution of ENSO (Philip and van

Oldenborgh 2006). A decrease in the strength of the trade winds is concurrent with a flattening of the thermocline, a reduction of upwelling in the eastern Pacific, and increased SST in the eastern relative to the western equatorial Pacific, thus resulting in further weakening of the trade winds (Collins et al., 2010).

We use the zonal wind stress index, Westerly Wind Bursts (WWBs), and Easterly Wind Bursts (EWBs) to study the wind stress over the tropical Pacific. The zonal wind stress index is defined as the wind stress averaged over the equatorial tropical Pacific (5° N-5° S; 120° E-80° W), whereas selecting only the positive (negative) values of the wind stress over the same region defines the WWBs (EWBs) (Hu and Fedorov 2016). ~~In the present study,~~

We find that the zonal wind stress is significantly reduced over most parts of the tropical Pacific, especially over the Niño3 region in both 4×CO_2 and G1 (Fig. 3a-e), in agreement with the ~~altered~~reduced zonal SST gradients in both scenarios (Fig. 1). The zonal wind stress weakens by 31 % and 10 % in 4×CO_2 and G1 (statistically significant at 99 % cl~~) (~~; Fig. 4a~~). The weakening in 4×CO_2 is compensated to some degree in G1 but the wind field does not recover completely to its preindustrial state~~), respectively. We also ~~observe significant~~ see a considerable weakening of zonal wind stress over the Niño3 region, both under 4×CO_2 and G1.

Formatted: English (U.S.)

The strength of WWBs increases by 13 % under G1 relative to piControl (99 % cl), while the EWBs decrease in strength by 7 ~~%.~~% (99 % cl). In comparison, the strength of both the WWBs and EWBs is reduced (99 % cl) under 4×CO_2, by 33 % and 28 %, respectively. The strong WWBs are more closely linked to positive SST anomalies than negative SST anomalies (Cai et al., 2015a) and thus are likely to ~~result in an~~ increase ~~in~~the frequency of extreme El Niño events (Hu and Fedorov 2016) in G1~~. The strength~~, which is important with regards to the mechanistic interpretation of ~~both the WWBs and EWBs are reduced (99 % cl) under 4×CO2, by 33 % and 28 %, respectively.~~ the ENSO changes below.

~~These findings in the 4×CO2 simulation agree with Philip and van Oldenborgh (2006), who, in several climate models, found up to 40 % reduction in zonal wind stress in the 23rd century.~~

3.1.4 Zonal and meridional sea surface temperature gradients

The ZSSTG between western and eastern equatorial Pacific is one of ~~its~~the characteristic features of the equatorial tropical Pacific. The ZSSTG is weak during an El Niño and strong during La Niña events (Latif et al., 2009). The ZSSTG is calculated as the difference between SST in the western Pacific Warm Pool (5° N-5° S; 100° E-126° E) and eastern equatorial Pacific (Niño3 region: 5° N-5° S; 160° E-150° W). The zonal SST gradient is reduced both in 4xCO_2 and ~~also in~~ G1 (Fig. 4b~~)~~, 99 % cl), but the reduction ~~relative to piControl~~ is ~~less~~smaller in G1 (11 %) than in 4xCO_2 (62 %).

Formatted: Subscript

The reduced zonal SST asymmetry in 4×CO_2 and G1 is consistent with the weakening of the trade winds and zonal wind stress, as noted in Sect. 3.1.3. The weakening of trade winds can result in reduced upwelling in the eastern equatorial Pacific, and east to west surface currents

(Collins et al., 2010), leading to an increase in El Niño events. Our results under 4xCO_2 are in agreement with Coats and Karnauskas (2017), who using several climate models found a weakening of the ZSSTG under the RCP8.5 scenario.

MSSTG is calculated as the SST averaged over the off-equatorial region (5° N-10° N; 150° W-90° W) minus SST averaged over the equatorial region (2.5° N-2.5° S; 150° W-90° W) (Cai et al., 2014). Reversal of sign or weakening of the MSSTG has been observed during extreme El Niño events, as the ITCZ moves over the equator~~.~~ (e.g., Cai et al., 2014). Overall there is a change in sign and reduction of MSSTG ~~both~~ in 4×CO_2 (~-111 ~~%),~~%, 99 % cl) and only decrease in G1 (~-9 ~~%)~~ (%, 99 % cl~~,~~) (Fig. ~~S2~~S3, and Table S2). The decrease in strength of MSSTG is an indication that extreme El Niño events are expected to increase (Cai et al., 2014) under solar geoengineering. The weakening of the MSSTG is qualitatively in agreement with previous studies under increased GHG forcings (e.g., Cai et al., 2014; Wang et al., 2017).

~~Wang et al. (2017) observed a weakening of the MSSTG in a multi-model ensemble under RCP2.6, however they did not find any evidence of change in the ZSSTG in RCP2.6 and RCP8.5.~~

3.1.5 Thermocline ~~depth~~

Previous studies (e.g., Vecchi and Soden 2007; Yeh et al., 2009) ~~showed~~revealed shoaling as well as a reduction in the east-west tilt of the equatorial Pacific thermocline under increased GHG scenarios. A decrease in thermocline depth and slope is a dynamical response to reduced zonal wind stress. Shoaling of the equatorial Pacific thermocline can result in positive SST anomalies in the eastern ~~equatorial~~tropical Pacific ~~and that~~, which in turn can affect the formation of El Niño (Collins et al., 2010).

Thermocline depth here is defined as the depth of the 20 °C (for piControl and G1~~)~~), and 24 °C (for 4×CO_2) isotherms averaged between 5° N and 5° S, following Phillip and van Oldenborgh (2006). Due to surface warming in GHG scenarios, the 20 °C isotherm deepens (Yang and Wang et al., 2009~~)~~), and this must be compensated by using a warmer isotherm (24 °C) as a metric in the 4×CO_2 case.

In 4xCO_2, the tropical Pacific thermocline depth (24 °C isotherm) shoals by 22 % (99 % cl, Fig. 4c), as expected from similar experiments (Vecchi and Soden 2007; Yeh et al., 2009). However, there is no statistically significant change in the mean thermocline depth in G1. ~~Sun shading completely offsets shoaling of the thermocline depth which is characteristic of GHG warming scenarios.~~ In 4xCO_2, most likely the weakened easterlies (as noticed in Sect. 3.1.3; e.g., Yeh et al., 2009, Wang et al., 2017) and greater ocean temperature stratification due to increased surface warming (see Sect. 4 and Cai et al., 2018) lead to a significant shoaling of the thermocline across the western and central equatorial Pacific. In contrast, relatively little change takes place between 130° W and 90° W. In a CMIP3 multimodel (SRESA1B scenario) ensemble, Yeh et al. (2009) found a more profound deepening of the thermocline in this part of the eastern equatorial Pacific; however, for example, Nowack et al. (2017) did not find such changes under 4xCO_2 (cf. their Fig. S9). One possible explanation

Formatted: English (U.S.)

Formatted: Justified

Formatted: Font: Not Bold

Formatted: Subscript

Formatted: Subscript

for this behaviour is the competing effects of upper-ocean warming (which deepens the thermocline) and the weakening of westerly zonal wind stress, causing thermocline shoaling (see Kim et al. 2011a).

3.1.6 Vertical velocity and Walker circulation

Under normal conditions, ~~in the tropical Pacific,~~ there is strong atmospheric upwelling over the western equatorial Pacific, SPCZ, and ~~that part of the ITCZ located north of the equatorial tropical Pacific, whereas~~ITCZ. In contrast, the relatively cold and dry eastern Pacific is dominated by atmospheric downwelling. This process, as simulated in HadCM3L, can be ~~clearly~~ seen in maps of Omega500-100 ~~in~~ (Fig. 5a~~.~~). The region of ascent over the SPCZ and ITCZ moves equatorward in 4×CO_2 (Fig 5b), consistent with the increase in SST and precipitation over the equatorial region (Fig. 1d and 2d). ~~In 4×CO_2, the convective center also moves towards the Niño3 region centered at ~150°W. These changes are largely offset in G1, which indicates that decreasing the downward shortwave flux can largely steer these atmospheric changes back to preindustrial state (Fig. 5c).~~ The convective centre also moves towards the Niño3 region and centres at ~150°W. While these changes in spatial patterns of atmospheric divergence and convergence are found to be corrected for G1 (Fig. 5c), significant differences in the strength of the atmospheric circulation remain, which in turn are coupled to the aforementioned changes in atmospheric stability. Specifically, both for 4×CO_2 and G1, upwelling decreases over the Warm Pool, but increases in the central Pacific and the eastern part of the Niño3 region (Fig. 5d-e). This picture is consistent with changes in the spatial extent and a weakening of the tropical PWC (Fig. 6a-c). In 4xCO2, the weakening and shifting of circulation patterns are consistent with multimodel results reported by Bayr et al. (2014) under GHG forcing. While mitigated, the PWC weakening found in G1 remains highly statistically significant (99 % cl; Fig. 6d-e).

Formatted: Font: Times New Roman, 12 pt, English (U.S.)

~~While spatial patterns in atmospheric divergence and convergence can be corrected in G1 (Fig. 5c), important differences remain. These are mostly associated with the magnitude of atmospheric convection. Specifically, a significant decrease in strength of upwelling is observed over the warm pool, while an increase is seen in the central pacific and the eastern part of Niño3 region (Fig. 5d-e); this happens both for 4×CO_2 and G1. The downwelling becomes weaker (i.e. less positive in Fig. 5e) in G1 over most parts of the eastern equatorial Pacific and over South America.~~

~~These changes are consistent with changes in the spatial extent and strength of the tropical PWC in 4×CO_2 and G1 (Fig. 6a-c). In 4×CO_2, the time-averaged western branch of the PWC extends further eastward and becomes broader, in agreement with the changes in Omega500-100 described above, while the eastern branch of the PWC is squeezed. The PWC reverts back to preindustrial spatial patterns in G1 (Fig. 6c).~~

~~Significant (90 % cl) changes occur in the strength of the PWC in 4×CO_2 and G1 relative to piControl (Fig. 6d-e). Both the western and eastern branches of the PWC become weaker in strength, whereas the vertical velocity strengthens in the central Pacific. Thus, G1 offsets the~~

~~changes in spatial pattern of PWC occurring under increased GHG forcing but fails to completely compensate changes in strength.~~

3.2 ENSO amplitude and frequency

In Sect. 3.1, we ~~noted~~described a variety of coupled, and highly significant changes in the tropical Pacific mean state, such as the weakening of zonal and meridional SST gradients, zonal wind stress, and PWC. ~~These~~It is well-known that such changes can affect ~~the~~ ENSO variability. ~~In this~~This section~~, we discuss~~ discusses various metrics used to ~~characterise~~characterize ENSO variability and ~~show~~unfolds how they change in 4xCO_2 and G1. Specifically, we investigate the amplitude of ENSO, changes in amplitude asymmetry between El Niño and La Niña events, and ENSO frequency.

3.2.1 ENSO amplitude

~~Three ENSO indices (Niño3, Niño4, and Niño3.4) are used to~~To characterize changes in ENSO~~. All three~~, this study uses two separate indices ~~are necessary~~for two different regions, because extreme warm and cold events are not ~~simply~~ mirror images of each other (Cai et al., 2015b). The Niño3 (Niño4) index is employed for studying characteristics of El Niño (La Niña) events in the eastern (central) Pacific region. ENSO amplitude is defined as the standard deviation of SST anomalies in a given ENSO region (e.g., Philip and van Oldenborgh 2006; Nowack et al., 2017). The maximum amplitude of warm events is defined as the maximum positive ENSO anomaly during the entire time series analysed (Gabriel and Robock 2015). Cold events are defined similarly, but using the maximum negative ENSO anomaly.

Formatted: Font: Times New Roman, 12 pt

In 4×CO_2, ~~all~~both eastern and central Pacific ENSO ~~indices show~~amplitudes undergo a statistically significant decrease (47~~-~~ and 64 ~~%), whereas in G1, Niño3 and Niño3.4 indices show an increase (5-8 %) in amplitude~~%, respectively, at 99 % cl ~~(~~, Table 1~~). Further, in 4×CO_2, all ENSO indices show a decrease in the~~ -2). The maximum amplitude of warm ~~(30-57 %)~~events in the eastern Pacific and cold ~~(19-36 %) events (Table 2-3). In G1, Niño4 and Niño3.4 indices indicate a decrease (7-11 %) in maximum amplitude of warm~~ events ~~but only~~in the ~~Niño4 index indicates an increase (20 %) in maximum amplitude of cold events. Thus, owing to an overall~~central Pacific are also significantly reduced (57 % and 36 % at 99 % cl, respectively; Table 3-4). Previous studies found that climate models produced mixed responses (both increases and decreases in amplitude) in terms of how ENSO amplitude change with global warming (see Latif et al. 2009; Collins et al. 2010; Vega-Westhoff and Sriver 2017). However, Cai et al. (2018) found an intermodel consensus, for models capable of reproducing ENSO diversity, for strengthening of ENSO amplitude~~, and strengthening (weakening) of~~ under A2, RCP4.5, and RPC8.5 transient scenarios. In contrast, in G1, the ~~maximum~~eastern Pacific ENSO amplitude gets strengthened (9 % at 99 % cl), and no statistically significant change is noticed in the central Pacific ENSO amplitude~~ of cold (warm) events,~~ .

Formatted: English (U.K.)

Formatted: English (U.K.)

Further, the maximum amplitude of cold events is strengthened in the central Pacific (20 % at 99 % cl), but no statistically significant change occurs in the eastern Pacific. A validation of these changes in ENSO amplitude using the E- and C-indices, as these indices represent SST anomalies similar to those of Niño3 and Niño4 index (Cai et al. 2015a), yields indeed very similar results (see Table 1-4). Thus, our simulations imply that significant changes can occur in ENSO events under solar geoengineering~~ could occur despite global mean surface temperatures being very similar in G1 and preindustrial conditions~~. Mechanistically, it is self-evident that these changes might be linked to the tropical Pacific SST overcooling of ca. 0.30 °C and the substantial SST gradient changes under G1 relative to piControl.

~~In general, the El Niño events are stronger than La Niña events, and~~However, the use of standard deviations to define ENSO amplitude is suboptimal, because amplitudes of El Niño and La Niña events are asymmetric, i.e., in general, El Niño events are stronger than La Niña events (An and Jin 2004; Schopf and Burgman 2006; Ohba and Ueda 2009; Ham 2017).~~ In the present study, the strengthening (weakening) of maximum amplitude of cold (warm) events indicates that asymmetry of cold and warm event's amplitude would change in both 4×CO_2 and G1.~~ The relative strength of ENSO warm and cold events can be measured by the skewness of SST over the ENSO regions (Vega-Westhoff and Sriver 2017). Following Ham (2017), we investigate the asymmetry ~~of~~in the amplitude of El Niño and La Niña events by comparing the skewness of detrended Niño3 SST anomalies in piControl with 4×CO_2 and G1.

We find that, relative to piControl, the Niño3 SST skewness is reduced ~~(~~both in 4×CO_2 (190 % at 99 % cl) ~~by 190 %, in 4×CO_2~~ and ~~by~~ G1 (65 % ~~in G1~~at 99 % cl) (Table 5). The E-Index also indicates reduced skewness under both 4~~). This~~×CO_2 (85 %) and G1 (28 %) at 99 % cl. The reduced skewness is further illustrated in maps showing differences in skewness between 4×CO_2 and G1 with piControl (Fig. ~~S3~~S4). Over the eastern equatorial Pacific, the SSTs are transformed from positively to negatively skewed under 4×CO_2 (Fig. ~~S3).~~S4b). Our results qualitatively agree with Ham (2017), who found a 40 % reduction in ENSO amplitude asymmetry using several CMIP5 models in the RCP4.5 scenario. In G1~~,~~ (Fig. S4e), the skewness of SSTs is reduced over the ~~entire~~eastern equatorial Pacific~~.~~, whereas it strengthens over the central equatorial Pacific region (at 99 % cl). The strengthening of skewness over the central equatorial Pacific is also consistent with increased C-Index skewness (66 % at 99 % cl) under G1 relative to piControl. Thus, due to the concurrent strengthening of the maximum amplitude of cold events and ~~weakening of warm events, and~~ reduction in the asymmetry of SST skewness, the intensity of cold events is predicted to increase compared to warm events under solar geoengineering.

~~Vega-Westhoff and Sriver (2017) also found a decrease in strength of ENSO amplitude in the RCP8.5 scenario in the Community Earth System Model (CESM). Our results also agree with Ham (2017) who found a 40 % reduction in ENSO amplitude asymmetry using several CMIP5 models in the RCP4.5 scenario.~~

3.2.2 El Niño frequency

Formatted: Font: Times New Roman, 12 pt

Formatted: English (U.S.)

Formatted: Font: Times New Roman, 12 pt, English (U.S.)

~~We chose a threshold value of rainfall for defining~~To study changes in El Niño frequency, we first need to define what constitutes an El Niño event. We here define extreme El Niño events ~~based on the work of Cai et al., (2014), who chose averaged~~ as episodes when monthly-mean DJF Niño3 total rainfall ~~exceeding~~exceeds 5 mm day^{-1} ~~for this~~, following the threshold ~~based on observations.~~definition by Cai et al~~., (2017)~~. (2014). However, as pointed out ~~that the trend~~by Cai et al. (2017), trends in Niño3 rainfall ~~is contributed~~are mainly driven by two ~~main~~ factors: (1) the change in the mean state of the tropical Pacific and (2) the change in frequency of extreme El Niño events. ~~In studying the~~ Therefore, since we want to focus on the changes in the extremes ~~only, the trend contributed by mean state changes should be subtracted~~, we need to remove contribution (1) from the raw Niño3 time series. ~~Hence, we~~We, therefore, fit a quadratic ~~trend~~polynomial to the time series of rainfall data from which all extreme El Niño events (DJF total rainfall > 5 mm day^{-1}) have been excluded and then subtract this trend from the raw Niño3 rainfall time series. Linearly detrending the rainfall time series produces similar results. Note that under piControl (observations), total rainfall of 5 mm day^{-1} is ~85th (~93rd) percentile in detrended Niño3 rainfall time series. Wang et al. (2020) termed events with rainfall > 5 mm day^{-1} as extreme convective El Niño events.

Formatted: English (U.K.)

~~Using the~~With detrended ~~time series, 8~~Niño3 total rainfall exceeding 5 mm day^{-1} as an extreme, three extreme and seven moderate ~~and 2 extreme~~ El Niño events can be identified from the historical record between 1979 and 2017 (Fig. 7a). ~~The MSSTG is negative during the 1982 and 1997 extreme events. The identification of extreme events is slightly sensitive to the choice of threshold. For example, a threshold of detrended Niño3 total rainfall of 5 mm day-1 does not recognize 2015 as an extreme El Niño year, since it has weak positive MSSTG. We repeat the same method with averaged DJF Niño3 rainfall anomalies greater the 3 and 4 mm day-1. Rainfall anomaly of 3 mm day-1 identifies 2015 as an extreme El Niño year whereas 4 mm day-1 does not (Fig. 7b). Since, a threshold of total rainfall > 5 mm day-1 does not recognize El Niño events having weak positive MSSTG as extreme El Niño events, we use all three threshold values (total rainfall > 5 mm day-1; and 3 and 4 mm day-1 rainfall anomaly) for detecting any change in extreme El Niño events under solar geoengineering experiment. Note that under piControl, total rainfall of 5 mm day-1 is ~95th percentile, whereas 4 (3) mm day-1 anomaly is ~94th (~90th) percentile in detrended Niño3 rainfall time series.~~

~~Since there exists a nonlinear relationship between SST and Niño3 rainfall, for this method to be applicable the Niño3 rainfall skewness should be at least +1 (see Cai et al., 2014). Further, the skewness criterion is used to avoid climate models simulating overly wet or dry conditions over the Niño3 region (Cai et al., 2017). HadCM3L simulates skewness of 2.06, -0.07, and 1.55 for piControl, 4×CO2, and G1, respectively. The reduced skewness of Niño3 rainfall under GHG forced climate indicates that nonlinear relationship between Niño3 rainfall and MSSTG completely breakdowns under 4×CO2. Below, we only focus our analysis on G1 for studying the changes in ENSO extremes.~~

~~With detrended Niño3 total rainfall exceeding 5 mm day-1 as an extreme, a~~A statistically significant ~~(99 % cl)~~ increase of ~~44 %~~526 % (99 % cl) in extreme El Niño events ~~is~~

~~observed~~can be seen under ~~G1 (65~~4×CO_2 (939 events) relative to piControl (~~45 events) (Fig. 7c-d). Thus, an extreme El Niño event occurring every ~22-yr under preindustrial conditions occurs every ~15-yr under solar geoengineered conditions. The moderate El Niño events~~ 150 events) (Fig. 7b-c). The geoengineering of climate (G1) largely offsets the increase ~~by 7 %~~in extreme El Niño frequency under ~~G1,~~4×CO_2 (Fig. 7d), however, ~~the change is not statistically significant. A statistically significant (95 %)~~compared to piControl, still a 17 % increase ~~of~~ in extremes and a 12 % increase in ~~frequency of~~the total number of El ~~Nino~~Niño events (~~number of extreme~~moderate plus ~~moderate events) is also observed with number of events increasing from 300 in piControl to 337 in G1~~extreme) can be seen at 95 % cl. Thus, an El Niño event occurring every ~3.3-yr under preindustrial conditions occurs every ~2.9-yr under solar geoengineered conditions.

~~Results similar to those with 5 mm day^{-1} are found when using detrended Niño3 rainfall anomaly of 3 and 4 mm day^{-1} as definition thresholds for extreme El Niño events. Specifically, the number of extreme events increase by ~40 % and ~42 % for Niño3 rainfall anomaly thresholds of 3 and 4 mm day^{-1} respectively, and the frequency of total (extreme plus moderate) events increase by ~12 % in both cases in G1 relative to piControl (Fig. S4a-d).~~

~~No statistically significant changes in the number of extreme El Niño events is detected when using ENSO indices based on SST. However, all SST based ENSO indices (Niño3, Niño4, and Niño3.4) indicate statistically significant increase of ~12 % in frequency of total (extreme plus moderate) number of El Niño events (ENSO index > 0.5 s.d.) (Table S4).~~

~~There is no evidence of changes in the frequency of central Pacific El Niño (El Niño Modoki) comparative to the frequency of eastern Pacific El Niño (canonical El Niño) in G1 relative to piControl (not shown).~~

~~We note that under~~A threshold of detrended Niño3 total rainfall of 5 mm day^{-1} recognizes events as extremes even when the MSSTG is positive and stronger, especially under 4×CO_2, which plausibly means that ITCZ might not shift over the equator for strong convection to occur during such extremes. The El Niño event of 2015 is a typical example of such events. We test our results with a more strict criterion by choosing only those events as extremes, which have characteristics similar to that of 1982 and 1997 El Niño events (i.e., Niño3 rainfall > 5 mm day^{-1} and MSSTG < 0). We declare events having characteristics similar to that of the 2015 event as moderate El Niño events (Fig. S5). Based on this method, we find a robust increase in the number of extreme El Niño events both in 4×CO_2 (924 %) and G1 (61 %) at 99 % cl. We also performed the same analysis by linearly detrending the rainfall time series and find similar results (Fig. S6).

An alternative approach to quantifying extreme El Niño events is based on Niño3 SST index > 1.75 s.d. as an extreme event threshold (Cai et al., 2014). We note that using this definition, no statistically significant change in the number of extreme El Niño events is detected in G1 (61 events), whereas they reduced from 57 in piControl to zero events in 4×CO_2 highlighting the dependency of specific results on the precise definition of El Niño events used. However, relative to piControl, Niño3 SST index indicates a statistically significant increase (decrease) of 12 % (46 %) in the frequency of the total number of El Niño events (Niño3 SST index > 0.5 s.d.) (Table S3) in G1 (4×CO_2). Further, we examine the change in extreme El Niño events using E-Index > 1.5 s.d. (see Cai et al., 2018) as threshold. The SST based E-Index identifies 79, 147, and 93 extreme El Niño events in piControl, 4×CO_2, and G1, respectively. Thus using E-Index, extreme El Niño events increase by 86 % (99 % cl) and 17 % (missing 95 % cl by three events) in 4×CO_2 and G1, respectively. Based on the E-index definition, we also see a statistically significant increase in the total number of El Niño events in 4×CO_2 (88%) and G1 (12 %) (Table S3). Note that Wang et al. (2020) showed that extreme convective events can still happen even if the E-index is not greater than 5 mm day^{-1} (cf. Figure 2 in Wang et al. 2020).

We highlight that both in 4×CO_2 and solar geoengineered climate, more weak and reversed MSSTG events occur relative to piControl (Fig. ~~S2~~S3). More frequent reversals of MSSTG result ~~into~~in a more frequent establishment of strong convection in the eastern equatorial Pacific. According to Cai et al. (2014), more frequent convection over the eastern tropical Pacific increases the sensitivity of rainfall by 25 % to positive SST anomalies. Further, in Sect. 3.1.3, we ~~observed~~found that WWBs (EWBs) are 13 % (7 %) stronger (weaker) than in piControl, which also ~~favors~~favours a higher frequency of El Niño events in G1. Thus, we conclude that changes in the tropical Pacific mean state~~,~~; in particular weakening of temperature gradients (MSSTG and ZSSTG), changes in zonal wind stress, and convection over the tropical Pacific (and consistent weakening of the PWC) are the ~~possible~~plausible causes of increased frequency of extreme El Niño events under G1.

3.2.3 La Niña frequency

During La Niña events, the ZSSTG, the PWC, and atmospheric convection in the western Pacific are stronger than ~~normal~~on average. Here, we present plots of Niño4 vs ZSSTG for piControl, 4×CO_2, and G1 (Fig. ~~7e-f).~~8a-c). In 4×CO_2, extreme La Nina events are reduced to zero relative to piControl, and a statistically significant (99 % cl) decrease occurs in moderate, weak, and total number (sum of extreme, moderate and weak events) of La Niña events. We ~~observe~~find a statistically significant (95 % cl) increase in extreme La Niña events in ~~the~~ G1 ~~experiment~~. The number of extreme La Niña events increases by 32 % (61 events) in G1 relative to piControl (46 events). Thus, an extreme La Niña event ~~occurring every ~22 yr in piControl~~ occurs every ~~~16 yr in G1. The other two ENSO indices (Niño3 and Niño3.4) also show statistically significant increases in extreme La Niña events in G1 (Table S5). The Niño3 (Niño3.4) shows ~400 % (~138 %) increase in extreme La Niña, meaning an extreme event occurring every ~124 (~62)~~22 years ~~over the Niño3 (Niño 3.4) region~~ in piControl ~~occurs~~and every ~~~25 (~26)~~16 years in G1. ~~Increased~~

The increased number of extreme El Niño events ~~results~~provides a possible mechanism for increased frequency of La Niña events, as they result in more heat discharge events causing cooling, hence providing conducive conditions for increased occurrence of La Niña events (Cai et al., 2015a, 2015b). In addition, the ocean becomes 4% more stratified under G1 relative to piControl (Fig. 15e, Table S7). The increased vertical ocean stratification in the

Formatted: English (U.S.)

Formatted: English (U.K.)

Formatted: English (U.K.)

Formatted: English (U.K.)

central equatorial Pacific steers cooling in the Niño4 region and, hence, can cause more frequent strong positive ZSSTG anomalies (Fig. S9c and S10b) resulting in an increased number of extreme La Niña events (see also Cai et al., 2015b).

Formatted: English (U.K.)

3.3 Spatial characteristics of ENSO

In Sect. 3.2, we showed that ~~the~~overall and maximum ~~amplitude of cold (warm) events is~~ENSO event amplitudes generally strengthened ~~(weakened) and that~~under G1, while the amplitude asymmetry between warm and cold events is significantly reduced~~ in G1 relative to piControl. Here we~~. In this section, we present composite anomalies, i.e. the average patterns of all El Niño and La Niña events. These composites provide process-based evidence for the strengthening (weakening) of extreme La Niña (El Niño) events in G1~~ relative to piControl. Using composite analysis, we .~~ We show that ~~for extreme La Niña (El Niño) events~~ the PWC, SST, and composite rainfall anomalies are strengthened ~~in G1 relative to piControl. The composite anomalies are shown for the extreme and the total (~~for extreme La Niña events, while they are weakened for extreme El Niño events under G1. For composite analysis, extreme ~~plus moderate) number of La Niña (~~El ~~Niño)~~Nino events ~~in piControl~~are selected with Niño3 rainfall > 5 mm day^{-1} and ~~G1. We also calculate differences of composite anomalies between G1~~MSSTG < 0 (Fig. S5) because it gives a more robust estimate as all events show a reversal of MSSTG, and ~~piControl (G1-piControl) to detect any significant change in ENSO characteristics under solar geoengineering~~more vigorous convection.

Formatted: English (U.K.)

Formatted: Font: Bold

3.3.1 Weakening of extreme El Niño ~~composites~~events in G1

The broad spatial ~~pattern~~patterns of composite SST (Fig. 9), rainfall (Fig. 10), and PWC (Fig. 11) anomalies for the extreme and total number of El Niño events in G1 ~~is~~are very similar to ~~that~~those of piControl~~ with stronger warm~~. During extreme El Niño events, in G1, we find reduced SST (Fig. 9e) and rainfall anomalies ~~in~~ (Fig. 10e) over the eastern and western equatorial Pacific ~~than in the off-equatorial and western Pacific region (Fig. 8a-d). However, the extreme El Niño composite difference (G1-piControl) indicates that warm anomalies over western, central, and eastern equatorial Pacific are weaker in G1 (Fig. 8e). The composite difference of total El Niño events also indicates statistically significant (90 % cl) weak warm~~with a consistent weakening of the eastern and western branch of PWC (Fig. 11e). We also note reduced SST (Fig. 9f) and rainfall (Fig. 10f) anomalies over the western ~~and, central equatorial~~ Pacific in ~~G1~~agreement with a weakening of western branch of PWC (Fig. ~~8f).~~11f) for the total number of El Niño events in G1. Thus, in general, extreme El Niño events tend to be weaker in G1 than in piControl.

~~The spatial pattern of composite rainfall anomalies for extreme and total El Niño events is alike both in G1 and piControl with peak positive rainfall anomalies centering at $\sim$145° W and $\sim$160° W, respectively (Fig. 9a-d). However, during extreme El Niño events, in accordance with weak warm SST anomalies over western, central, and eastern equatorial Pacific (Fig. 8e), the positive rainfall anomalies are also weaker (Fig. 9e). The composite difference for total El Niño events also indicates weaker positive rainfall anomalies over the central Pacific (Fig. 9f).~~

~~During El Niño events, the PWC reverses in sign and direction with stronger atmospheric upwelling over the eastern Pacific and downwelling over the western Pacific. The spatial patterns of PWC for the extreme and total number of El Niño events are similar both under G1 and piControl (Fig. 10a-d). During extreme (total number of) El Niño events the upwelling is centered at ~145° W (~160° W) both in G1 and piControl. In G1 relative to piControl, the atmospheric upwelling (downwelling) becomes weak over eastern (western) equatorial Pacific during extreme El Niño events (Fig. 10e) which agrees with reduced SST and rainfall anomalies over these regions (see Fig. 8e and 9e). For total El Niño events, in contrast to extreme El Niño events, the deep convection between 600 and 200 hPa over eastern Pacific is strengthened under G1 relative to piControl whereas the atmospheric downwelling becomes weak over western Pacific (Fig. 10f). Thus, during extreme El Niño events the PWC is weaker in G1 than in piControl.~~

We conclude that, in our simulations, extreme El Niño events are more frequent but slightly less ~~powerful~~intense in a solar geoengineered climate than in preindustrial conditions. We further confirm this with a histogram of detrended Niño3 SST anomalies (Fig. ~~S5a~~S7a). Though more frequent positive Niño3 SST anomalies occur under G1 (between 1~~.5~~ and ~~2.5~~3 °C~~)~~), the mean Niño3 SST anomaly is weaker in G1 (~~2.38~~1.95 °C) than in piControl (2.~~16~~23 °C) at 99 % cl. Thus, the strength of extreme El Niño events is reduced by ~~~9~~12 % in G1 compared to piControl. However, no statistically significant shift in histograms of Niño3 SST anomalies is detected for the total number of El Niño events (Fig. ~~S5b~~S7b).

3.3.2 Strengthening of La Niña ~~composites~~ events in G1

The ~~composite~~broad spatial patterns of composite SST~~, and the~~ (Fig 12a-d), rainfall (Fig. 13a-d) and PWC (14a-d) anomalies~~,~~ for the extreme and total number of La Niña events are similar under G1 and piControl~~ (Fig 11a-d and Fig. 12a-d).~~. During the extreme and total number of La Niña events, the negative SST ~~anomalies are stronger~~ and ~~more stretched towards western Pacific than that for the total La Niña events. The peak negative~~ rainfall anomalies~~ occur in the Niño4 region for both for extreme~~, and ~~total La Niña events composites. The composite differences of SSTs (Fig. 11e-f)~~both east and ~~rainfall (Fig. 12e-f) anomalies for both extreme and total La Niña events show that negative SST and rainfall anomalies are stronger in G1 than in piControl. Thus, under G1 the extreme and total events are stronger than in piControl. These composite differences also show that during extreme and total La Niña events, the western Pacific and western coast of south America is warmer and wetter under G1 compared to piControl.~~

~~The PWC is~~ west branch of PWC are strengthened ~~during La Niña events. The spatial pattern of composite PWC for extreme and total La Niña events is similar both under G1 and piControl (Fig. 13a-d). However, the composite differences indicate that PWC is stronger in G1 than in piControl both for extreme and total La Niña events (Fig. 13e-f) consistent with stronger negative SST and rainfall anomalies in the eastern and central equatorial Pacific.~~

indicating an overall intensification of La Niña events in G1 relative piControl. We note that most of the stronger negative SST anomalies occur over the eastern equatorial Pacific~~ under~~

~~G1 compared to piControl indicating an overall increase in strength of La Niña events in solar geoengineered climate (Fig. 11e-f).~~. We ~~further~~ confirm ~~this with~~strengthening of La Niña events by plotting histograms of detrended Niño3 SST anomalies for~~ extreme and total number of La Niña events based on the Niño4 SST index (Fig. S5c-d). Figures S5c-d clearly show that under G1 compared to piControl stronger negative SST anomalies occur over eastern equatorial Pacific during~~ the extreme (piControl: -1.45 °C; G1: -1.68 °C) and the total number of La Niña events (piControl: -1.03 °C; G1: -1.22 °C~~).~~) based on the Niño4 SST index (Fig. S7c-d). Thus, we conclude that the strength of extreme (total number of) La Niña events is increased by ~16 % (~18 %) in G1 compared to piControl.

44 Mechanisms behind the changes in ENSO variability

4.1 Under greenhouse gas forcing

The reduced ENSO amplitude under 4×CO_2 is mainly caused by stronger hf and weaker BJ feedback relative to piControl (Fig. 15a-b, and Table S5-6). More rapid warming over the eastern than western equatorial Pacific regions reduces the SST asymmetry between western and eastern Pacific (Fig. 1d), resulting in the weakening of ZSSTG (Fig. 4b) that significantly weakens the zonal winds stress (Fig. 4a) and hence PWC (Fig. 6b, d, see Bayr et al., 2014). The overall reduction of zonal wind stress reduces the BJ feedback, which, in turn, can weaken the ENSO amplitude. Climate models show an inverse relationship between hf feedback and ENSO amplitude (Lloyd et al., 2009, 2011; Kim and Jin 2011b). The increased hf feedback might be the result of enhanced clouds due to strengthened convection (Fig. 5b, d) and stronger evaporative cooling in response to enhanced SSTs under 4×CO_2 (Knutson and Manabe 1994; Kim and Jin 2011b). Kim and Jin (2011a, b) found intermodel consensus on the strengthening of hf feedback in CMIP3 models under enhanced GHG warming scenario (Ferret and Collins 2019). Further, we see increased ocean stratification under 4×CO_2 (Fig. 15d and Table S7). A more stratified ocean is associated with an increase in both the El Niño events and amplitude in the eastern Pacific (Wang et al. 2020). It can also modify the balance between feedback processes (Dewitte et al., 2013). Enhanced stratification may also cause negative temperature anomalies in the central to the western Pacific through changes in thermocline tilt (Dewitte et al., 2013). Since the overall ENSO amplitude decreases in our 4xCO_2 simulation, we, thus, conclude that the ocean stratification mechanisms cannot be the dominant factor here, but that hf and BJ feedbacks must more than cancel out the effect of ocean stratification on ENSO amplitude.

The increased frequency of extreme El Niño events under 4×CO_2 is due to change in the mean position of the ITCZ (Fig. S2), causing frequent reversals of MSSTG (Fig. S3), and eastward extension of the western branch of PWC (Fig. 6), which both result in increased rainfall over the eastern Pacific (see Wang et al. 2020). This is due to greater east equatorial than off-equatorial Pacific warming (see Cai et al. 2020), which shifts the mean position of ITCZ towards the equator (Fig. S2). Simultaneously more rapid warming of the eastern than western equatorial Pacific reduces the ZSSTG, and hence zonal wind stress, as also evident from the weakening and shift of the PWC (Fig. 6) and increased instances of negative ZSSTG anomalies (Fig. S9). Ultimately, this leads to more frequent vigorous convection over the

Niño3 region (Fig. 5d), and enhanced rainfall (Fig. 2d, S8). Therefore, despite the weakening of the ENSO amplitude under 4×CO_2, rapid warming of the eastern equatorial Pacific causes frequent reversals of meridional and zonal SST gradients, resulting in an increased frequency of extreme El Niño events (see also Cai et al., 2014; Wang et al., 2020).

We note that under GHG forcing, HadCM3L does not simulate an increase in the frequency of extreme La Niña events as found by Cai et al. (2015b) using CMIP5 models. However, it does show an increase in the total number of La Niña events (Table S4). In a multimodel ensemble mean, Cai et al. (2015b) found that the western Pacific warms more rapidly than the central Pacific under increased GHG forcing, resulting in strengthening of the zonal SST gradient between these two regions. Strengthening of this zonal SST gradient and increased vertical upper ocean stratification provide conducive conditions for increased frequency of extreme La Niña events (Cai et al., 2015b). One reason why we do not see an increase in the frequency of central Pacific extreme La Niña events might be that HadCM3L does not simulate more rapid warming of the western Pacific compared to the central Pacific as noticed by Cai et al. (2015b) (compare our Fig. 1d with Fig. 3b in Cai et al., 2015b), hence, as stronger zonal SST gradient does not develop, across the equatorial Pacific, as needed for extreme La Niña events to occur (see Fig. S9a, c and S10).

4.2 Under solar geoengineering

G1 over cools the upper ocean layers, whereas the GHG-induced warming in the lower ocean layers is not entirely offset, thus increasing ocean stratification (Fig. 15). The increased stratification boosts atmosphere-ocean coupling (see Cai et al., 2018), which favours enhanced westerly wind bursts (Fig. 4a) (e.g., Capotondi et al., 2018) to generate stronger SST anomalies over the eastern Pacific (Wang et al. 2020). The larger cooling of the western Pacific than the eastern Pacific can also enhance westerly wind bursts reinforcing the BJ feedback and hence SST anomalies in the eastern Pacific. We conclude that increased ocean stratification, along with stronger BJ feedback, is the most likely mechanism behind the overall strengthening of ENSO amplitude under G1.

The increased frequency of extreme El Niño events under G1 can be linked to the changes in MSSTG and ZSSTG (see Cai et al., 2014, and Fig. S3, S9). The eastern off-equatorial Pacific cools more than the eastern equatorial regions, providing relatively more conducive conditions for convection to occur through a shift of ITCZ over to the Niño3 region (Fig. 1e). At the same time, the larger cooling of the western equatorial Pacific than of the eastern equatorial Pacific reduces the ZSSTG and convective activity over the western Pacific, which leads to a weakening of the western branch of PWC (Fig. 6e). Hence we see reduced rainfall over the western Pacific and enhanced rainfall from the Niño3 to the central Pacific region (Fig 2e). These mean state changes, strengthening of convection between ~140° W and ~150° E, and more reversals of the MSSTG and ZSSTG (Fig. S3) result in an increased number of extreme El Niño events in G1 than in piControl (Fig. 7).

5 Discussion and conclusions

In this paper, we have ~~analysed~~analyzed the impact of abruptly increased GHG forcing ($4\times CO_2$~~)~~), and solar geoengineering (G1~~)~~), on the tropical Pacific mean climate and ENSO extremes. Previous solar geoengineering studies did not show any statistically significant change in the PWC (e.g., Guo et al., 2018) or ENSO frequency and amplitude (e.g., Gabriel and Robock 2015). However, those results were strongly limited by the ~~–~~length of the respective ~~GeoMIP~~ simulations, which made changes ~~difficult~~challenging to detect, given the high ~~climate~~ tropical Pacific climate variability. This ~~problem was~~limitation has been overcome here by using long (1000~~ years~~-year) climate model simulations, carried out with HadCM3L. The longer record makes it possible to detect even relatively small changes between the preindustrial and G1 scenarios within the chosen model system.

Formatted: Font: Times New Roman, 12 pt, English (U.S.)

~~We find that manipulating the downward shortwave flux through~~To conclude, solar geoengineering can compensate ~~some~~many of the ~~greenhouse~~GHG-induced changes in the tropical Pacific, but, importantly, not all~~. Importantly, manipulating~~ of them. In particular, controlling the downward shortwave flux cannot correct one of the climate ~~system's~~system's most dominant ~~mode~~modes of variability, i.e., ENSO, wholly back to preindustrial conditions. ~~Specifically~~The ENSO feedbacks (Bjerkness and heat flux) and more stratified ocean temperatures may induce ENSO to behave differently under G1 than under piControl and $4\times CO_2$. Different meridional distributions of shortwave and longwave forcings (e.g., Nowack et al., 2016) resulting in the surface ocean overcooling, and residual warming of the deep ocean are the plausible reasons for the solar geoengineered climate not reverting entirely to the preindustrial state. However, we ~~find that:~~note that this is a single model study, and more studies are needed to show the robustness and model-dependence of any results discussed here, e.g. using long-term multimodel ensembles from GeoMIP6 (Kravitz et al., 2015), once the data are released. The long-term Stratospheric Aerosol Geoengineering Large Ensemble (GLENS; Tilmes et al., 2018) data can also be explored to investigate ENSO variability under geoengineering. We summarize our key findings as follows:

Formatted: English (U.S.)

Formatted: English (U.S.)

1. The warming over the tropical Pacific under increased GHG forcing ($4\times CO_2$) is overcompensated under solar sunshade ~~(G1)~~ geoengineering (G1), resulting, by design, in ~~a cooling~~tropical mean overcooling of approximately 0.3 °C. This overcooling is more pronounced in the western tropical Pacific and SPCZ than in the eastern Pacific under the G1 scenario. ~~This shows that even in an ideal situation, where shading is applied as soon as GHG forcing is introduced, the climate will experience changes in regional gradients. The implication is that solar engineering experiments could benefit from applying spatially variable shadings to redress some of the changes induced by the GHGs.~~
2. The reduced SST and rainfall asymmetry~~,~~ between the warm pool and the cold tongue, ~~observed~~seen under $4\times CO_2$, is mostly corrected in G1, but regionally important differences remain relative to preindustrial conditions. The tropical Pacific is 5 % wetter in $4\times CO_2$, whereas it is 5 % drier in G1 relative to piControl. ~~Solar~~In particular, solar geoengineering results in decreased rainfall over the warm pool, SPCZ, and ITCZ and ~~an increase~~increased rainfall over the central and eastern equatorial Pacific.

3. The preindustrial median position of ITCZ~~ north of the equator~~ (154° W-82° W; 7.5° N) changes significantly under 4×CO_2 and moves over the equator (154° W-82° W; 0°). G1 restores the ITCZ to its preindustrial position (154° W-82° W; 7.5° N).

4. The increased GHG forcing results in 31 % reduction in zonal wind stress over the tropical Pacific. G1 fails to ~~completely~~ compensate this reduction~~,~~ entirely and results in weakening the zonal wind stress by 10 % with a 13 % (7 %) increase (decrease) in WWBs (EWBs), thus providing more conducive conditions for El Niño extremes.

5. Under solar geoengineering, both ZSSTG and MSSTG are reduced by 11 % and 9 %, respectively. More frequent reversal of MSSTG occurs in G1 relative to piControl.

6. In 4×CO_2, the thermocline ~~shoals by 22 %~~flattens over the tropical Pacific, ~~however~~and G1 ~~completely~~ recovers ~~it to~~ its preindustrial ~~orientation~~condition.

7. The PWC becomes weaker both under 4×CO_2 and G1 scenarios.

8. The increased GHG forcing results in a weakening of ENSO amplitude~~ by 30-57 %~~, whereas solar geoengineering strengthens it ~~by 5-8 %~~ relative to preindustrial climate. The maximum amplitude of ~~warm (~~cold~~)~~ events is enhanced under G1.

~~8.~~9. The reduced ~~(increased) under G1~~ENSO amplitude under 4×CO_2 is mainly due to enhanced hf feedback, whereas the increase under G1 is mainly caused by enhanced BJ feedback and ocean stratification.

~~9.~~10. The ENSO amplitude asymmetry between warm and cold events is reduced under G1 relative to piControl.

~~10.~~11. The frequency of extreme El Niño events increases by ~~44~~61 % in G1 relative to piControl.~~ Hence, an extreme El Niño event occurring every ~22-yr under preindustrial conditions occurs every ~15-yr under solar geoengineered conditions.~~ Further, the frequency of the total number~~ (extreme plus moderate)~~ of El Niño events also increases by 12 %. Thus, an El Niño event occurring every ~3.3-yr under preindustrial conditions occurs every ~2.9-yr under solar geoengineered climate. The reason for the occurrence of more extreme El Niño events under G1 is more frequent reversals of MSSTG compared to piControl.

~~11.~~12. The frequency of extreme La Niña events increases by 32 % under G1 relative to piControl. Thus, an extreme La Niña event occurring every ~22-yr in piControl occurs every ~16-yr in G1.

~~12. The extreme El Niño events are ~9 % weaker whereas all La Niña events are ~18 % stronger under G1 compared to piControl.~~

Author contribution. Long Cao developed the model code and performed the simulations. Abdul Malik formulated the research questions, defined the methodology with the help of all co-authors, and performed the scientific analysis. Abdul Malik prepared the manuscript with contributions from all co-authors.

Competing interests. The authors declare that they have no conflict of interest.

Data availability. Data are available upon request from Long Cao (longcao@zju.edu.cn).

Formatted: Line spacing: Multiple 1.15 li

Formatted: Font: Bold, English (U.S.)

Formatted: List Paragraph

Acknowledgments

~~This work was supported by the~~ The Swiss National Science Foundation supported this work under the grant EarlyPostdoc. Mobility (P2BEP2_175255). Peer J. Nowack is funded through an Imperial College Research Fellowship. GPCP Precipitation and NCEP Reanalysis data was provided by the NOAA/OAR/ESRL PSD, Boulder, Colorado, USA, from their Web site at https://www.esrl.noaa.gov/psd/. ~~PJN is supported through an Imperial College Research Fellowship.~~The ERA5 data was downloaded from https://cds.climate.copernicus.eu/cdsapp#!/home.

Formatted: Line spacing: Multiple 1.15 li

References

Adler, R. F., Huffman, G. J., Chang, A., Ferraro, R., Xie, P-P., Janowiak, J., Rudolf, B., Schneider, U., Curtis, S., Bolvin, D., Gruber, A., Susskind, J., Arkin, P., and Nelkin, E.: The version-2 Global Precipitation Climatology Project (GPCP) monthly precipitation analysis (1979–Present), J. Hydrometeorol., 4, 1147–1167, https://doi.org/10.1175/1525-7541(2003)004<1147:TVGPCP>2.0.CO;2, 2003.

An, S-II., and Jin, F-F.: Nonlinearity and Asymmetry of ENSO, J. Climate., 17, 2399–2412, https://doi.org/10.1175/1520-0442(2004)017<2399:NAAOE>2.0.CO;2, 2004.

Bala, G., Duffy, P. B., and Taylor, K. E.: Impact of geoengineering schemes on the global hydrological cycle. Proc. Natl. Acad. Sci. U. S. A., 105, 7, 664–7, 669, https://doi.org/10.1073/pnas.0711648105, 2008.

Bayr, T., Dommenget, D., Martin, T., Power, S. B.: The eastward shift of the Walker circulation in response to global warming and its relationship to ENSO variability. Clim. Dyn., 43, 2747–2763, https://doi.org/10.1007/s00382-014-2091-y, 2014.

Bellenger, H., Guilyardi, E., Leloup, J., Lengaigne, M., Vialard, J.: ENSO representation in climate models: from CMIP3 to CMIP5. Clim. Dyn., 42, 1999–2018, http://doi. 10.1007/s00382-013-1783-z, 2014.

Boer, G. J., Yu, B., Kim, S., ~~and~~ Flato, G. M.: Is there observational support for an El Niño-like pattern of future global warming~~?,~~? Geophys. Res. Lett., 31, 1–4, https://doi.org/10.1029/2003GL018722, 2004.

Formatted: Line spacing: Multiple 1.15 li

Bove, M. C., Elsner, J. B., Landsea, C. W., Niu, X., O Brien, J. J.: Effect of El Niño on U.S. landfalling hurricanes, revisited, B. Am. Meteorol. Soc., 79 (11), 2477-2482, https://doi.org/10.1175/1520-0477(1998)079<2477:EOENOO>2.0.CO;2, 1998.

Cai, W., Borlace, S., Lengaigne, M., van Rensch, P., Collins, M., Vecchi, G., Timmermann, A., Santoso, A., McPhaden, M. J., Wu, L., England, M. H., Wang, G., Guilyardi, E., and Jin, F-F.: Increasing frequency of extreme El Niño events due to greenhouse warming, Nat. Clim. Change., 4(2), 111–116, https://doi.org/10.1038/nclimate2100, 2014.

Cai, W., Santoso, A., Wang, G., Yeh, S. W., An, S. Il, Cobb, K. M., Collins, M., Guilyardi, E., Jin, F-F., Kug, J-S., Lengaigne, M., McPhaden, M. J., Takahashi, K., Timmermann, A., Vecchi, G., Watanabe, M., and Wu, L.: ENSO and greenhouse warming. Nat. Clim. Change., 5(9), 849–859. https://doi.org/10.1038/nclimate2743, 2015a.

Cai, W., Wang, G., Dewitte, B., Wu, L., Santoso, A., Takahashi, K., Yang, Y., Carréric, A., McPhaden, M. J.: Increased variability of eastern Pacific El Niño greenhouse warming. Nature, 564, 201-206, https://doi.org/10.1038/s41586-018-0776-9, 2018.

Cai, W., Wang, G., Santoso, A., Lin, X., and Wu, L.: Definition of Extreme El Niño and Its Impact on Projected Increase in Extreme El Niño Frequency. Geophys. Res. Lett., 44(21), 11184-11190, https://doi.org/10.1002/2017GL075635, 2017.

Cai, W., Wang, G., Santoso, A., Mcphaden, M. J., Wu, L., Jin, F-F., Timmermann, A., Collins, M., Vecchi, G., Lengaigne, M., England, M. H., Dommenget, D., Takahashi, K., and Guilyardi, E.: Increased frequency of extreme La Niña events under greenhouse warming, Nat. Clim. Change., 5(2), 132–137, https://doi.org/10.1038/nclimate2492, 2015b.

Cao, L., Duan, L., Bala, G., and Caldeira, K.: Simulated long-term climate response to idealized solar geoengineering, Geophys. Res. Lett., 43(5), 2209-2217, https://doi.org/10.1002/2016GL068079, 2016.

Capotondi, A., Wittenberg, A., Masina, S.: Spatial and temporal structure of Tropical Pacific interannual variability in 20th century coupled simulations, ~~Ocean~~ocean. Model., 15(3-4), 274-298, https://doi.org/10.1016/j.ocemod.2006.02.004, 2006.

Chen, L., Li, T., Yu, Y., and Behera, S. K.: A possible explanation for the divergent projection of ENSO amplitude change under global warming~~.~~, Clim. Dynam., 49(11–12), 3799–3811, https://doi.org/10.1007/s00382-017-3544-x, 2017.

~~Collins, M., Tett~~Chung, C. T. Y., Power, S. ~~F.~~ B., Arblaster, J. M., Rashid, H. A., Roff, G. L.: Non-linear precipitation response to El Niño and ~~Cooper, C.: The internal climate variability of HadCM3, a version of~~global warming in the ~~Hadley Centre coupled model without flux adjustments~~Indo-Pacific. Clim~~Dynam, 17(1), 61–81~~. Dyn., 42, 1837–1856, https://doi.org/10.1007/~~s003820000094, 2001~~s00382-013-1892-8, 2014.

Coats, S., Karnauskas, K. B.: Are Simulated and Observed Twentieth-Century Tropical Pacific Sea Surface Temperature Trends Significant Relative to Internal Variability? Geophys. Res. Lett., 44, 9928–9937, https://doi.org/10.1002/2017GL074622, 2017.

Collins, M., An, S.-I., Cai, W., Ganachaud, A., Guilyardi, E., Jin, F.-F., Jochum, M., Lengaigne, M., Power, S., Timmermann, A., Vecchi, G., and Wittenberg, A.: The impact of global warming on the tropical Pacific Ocean and El Niño. Nature Geoscience, 3(6), 391–397, https://doi.org/10.1038/ngeo868, 2010.

Copernicus Climate Change Service (C3S).: ERA5: Fifth generation of ECMWF atmospheric reanalyses of the global climate. Copernicus Climate Change Service Climate Data Store (CDS), January 2020. https://cds.climate.copernicus.eu/cdsapp#!/home, https://doi.org/10.24381/cds.f17050d7, 2017.

Cox, P. M., Betts, R. A., Jones, C. D., Spall, S. A., and Totterdell, I. J.: Acceleration of global warming due to carbon-cycle feedbacks in a coupled climate model, Nature, https://doi.org/10.1038/35041539, 2000.

Crutzen, P. J: Albedo enhancement by stratospheric sulfur injections: A contribution to resolve a policy dilemma?, Climatic Change, 77(3–4), 211–219, https://doi.org/10.1007/s10584-006-9101-y, 2006.

Curry, C. L., Sillmann, J., Bronaugh, D., Alterskjaer, K., Cole, J. N. S., Ji, D., Kravitz, B., Kristjánsson, J. E., Moore, J. C., Muri, H., Niemeier, U., Robock, A., Tilmes, S., and Yang, S.: A multimodel examination of climate extremes in an idealized geoengineering experiment, J. Geophys. Res-Atmos., 119(7), 3900–3923, https://doi.org/10.1002/2013JD020648, 2014.

Formatted: Line spacing: Multiple 1.15 li

Formatted: Line spacing: Multiple 1.15 li

Formatted: Line spacing: Multiple 1.15 li

Dewitte, B., Yeh, S-W., Thual, S.: Reinterpreting the thermocline feedback in the western-central equatorial Pacific and its relationship with the ENSO modulation. Clim Dyn, 41, 819–830, https://doi.org/10.1007/s00382-012-1504-z, 2013.

Essery, R., and Clark, D. B.: Developments in the MOSES 2 land-surface model for PILPS 2e, Global Planet. Change., 38(1-2), 161–164~~.,~~, https://doi.org/10.1016/S0921-8181(03)00026-2, 2003.

Ferret, S., Collins, M.: ENSO feedbacks and their relationships with the mean state in a flux adjusted ensemble. Clim. Dyn., 52, 7189–7208, https://doi.org/10.1007/s00382-016-3270-9, 2019.

Gabriel, C. J., and Robock, A.: Stratospheric geoengineering impacts on El Niño/Southern Oscillation, Atmos. Chem. Phys., 15(20), 11949–11966, https://doi.org/10.5194/acp-15-11949-2015, 2015.

Gandhi, S. M., Sarkar, B. C.: Conventional and Statistical Resource/Reserve Estimation, in: Essentials of Mineral Exploration and Evaluation, Elsevier,1st Edition, 271-288, https://doi.org/10.1016/C2015-0-04648-2, 2016.

Gibbons, J. D., and Chakraborti, S~~., :~~.: Nonparametric Statistical Inference, 5th Ed., Statistics: Textbooks & Monographs, Chapman and Hall/CRC Press, Taylor and Francis Group, 2011.

Govindasamy, B., Caldeira, K.: Geoengineering Earth's radiation balance to mitigate CO2-induced climate change, Geophys. Res. Lett., 27(14), 2141-2144, https://doi.org/10.1029/1999GL006086, 2000.

Guilyardi, E.: El Niño–mean state–seasonal cycle interactions in a ~~multi-model~~multimodel ensemble, Clim. Dynam., 26(4), 329-348, https://doi.org/10.1007/s00382-005-0084-6~~-~~, 2006.

Guo, A., Moore, J. C., and Ji, D.: Tropical atmospheric circulation response to the G1 sunshade geoengineering radiative forcing experiment, Atmos. Chem. Phys., 18, 8689-8706, https://doi.org/10.5194/acp-18-8689-2018, 2018.

Ham, Y.: A reduction in the asymmetry of ENSO amplitude due to global warming: The role of atmospheric feedback, Geophys. Res. Lett., 44(16), 8576–8584, https://doi.org/10.1002/2017GL074842, 2017.

Hollander, M., and Wolfe D. A.: ~~Nonparametric~~Non-parametric Statistical Methods, 2nd Ed., John Wiley and Sons, Inc., 1999.

Hong, Y., Moore J. C., Jevrejeva, S., Ji, D., Phipps, S. J., Lenton~~.,~~, A., Tilmes, S., Watanabe, S., and Zhao, L.: Impact of the GeoMIP G1 sunshade geoengineering experiment on the Atlantic meridional overturning circulation, Environ. Res. Lett., 12(3), https://doi.org/10.1088/1748-9326/aa5fb8, 2017.

Hu, S., and Fedorov, A. V.: Exceptionally strong easterly wind burst stalling El Niño of 2014, P. Natl. Acad. Sci. USA., 113(8), 2005-2010, https://doi.org/10.1073/pnas.1514182113, 2016.

Huang, P., and Ying, J.: A multimodel ensemble pattern regression method to correct the tropical pacific SST change patterns under global warming. J. Climate., 28(12), 4706–4723, https://doi.org/10.1175/JCLI-D-14-00833.1, 2015.

Formatted: Line spacing: Multiple 1.15 li

Formatted: Line spacing: Multiple 1.15 li

Formatted: Line spacing: Multiple 1.15 li

Kim, S. T., Cai, W., Jin, F.-F., Santoso, A., Wu, L., Guilyardi, E., and An, S.-I.: Response of El Niño sea surface temperature variability to greenhouse warming. Nat. Clim. Change., 4(9), 786–790, https://doi.org/10.1038/nclimate2326, 2014.

Kim, S. T., Jin, F-F.: An ENSO stability analysis. Part I: results from a hybrid coupled model. Clim Dyn., 36, 1593–1607, https://doi. 10.1007/s00382-010-0796-0, 2011a.

Kim, S. T., Jin, F-F.: An ENSO stability analysis. Part II: results from the twentieth and twenty-first century simulations of the CMIP3 models. Clim Dyn., 36, 1609–1627, https://doi. 10.1007/s00382-010-0872-5, 2011b.

Knutson, T. R., Manabe, S.: Impact of increased CO_2 on simulated ENSO-like phenomena. Geophys. Res. Lett., 21, 2295-2298, https://doi.org/10.1029/94GL02152, 1994.

Kohyama, T., Hartmann, D. L., and Battisti, D. S.: La Niña-like mean-state response to global warming and potential oceanic roles, J. Climate., 30(11), 4207–4225, https://doi.org/10.1175/JCLI-D-16-0441.1, 2017.

Kravitz, B., Caldeira, K., Boucher, O., Robock, A., Rasch, P. J., Alterskjær, K., Karam, D. B., Cole, J. N. S., Curry, C. L., Haywood, J. M., Irvine, P. J., Ji, D., Jones, A., Kristjánsson, J. E., Lunt D. J., Moore, J. C., Niemeier, U., Schmidt, H., Schulz, M., Singh, B., Tilmes, S., Watanabe, S., Yang, S., Yoon, J-H.: Climate model response from the Geoengineering Model Intercomparison Project (GeoMIP), J. Geophys. Res-Atmos., 118, 8320–8332, https://doi.org/10.1002/jgrd.50646, 2013b.

Kravitz, B., Forster, P. M., Jones, A., Robock, A., Alterskjær, K., Boucher, O., Jenkins, A. K. L., Korhonen, H., Kristjánsson, J. E., Muri H., Niemeier, U., Partanen, A-I., Rasch, P. J., Wang, H., Watanabe, S.: Sea spray geoengineering experiments in the geoengineering model intercomparison project (GeoMIP): Experimental design and preliminary results, J. Geophys. Res-Atmos., 118(19), 11175–11186, https://doi.org/10.1002/jgrd.50856, 2013a.

Kravitz, B., Robock, A., Boucher, O., Schmidt, H., Taylor, K. E., Stenchikov, G., and Schulz, M.: The Geoengineering Model Intercomparison Project (GeoMIP), Atmos. Sci. Lett., 12(2), 162–167, https://doi.org/10.1002/asl.316, 2011.

Kravitz, B., Robock, A., Tilmes, S., Boucher, O., English, J. M., Irvine, P. J., Jones, A., Lawrence, M. G., MacCracken, M., Muri, H., Moore, J. C., Niemeier, U., Phipps, S. J., Sillmann, J., Storelvmo, T., Wang, H., and Watanabe, S.: The Geoengineering Model Intercomparison Project Phase 6 (GeoMIP6): simulation design and preliminary results, Geosci. Model Dev., 8, 3379–3392, https://doi.org/10.5194/gmd-8-3379-2015, 2015.

Latif, M., and Keenlyside, N. S.: El Niño/Southern Oscillation response to global warming, P. Natl. Acad. Sci. USA., 106 (49), 20578-20583, 10.1073/pnas.0710860105, 2009.

Liu, Z., Vavrus, S., He, F., Wen, N., and Zhong, Y.: Rethinking tropical ocean response to global warming: The enhanced equatorial warming. J. Climate., 18(22), 4684–4700, https://doi.org/10.1175/JCLI3579.1, 2005.

Lloyd, J., Guilyardi, E., Weller, H.: The role of atmosphere feedbacks during ENSO in the CMIP3 models. Part II: using AMIP runs to understand the heat flux feedback mechanisms. Clim. Dyn., 37,1271–1292, https://doi.org/10.1007/s00382-010-0895-y, 2011.

Formatted: Line spacing: Multiple 1.15 li

Formatted: Line spacing: Multiple 1.15 li

Lloyd, J. E., Guilyardi, E., Weller, H., Slingo, J.: The role of atmosphere feedbacks during ENSO in the CMIP3 models Atmos. Sci. Lett., 10, 170-176, https://doi.org/10.1002/asl.227~~170–176~~, 2009.

Lunt, D. J., Ridgwell, A, Valdes, P. J., Seale, A.: Sunshade World: A fully coupled GCM evaluation of the climatic impacts of geoengineering, Geophys. Res. Lett., 35(L12710), https://doi.org/10.1029/2008GL033674, 2008.

Luo, Y., Lu, J., Liu, F., and Liu, W.: Understanding the El Niño-like oceanic response in the tropical Pacific to global warming, Clim. Dynam., 45(7–8), 1945–1964, https://doi.org/10.1007/s00382-014-2448-2, 2015.

Malik, A., Brönnimann, S., Stickler, A., Raible, C. C., Muthers, S., Anet, J., Rozanov, E., Schmutz, W.: Decadal to multi-decadal scale variability of Indian summer monsoon rainfall in the coupled ocean-atmosphere-chemistry climate model SOCOL-MPIOM, Clim. Dynam., 49(9–10), 3551–3572, https://doi.org/10.1007/s00382-017-3529-9, 2017.

Meehl G. A., Washington, W. M.: El Niño like climate change in a model with increased atmospheric CO2 concentrations, Nature, 382, 1996.

Moore, T. R., Matthews, H. D., Simmons, C., and Leduc, M.: Quantifying changes in extreme weather events in response to warmer global temperature, Atmos. Ocean., 53(4), 412–425, https://doi.org/10.1080/07055900.2015.1077099, 2015.

Nowack, P. J., Abraham, N. L., Braesicke, P., and Pyle, J. A.: Stratospheric ozone changes under solar geoengineering: implications for UV exposure and air quality, Atmos. Chem. Phys., 16, 4191–4203, https://doi.org/10.5194/acpd-15-31973-2015, 2016.

Nowack, P. J., Abraham, N. L., Braesicke, P., and Pyle J. A.: The impact of stratospheric ozone feedbacks on climate sensitivity estimates, J. Geophys. Res. Atmos., 123, 4630–4641, https://doi.org/10.1002/2017JD027943, 2018.

Nowack, P. J., Abraham, N. L., Maycock, A. C., Braesicke, P., Gregory, J. M., Joshi, M. M., Osprey, A., and Pyle, J. A.: A large ozone-circulation feedback and its implications for global warming assessments, Nat. Clim. Chang., 5(1), 41–45, https://doi.org/10.1038/nclimate2451, 2015.

Nowack, P. J., Braesicke, P., Abraham, N. L., and Pyle J. A.: On the role of ozone feedback in the ENSO amplitude response under global warming, Geophys. Res. Lett., 44, 3858–3866, https://doi.org/10.1002/2016GL072418, 2017.

Ohba, M., Ueda H.: Role of ~~nonlinear atmospheric~~non-linear atmospheric response to SST on the asymmetric transition process of ENSO, 177–192. https://doi.org/10.1175/2008JCLI2334.1, 2009.

Pachauri, R. K., Allen, M. R., Barros, V. R., Broome, J., Cramer, W., Christ, R., Church, J. A., Clarke, L., Dahe, Q., Dasgupta, P., Dubash, N. K., Edenhofer, O., Elgizouli, I., Field, C. B., Forster, P., Friedlingstein, P., Fuglestvedt, J., Gomez-Echeverri, L., Hallegatte, S., Hegerl, G., Howden, M., Jiang, K., Jimenez Cisneroz, B., Kattsov, V., Lee, H., Mach, K. J., Marotzke, J., Mastrandrea, M. D., Meyer, L., Minx, J., Mulugetta, Y., O'Brien, K., Oppenheimer, M., Pereira, J. J., Pichs-Madruga, R., Plattner, G. K., Pörtner, H. O., Power, S. B., Preston, B., Ravindranath, N. H., Reisinger, A., Riahi, K., Rusticucci, M., Scholes, R., Seyboth, K., Sokona, Y., Stavins, R., Stocker, T. F., Tschakert, P., van Vuuren, D., and van Ypserle, J. P.: Climate change 2014: synthesis report, contribution of Working Groups I, II and III to the Fifth Assessment Report of the Intergovernmental

Formatted: Line spacing: Multiple 1.15 li

Panel on Climate Change, Pachauri, R., and Meyer, L., (Eds.) , Geneva, Switzerland, IPCC, 151 p., ISBN: 978-92-9169-143-2, 2014.

Park, W., Keenlyside, N., Latif, M., Ströh, A., Redler, R., Roeckner, E., and Madec, G.: Tropical Pacific climate and its response to global warming in the Kiel Climate Model. J. Climate., 22(1), 71–92, https://doi.org/10.1175/2008JCLI2261.1, 2009.

Philip, S. Y., and van Oldenborgh, G. J.: Shifts in ENSO coupling processes under global warming, Geophys. Res. Lett., 33(11), 1–5, https://doi.org/10.1029/2006GL026196, 2006.

Power, S., Delage, F., Chung, C., Kociuba, G., Keay, K.: Robust twenty-first-century projections of El Niño and related precipitation variability. Nature, 502, 541–545, https://doi.org/10.1038/nature12580, 2013.

Rayner, N. A., Parker, D. E., Horton, E. B., Folland, C. K., Alexander, L. V, Rowell, D. P., … Kaplan, A.: Global analyses of sea surface temperature~~-~~, sea ice~~-~~, and night marine air temperature since the late nineteenth century, J. Geophys. Res-Atmos., 108(D14), https://doi.org/10.1029/2002JD002670, 2003.

Ropelewski, C. F., and Halpert, M. S.: Global and regional scale precipitation patterns associated with the El Niño/Southern Oscillation, Mon Weather Rev., https://doi.org/10.1175/1520-0493(1987)115<1606:GARSPP>2.0.CO;2, 1987.

Santoso, A., Mcphaden, M. J., and Cai, W.: The defining characteristics of ENSO extremes and the strong 2015/2016 El Niño, Rev. Geophys., 55(4), 1079–1129, https://doi.org/10.1002/2017RG000560, 2017.

Schmidt, H., Alterskjær, K., Alterskjær, K., Bou Karam, D., Boucher, O., Jones, A., … Timmreck, C.: Solar irradiance reduction to counteract radiative forcing from a quadrupling of CO2: ~~Climate~~climate responses simulated by four earth system models, Earth. Syst. Dynam., 3(1), 63–78, https://doi.org/10.5194/esd-3-63-2012, 2012.

Schopf, P. S., and Burgman R. J.: A simple mechanism for ENSO residuals and asymmetry, J. Climate., 19, 3167–3179, 2006.

Stevenson, S., Fox-Kemper, B.: ENSO model validation using wavelet probability analysis, J. Climate., 23, 5540–5547, https://doi.org/10.1175/2010JCLI3609.1, 2010.

Stocker T. F., Qin D., Plattner, G. K., Tignor M., Allen, S. K., Boschung, J., Nauels, A., Xia, Y., Bex, V., Midgley P. M. (Eds.): Summary for Policymakers, in: Climate Change 2013: The Physical Science Basis. Contribution of Working Group I to the Fifth Assessment Report of the Intergovernmental Panel on Climate Change, Cambridge University Press, Cambridge, UK and New York, NY, USA, https://doi.org/10.1017/CBO9781107415324.004, 2013.

Sun, N., Zhou, T., Chen, X., Endo, H., Kitoh, A., Wu, B.: Amplified tropical Pacific rainfall variability related to background SST warming. Clim Dyn 54, 2387–2402, https://doi.org/10.1007/s00382-020-05119-3, 2020.

Tilmes, S., Richter, J. H., Kravitz, B., MacMartin, D. G., Mills, M. J., Simpson, I. R., Glanville, A. S., Fasullo, J. T., Phillips, A. S., Lamarque, J., Tribbia, J., Edwards, J., Mickelson, S Gosh, S.: CESM1(WACCM) Stratospheric Aerosol Geoengineering Large Ensemble (GLENS) Project. Bull. Amer. Meteor. Soc., 99 (11), 2361–2371, https://doi.org/10.1175/BAMS-D-17-0267.1, 2018.

Formatted: Line spacing: Multiple 1.15 li

Formatted: German (Germany)

Valdes, P. J., Armstrong, E., Badger, M. P. S., Bradshaw, C. D., Bragg, F., Crucifix, M., Davies-Barnard, T., Day, J. J., Farnsworth, A., Gordon, C., Hopcroft, P. O., Kennedy, A. T., Lord, N. S., Lunt, D. J., Marzocchi, A., Parry, L. M., Pope, V., Roberts, W. H. G., Stone, E. J., Tourte, G. J. L., and Williams, J. H. T.: The BRIDGE HadCM3 family of climate models: HadCM3@Bristol v1.0, Geosci. Model Dev., 10, 3715–3743, https://doi.org/10.5194/gmd-10-3715-2017, 2017.

van Oldenborgh, G. J., Philip, S. Y., and Collins, M.: El Niño in a changing climate: A ~~multi-model~~multimodel study, ~~Ocean~~ocean. Sci., 1(2), 81–95, https://doi.org/10.5194/os-1-81-2005, 2005.

Vecchi G. A., Soden B. J., (2007). Global warming and the weakening of the tropical circulation, J. Climate., 20, 4316–4340, https://doi.org/10.1175/JCLI4258.1, 2007.

Vecchi, G. A., Soden, B. J., Wittenberg, A. T., Held, I. M., Leetmaa, A., and Harrison, M. J: Weakening of tropical Pacific atmospheric circulation due to anthropogenic forcing, Nature, 441, 73–76, https://doi.org/10.1038/nature0474, 2006.

Vecchi, G. A., and Wittenberg, A. T.: El Niño and our future climate: where do we stand? Wiley Interdiscip. Rev. Clim. Chang., 1(2), 260–270, https://doi.org/10.1002/wcc.33, 2010.

Vega-Westhoff, B., and Sriver, R. L: Analysis of ~~ENSO’s~~ENSO's response to unforced variability and anthropogenic forcing using CESM, Scientific Reports, 7(1), 1–10, https://doi.org/10.1038/s41598-017-18459-8, 2017.

Wang, G., Cai, W., Santoso, A.: Stronger Increase in the Frequency of Extreme Convective than Extreme Warm El Niño Events under Greenhouse Warming. J. Climate, 33(2), 675–690, https://doi.org/10.1175/JCLI-D-19-0376.1, 2020.

Wang, G., Cai, W., Gan, B., Wu, L., Santoso, A., Lin, X., Chen, Z., and McPhaden, M. J.: Continued increase of extreme El Ninõ frequency long after 1.5 C warming stabilization~~,~~. Nat. Clim. Change., 7(8), 568–572, https://doi.org/10.1038/NCLIMATE3351, 2017.

Wang, Y., Luo, Y., Lu, J., and Liu, F.: Changes in ENSO amplitude under climate warming and cooling, Clim. Dynam., 53–53. https://doi.org/10.1007/s00382-018-4224-1, 2018.

Watanabe, M., Kug, J-S., Jin, F-F., Collins, M., Ohba, M., Wittenberg, A. T.: Uncertainty in the ENSO amplitude change from the past to the future. Geophys. Res. Lett., 39(L20703), https://doi.org/10.1029/2012GL053305, 2012.

Wigley, T., M., L.: A combined mitigation/geoengineering approach to climate stabilization, Science, 314(5798), 452-454, 10.1126/science.1131728, 2006.

Yang, H., Wang F.: Revisiting the thermocline depth in the equatorial Pacific, J. Climate., 22, 3856–3863, https://doi.org/10.1175/2009JCLI2836.1, 2009.

Yang, S., Li, Z., Yu, J.-Y., Hu, X., Dong, W., and He, S.: El Niño–Southern oscillation and its impact in the changing climate, Natl Sci Rev, nwy046, https://doi.org/10.1093/nsr/nwy046, 2018.

Yeh, S. W., Kug, J. S., Dewitte, B., Kwon, M. H., Kirtman, B. P., and Jin, F. F; El Niño in a changing climate, Nature, 461(7263), 511–514, https://doi.org/10.1038/nature08316, 2009.

Formatted: Line spacing: Multiple 1.15 li

Formatted: German (Germany)

Formatted: Line spacing: Multiple 1.15 li

Formatted: Line spacing: Multiple 1.15 li

Zelle, H., van Oldenborgh, G. J., Burgers, G., and Dijkstra, H.: El Niño and greenhouse warming: results from ensemble simulations with the NCAR CCSM, J. Climate., 18, 4669-4683, https://doi.org/10.1175/JCLI3574.1, 2005.

Zhou, Z. Q., and Xie, S. P: Effects of climatological model biases on the projection of tropical climate change, J. Climate., 28(24), 9909–9917, https://doi.org/10.1175/JCLI-D-15-0243.1, 2015.

Formatted: Font: Not Bold

Formatted: Indent: Left: 0 cm, First line: 0 cm

Figures and Figure Captions

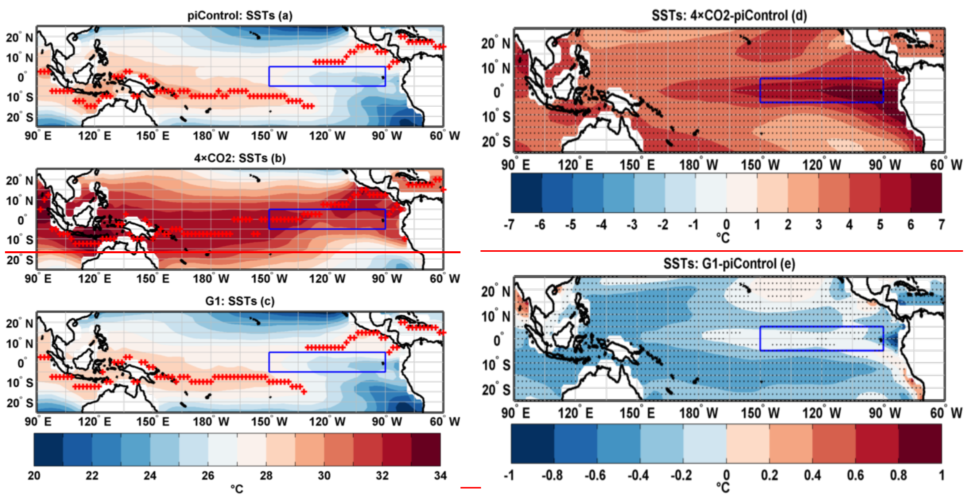

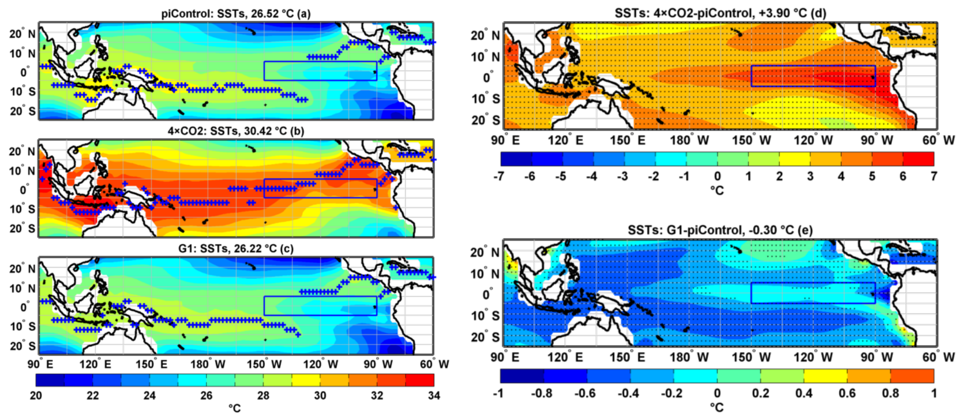

Figure 1. Tropical Pacific SST mean DJF climatology (a) piControl (b) 4×CO_2 (c) G1 (d) difference 4×CO_2-piControl and (e) difference G1-piControl. The ~~red~~blue plus sign in a-~~e~~c indicates latitudes with maximum SSTs. Stipples indicate grid points where the difference is statistically significant at ~~90~~99 % cl using a non-parametric Wilcoxon rank~~-~~sum test. The box in the eastern Pacific identifies the Niño3 region. The numbers in a-c represent a mean temperature in the corresponding simulation, and numbers in d-e represent an area-averaged difference of piControl with 4×CO_2 and G1, respectively, in the tropical Pacific region (25° N-25° S; 90° E-60° W).

Formatted: Font: Times New Roman, 12 pt

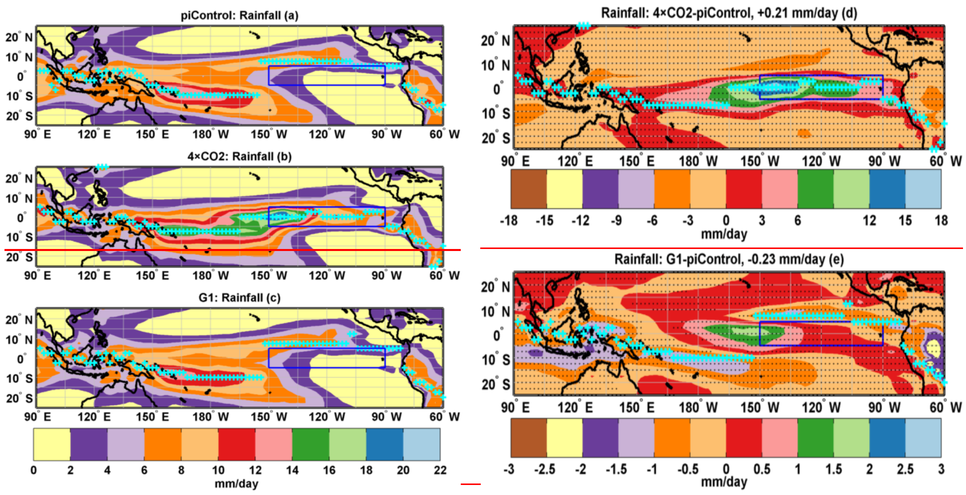

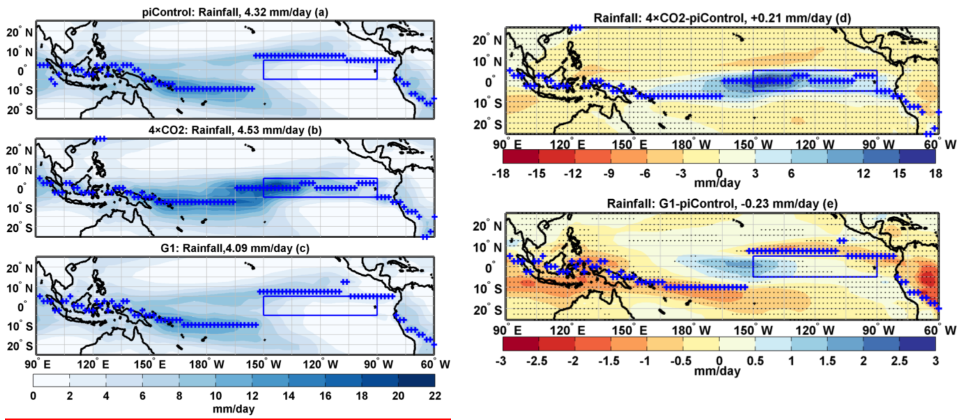

Figure 2. Tropical Pacific rainfall mean DJF climatology (a) piControl (b) 4×CO_2 (c) G1 (d) difference: 4×CO_2-piControl; the ~~cyan~~blue plus ~~sign~~signs indicate the position of ITCZ under 4×CO_2 and (e) difference: G1-piControl; the ~~cyan~~blue plus ~~sign~~signs indicate the position of ITCZ under G1. In a-c, the ~~cyan~~blue plus signs indicate the position of ITCZ for the corresponding experiment. Stipples indicate grid points where the difference is statistically significant at ~~90~~99 % cl using a non-parametric Wilcoxon rank~~-~~sum test. The numbers in a-c represent mean rainfall in the corresponding simulation, and numbers in d-e represent an area-averaged difference of piControl with 4×CO_2 and G1, respectively, in the tropical Pacific region (25° N-25° S; 90° E-60° W).

Formatted: English (U.S.)

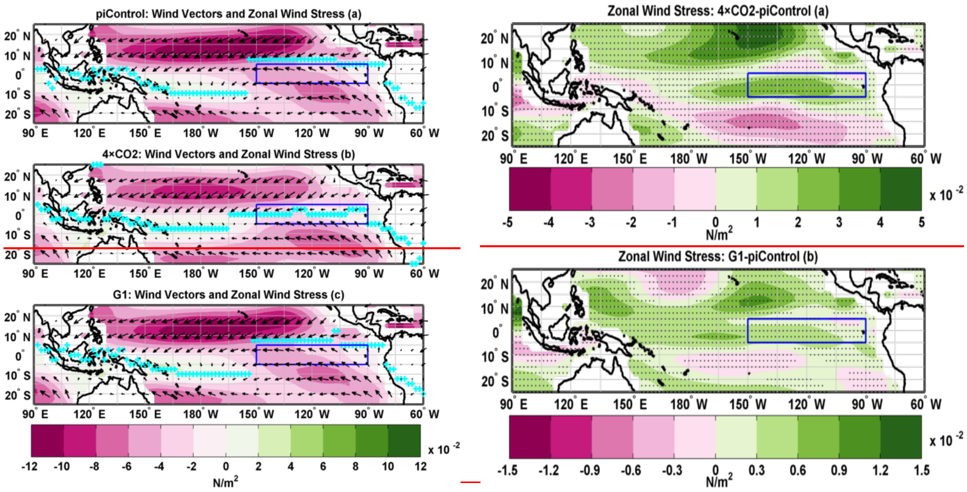

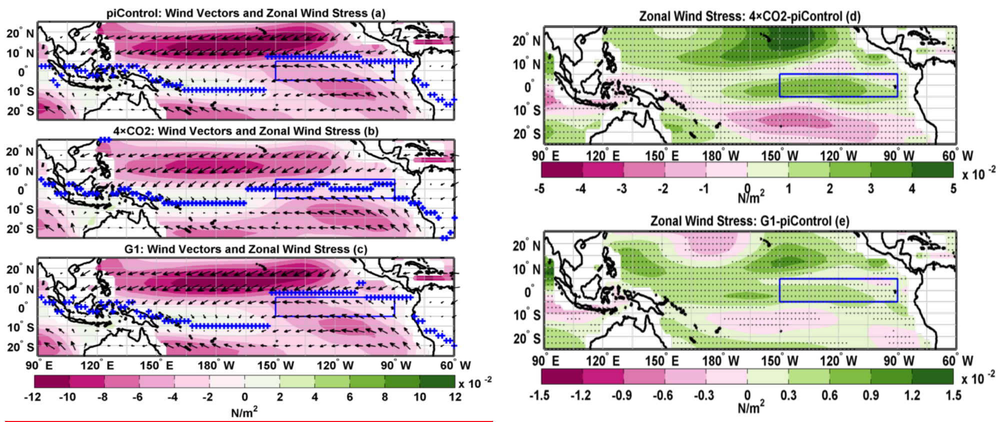

Figure 3. Tropical Pacific zonal wind stress mean DJF climatology (a) piControl (b) 4×CO_2 (c) G1 (d) difference: 4×CO_2-piControl and (e) difference: G1-piControl. Black arrows indicate the direction of 10 m wind. The ~~cyan~~blue plus sign in a-~~e~~c indicates latitudes with maximum rainfall. Stipples indicate grid points where the difference is statistically significant at ~~90~~99 % cl using a non-parametric Wilcoxon rank~~-~~-sum test.

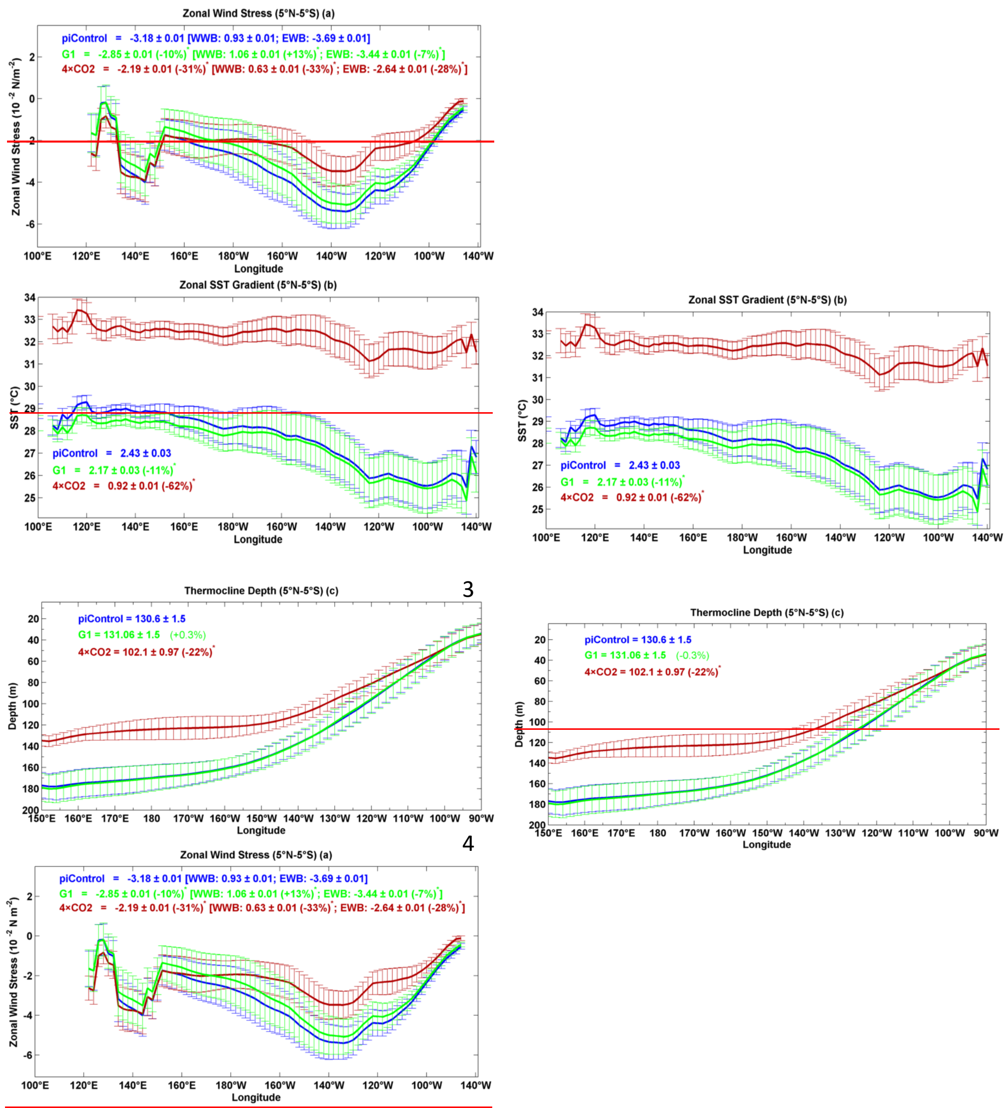

Figure 4. DJF mean climatology of (a) zonal wind stress, (b) zonal SST gradient, and (c) thermocline depth. Error bars indicate ±1 s.d. calculated over the simulated period. Numbers with an asterisk indicate that the percentage change is statistically significant at 99 % cl.

Formatted: Font: Bold

Formatted: Justified

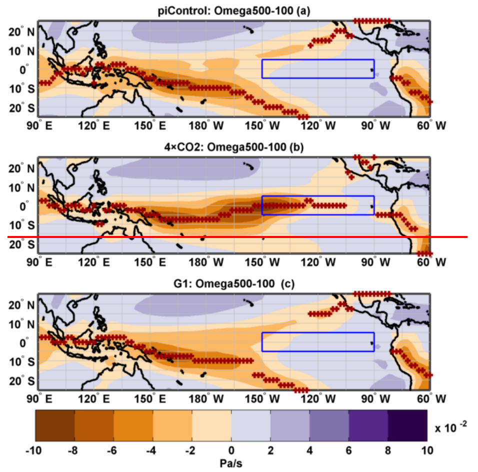

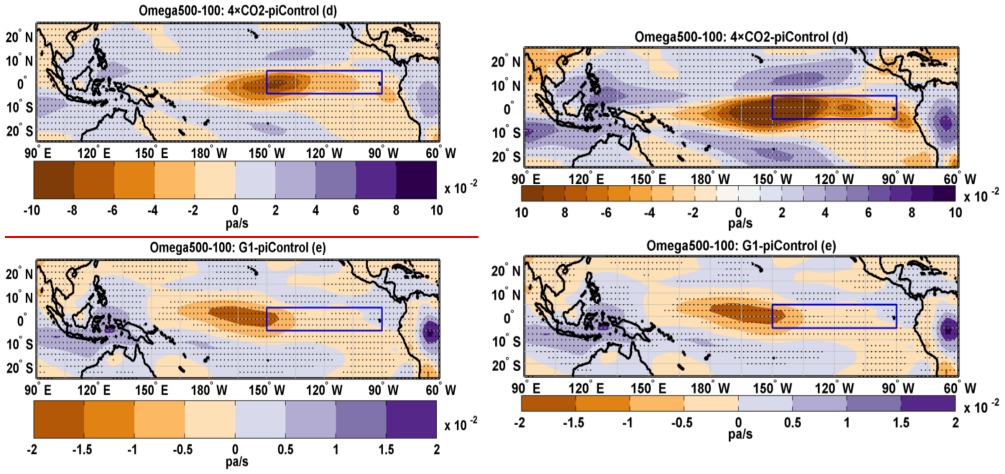

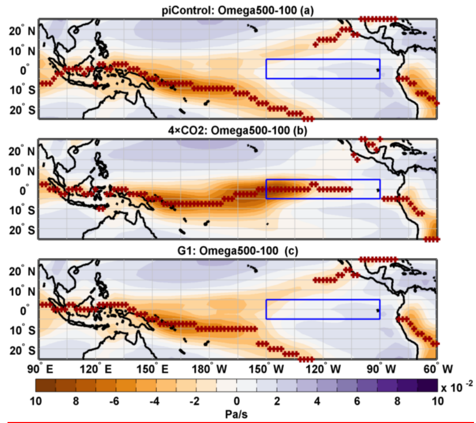

Figure 5. Tropical Pacific mean DJF climatology of vertical velocity averaged between 500- and 100-hPa (Omega500-100) (a) piControl (b) 4×CO_2 (c) G1 (d) difference: 4×CO_2-piControl and (e) difference: G1-piControl. In a-c, the brown plus sign ~~indicate~~indicates

latitudes where maximum upwelling occurs. Stipples indicate grid points where the difference is statistically significant at ~~90~~99 % cl using a non-parametric Wilcoxon rank~~-~~-sum test.

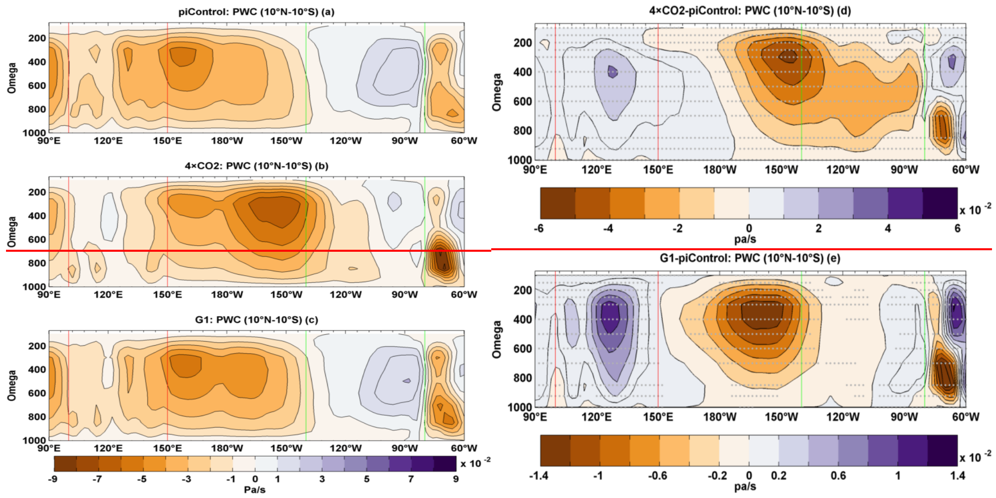

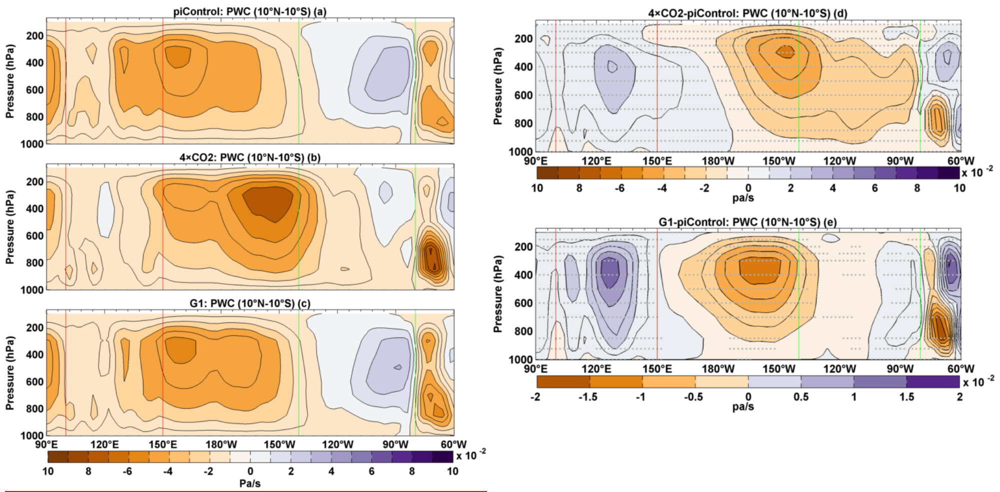

Figure 6. Mean DJF climatology of tropical Pacific Walker Circulation averaged over 90° E-60° W and 10° N-10° S (a) piControl (b) 4×CO_2 (c) G1 (d) difference: 4×CO_2-piControl and (e) difference: G1-piControl. Green (red) vertical lines show the longitudinal spread of the eastern (western) Pacific. Stipples indicate grid points where the difference is statistically significant at ~~90~~99 % cl using a non-parametric Wilcoxon rank~~-~~-sum test.

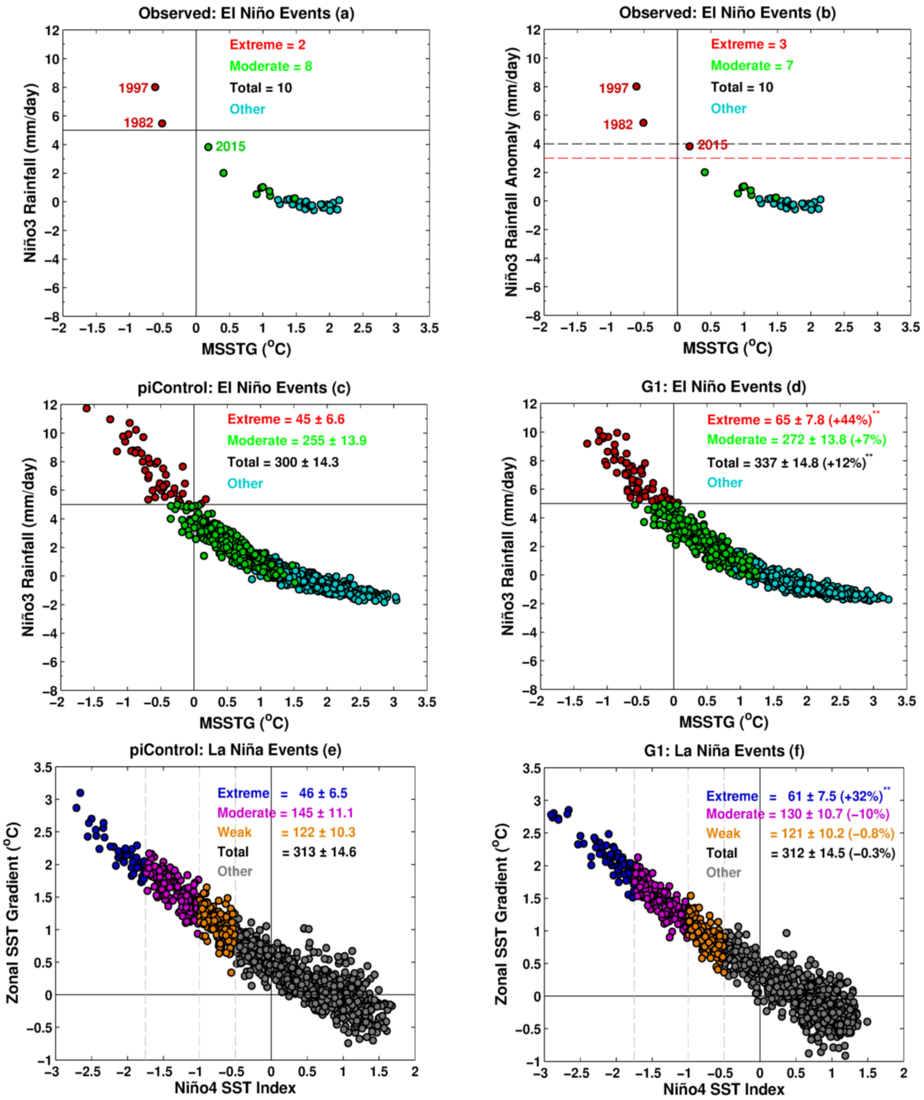
Observed: El Niño Events (a)
Extreme = 2
Moderate = 8
Total = 10
Other
1997
1982
2015
Niño3 Rainfall (mm/day)
MSSTG (°C)
Observed: El Niño Events (b)
Extreme = 3
Moderate = 7
Total = 10
Other
1997
1982
2015
Niño3 Rainfall Anomaly (mm/day)
MSSTG (°C)
piControl: El Niño Events (c)
Extreme = 45 ± 6.6
Moderate = 255 ± 13.9
Total = 300 ± 14.3
Other
Niño3 Rainfall (mm/day)
MSSTG (°C)
G1: El Niño Events (d)
Extreme = 65 ± 7.8 (+44%)**
Moderate = 272 ± 13.8 (+7%)
Total = 337 ± 14.8 (+12%)**
Other
Niño3 Rainfall (mm/day)
MSSTG (°C)
piControl: La Niña Events (e)
Extreme = 46 ± 6.5
Moderate = 145 ± 11.1
Weak = 122 ± 10.3
Total = 313 ± 14.6
Other
Zonal SST Gradient (°C)
Niño4 SST Index
G1: La Niña Events (f)
Extreme = 61 ± 7.5 (+32%)**
Moderate = 130 ± 10.7 (−10%)
Weak = 121 ± 10.2 (−0.8%)
Total = 312 ± 14.5 (−0.3%)
Other
Zonal SST Gradient (°C)
Niño4 SST Index

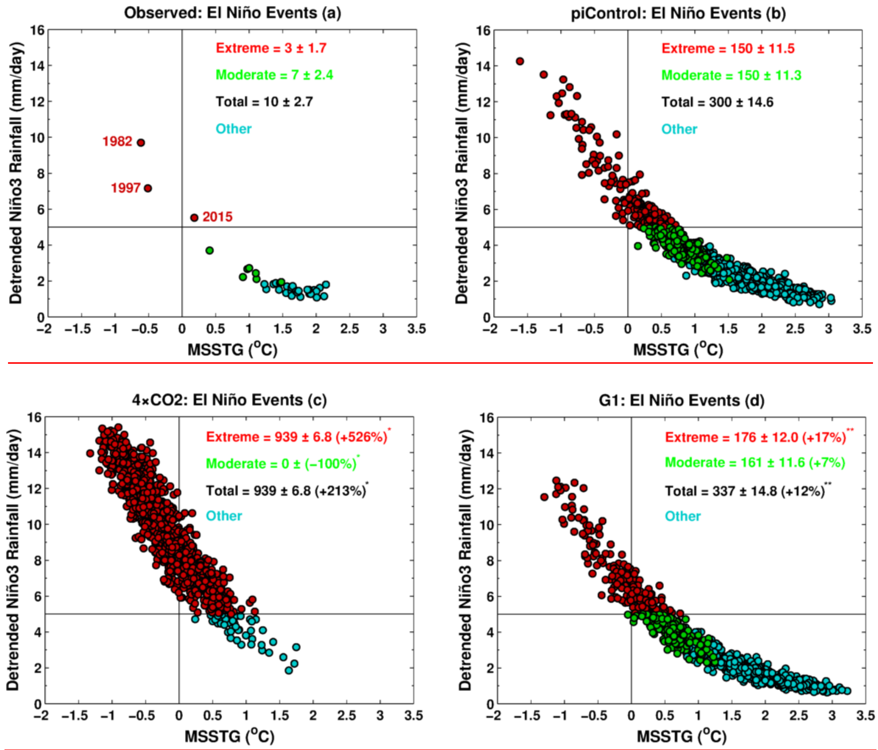

Figure 7. ~~Observed relationship between MSSTG and Niño3 rainfall when extreme El Niño is defined with (a) Niño3 total rainfall > 5 mm day^{-1} (b) Niño3 rainfall anomaly > 3 or 4 mm day^{-1}. Simulated relationship~~Relationship between MSSTG and Niño3 rainfall for (~~c)~~ a) observations (b) piControl (c) 4×CO_2, and (d) G1. ~~Simulated relationship between Niño4 and ZSSTG for (e) piControl and (f) G1. In b the~~ A solid black horizontal line indicates a threshold value of 5 mm day^{-1}. ~~In a, c and d the dashed red (black) horizontal line indicates~~See text for the definition of extreme, moderate, and total El Niño events. A single (double) asterisk indicates that the change in frequency, relative to piControl, is statistically significant at 99 % (95 %) cl. Numbers with a ± symbol indicate s.d. calculated with 10,000 bootstrap realizations. Following Cai et al. (2014), a non-ENSO related trend has been removed from the rainfall time series.

Formatted: Font: Bold

Formatted: English (U.K.)

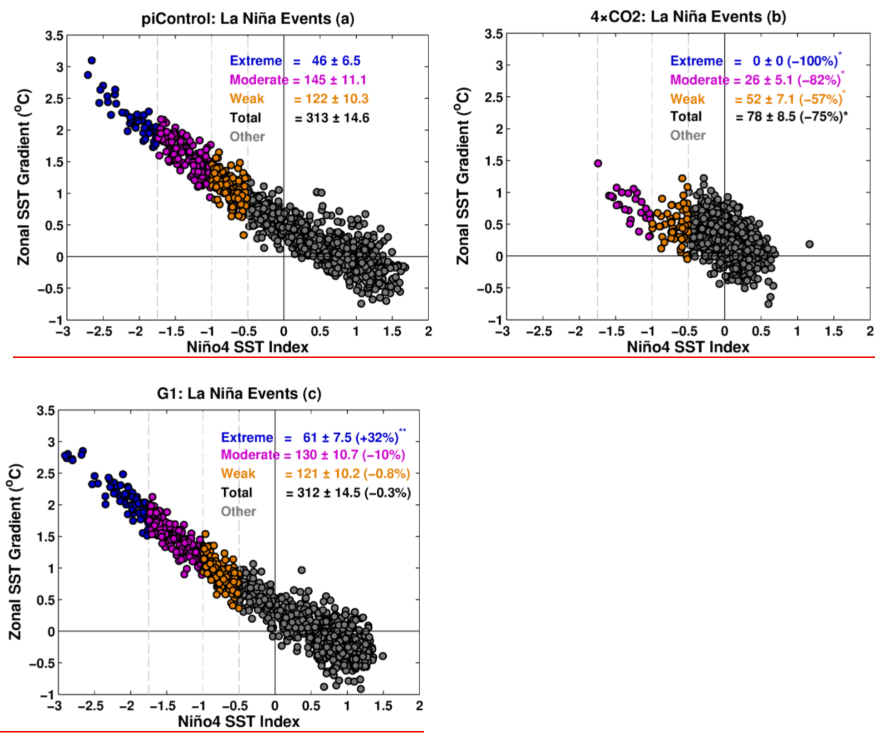

Figure 8. Relationship between ZSSTG and Niño4 SST index for (a) piControl (b) 4×CO_2 and (c) G1. Dashed grey vertical lines indicate threshold ~~anomaly~~values of ~~3 (4) mm day~~-1.75, -1, and -0.5 s.d. See text for the definition of extreme, moderate, weak, and total ~~El Niño (~~La Niña~~)~~ events. ~~The~~A single (double) asterisk indicates that the change in frequency is statistically significant at 99 % (95 ~~%~~%) cl. Numbers with a ± symbol indicate s.d. calculated with 10,000 bootstrap realizations.

Formatted: English (U.K.), Not Superscript/ Subscript

Formatted: English (U.K.)

Formatted: English (U.S.)

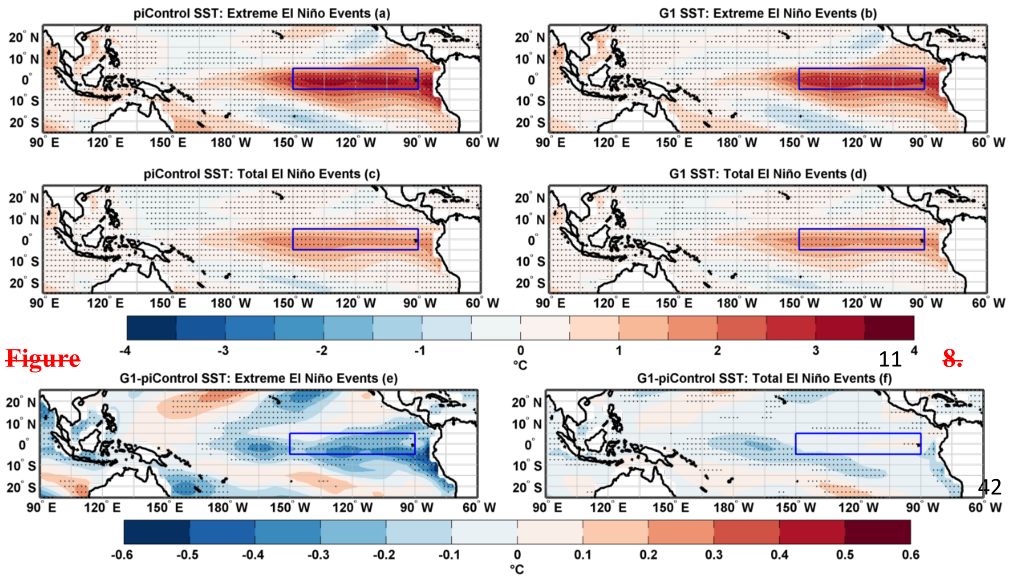

~~**Figure 8.**~~

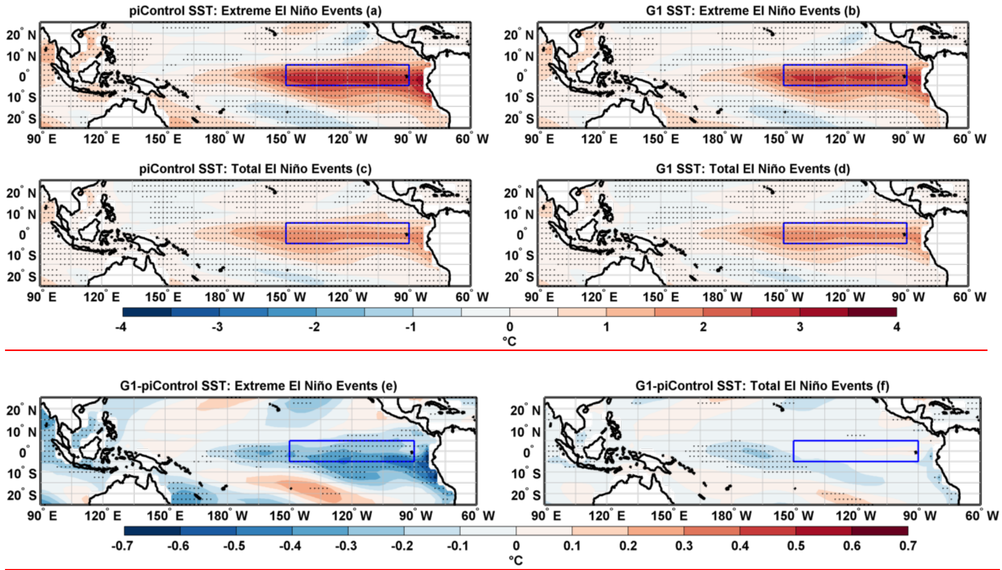

Figure ~~8~~9. Composites of SST anomalies for extreme El Niño events in (a) piControl and (b) G1. Composites of SST anomalies for the total number of El Niño events in (c) piControl and (d) G1. Composite differences (G1-piControl) of SST anomalies for (e) extreme El Niño events and (f) total number of El Niño events. Stipples indicate grid points with statistical significance at ~~90~~99 % cl using a non-parametric Wilcoxon rank~~-~~-sum test. The blue box in the eastern Pacific identifies the Niño3 region.

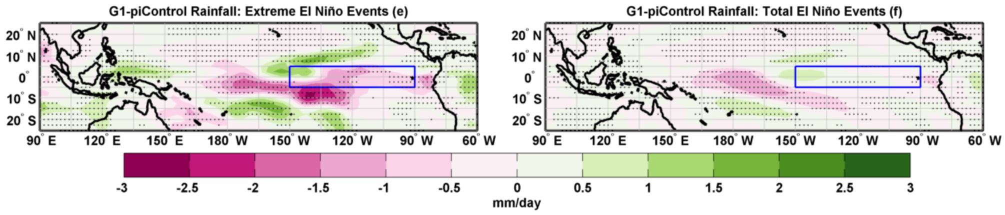
G1-piControl Rainfall: Extreme El Niño Events (e)
G1-piControl Rainfall: Total El Niño Events (f)
mm/day

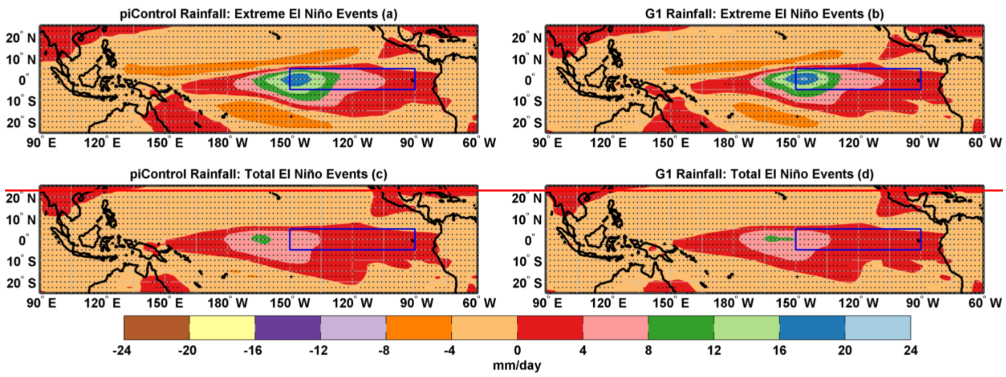
piControl Rainfall: Extreme El Niño Events (a)
G1 Rainfall: Extreme El Niño Events (b)
piControl Rainfall: Total El Niño Events (c)
G1 Rainfall: Total El Niño Events (d)
mm/day

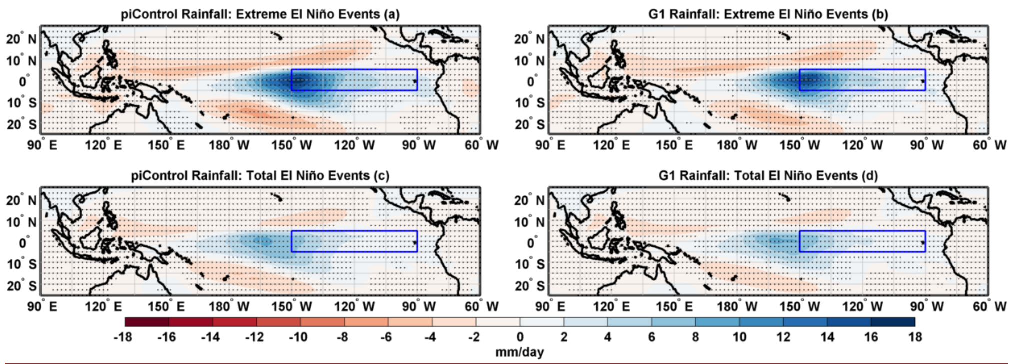
piControl Rainfall: Extreme El Niño Events (a)
G1 Rainfall: Extreme El Niño Events (b)
piControl Rainfall: Total El Niño Events (c)
G1 Rainfall: Total El Niño Events (d)
mm/day

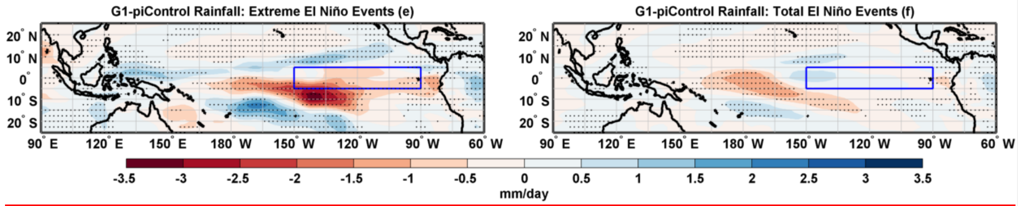

Figure ~~9~~10. Composites of rainfall anomalies for extreme El Niño events in (a) piControl and (b) G1. Composites of rainfall anomalies for the total number of El Niño events in (c) piControl and (d) G1. Composite differences (G1-piControl) of rainfall anomalies for (e) extreme El Niño events and (f) total number of El Niño events. Stipples in a-d and f (e) indicate grid points with statistical significance at ~~90~~99 (95) % cl using a non-parametric Wilcoxon rank~~-~~-sum test. The blue box in the eastern Pacific identifies the Niño3 region.

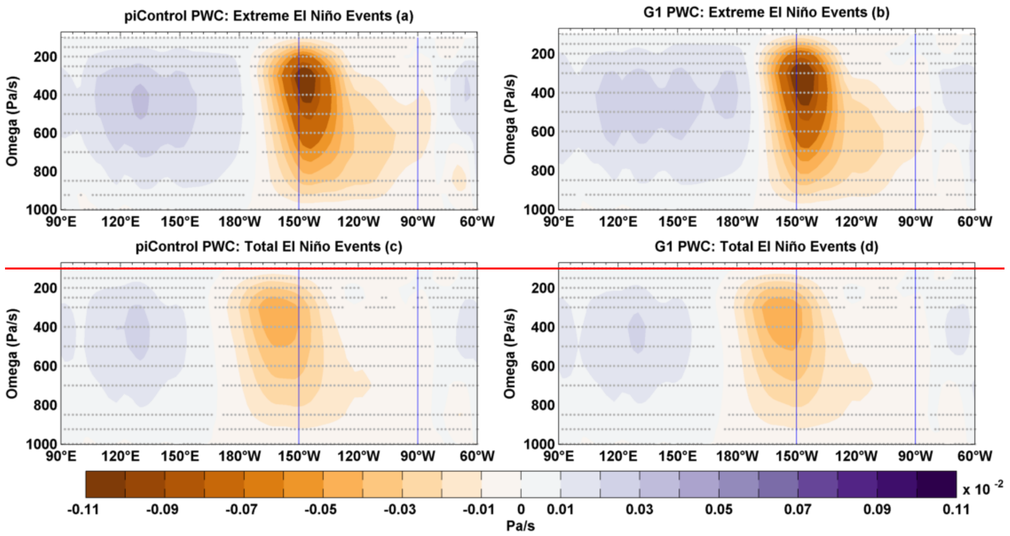
piControl PWC: Extreme El Niño Events (a)
G1 PWC: Extreme El Niño Events (b)
piControl PWC: Total El Niño Events (c)
G1 PWC: Total El Niño Events (d)
Omega (Pa/s)
200
400
600
800
1000
90°E 120°E 150°E 180°W 150°W 120°W 90°W 60°W
x 10 -2
-0.11 -0.09 -0.07 -0.05 -0.03 -0.01 0 0.01 0.03 0.05 0.07 0.09 0.11
Pa/s

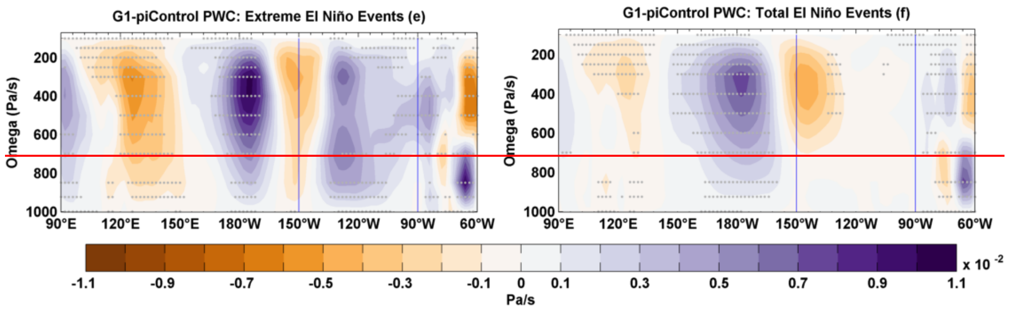
G1-piControl PWC: Extreme El Niño Events (e)
G1-piControl PWC: Total El Niño Events (f)
Omega (Pa/s)
200
400
600
800
1000
90°E 120°E 150°E 180°W 150°W 120°W 90°W 60°W
x 10 -2
-1.1 -0.9 -0.7 -0.5 -0.3 -0.1 0 0.1 0.3 0.5 0.7 0.9 1.1
Pa/s

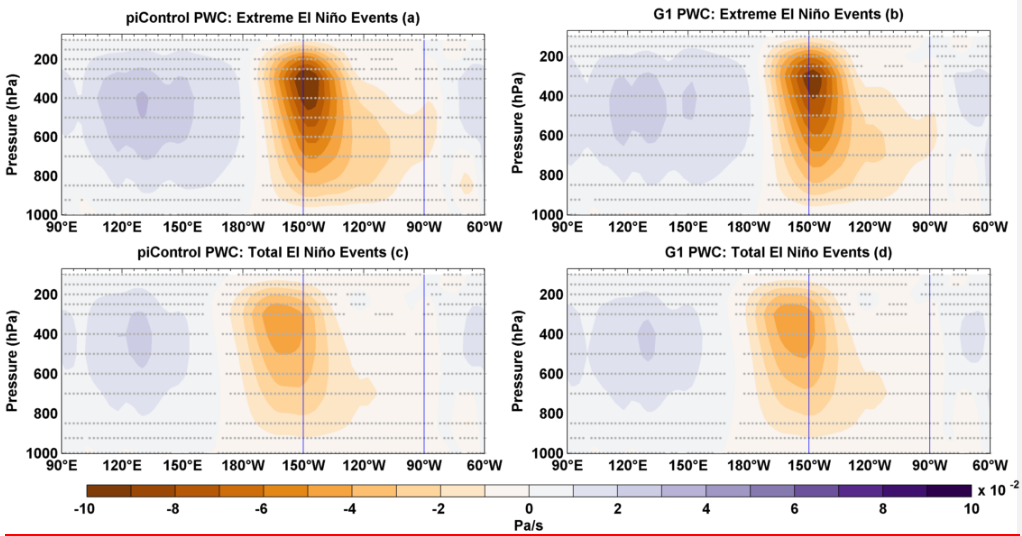
piControl PWC: Extreme El Niño Events (a)
G1 PWC: Extreme El Niño Events (b)
piControl PWC: Total El Niño Events (c)
G1 PWC: Total El Niño Events (d)
Pressure (hPa)
200
400
600
800
1000
90°E 120°E 150°E 180°W 150°W 120°W 90°W 60°W
x 10 -2
-10 -8 -6 -4 -2 0 2 4 6 8 10
Pa/s

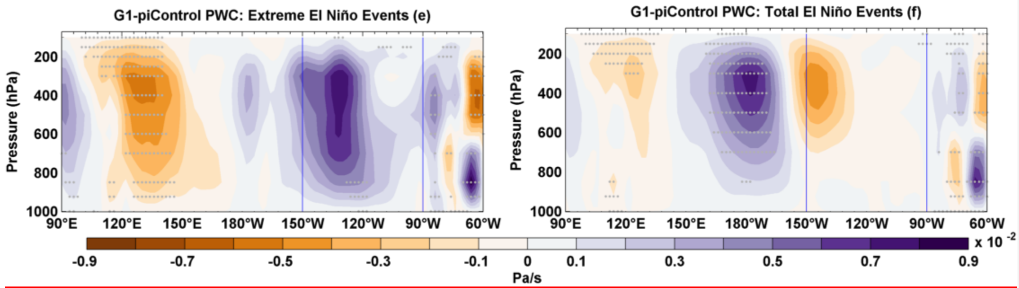

Figure ~~10~~11. Composites of PWC anomalies for extreme El Niño events in (a) piControl and (b) G1.

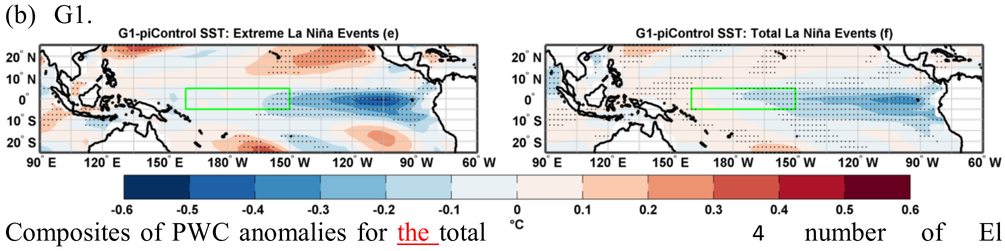

Composites of PWC anomalies for the total number of El Niño events in (c) piControl and (d) G1. Composite differences (G1-piControl) of PWC for (e) extreme El Niño events and (f) total number of El Niño events. Stipples indicate grid points with statistical significance at ~~90~~99 % cl using a non-parametric Wilcoxon rank~~-~~-sum test. The ~~box indicates~~blue vertical lines indicate the ~~Niño4~~Niño3 region.

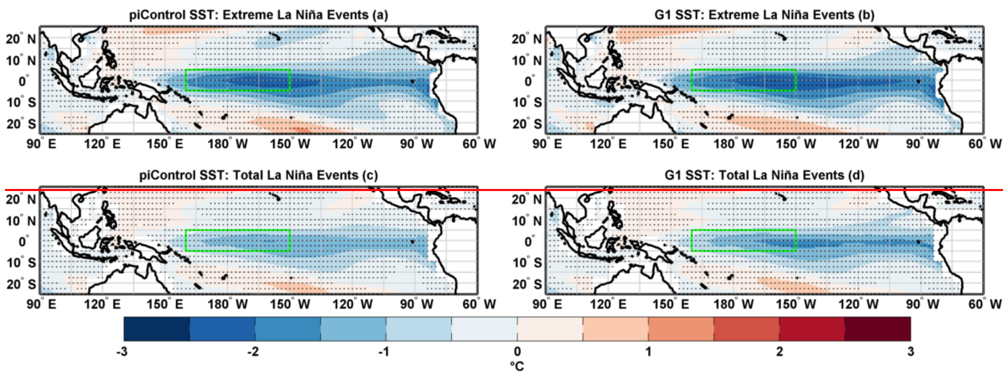

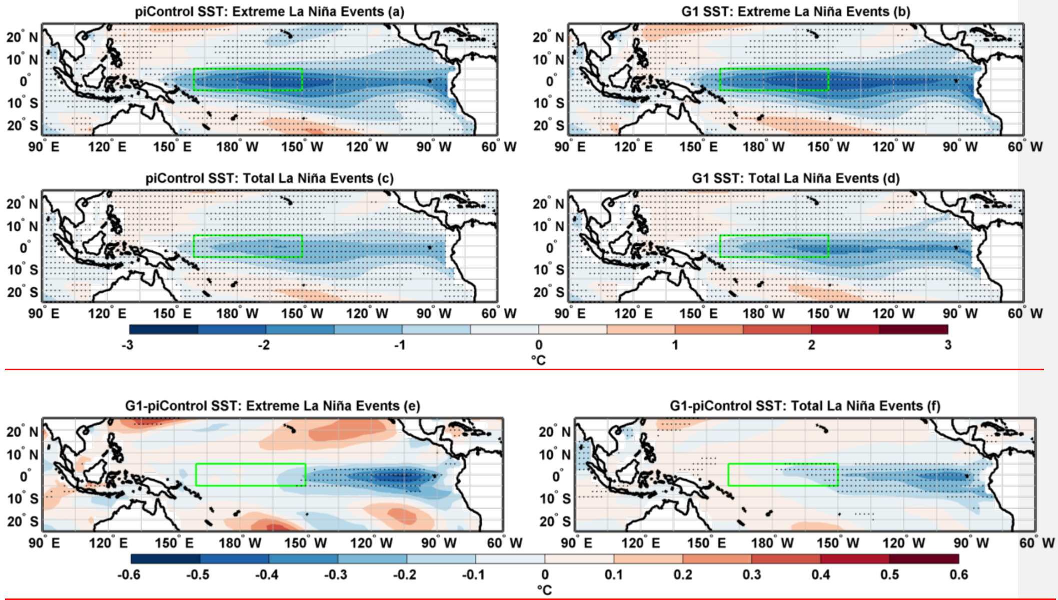

Figure ~~11~~12. Composites of SST anomalies for extreme La Niña events in (a) piControl and (b) G1. Composites of SST for the total number of La Niña events in (c) piControl and (d) G1. Composite differences (G1-piControl) of SST for (e) extreme La Niña events and (f) the total number of La Niña events. Stipples indicate grid points with statistical significance at ~~90~~99 % cl using a non-parametric Wilcoxon rank~~-~~-sum test. The green box indicates the Niño4 region.

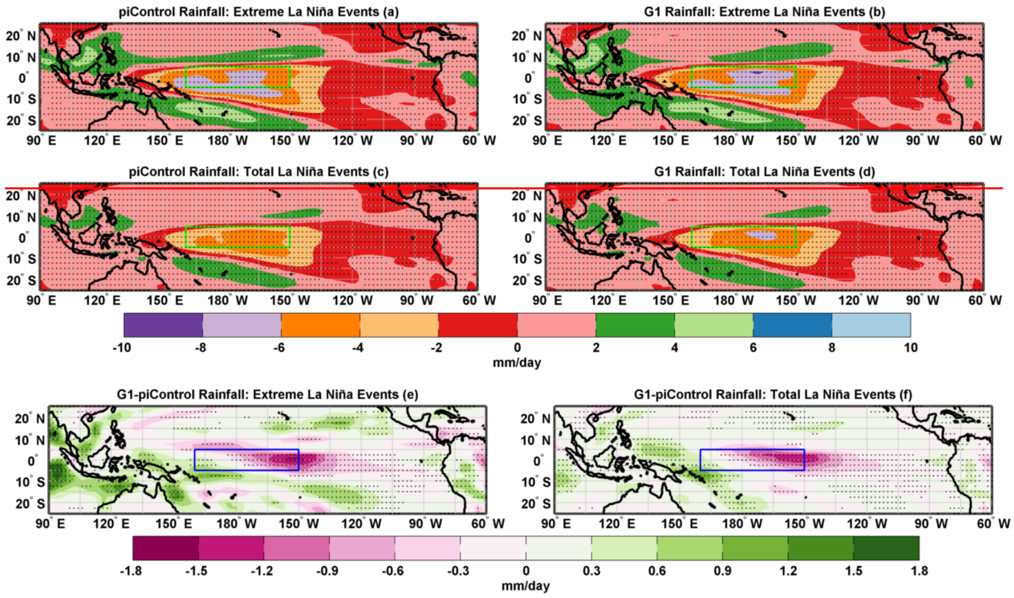

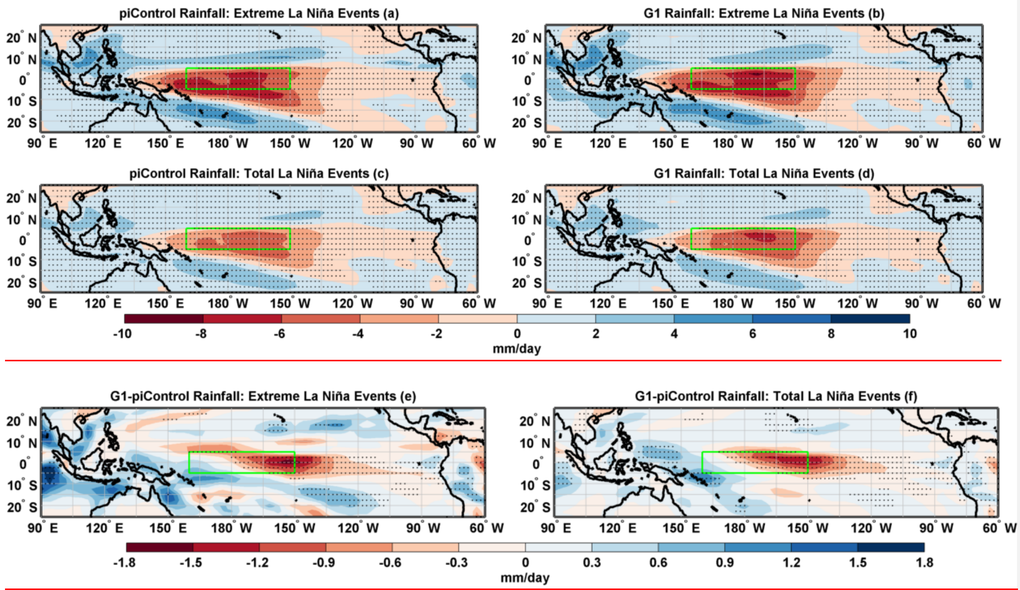

Figure ~~12~~13. Composites of rainfall anomalies for extreme La Niña events in (a) piControl and (b) G1. Composites of rainfall anomalies for the total number of La Niña events in (c) piControl and (d) G1. Composite differences (G1-piControl) of rainfall for (e) extreme La Niña events and (f) the total number of La Niña events. Stipples indicate grid points with statistical significance at ~~90~~99 % cl using a non-parametric Wilcoxon rank~~-~~-sum test. The green box indicates the Niño4 region.

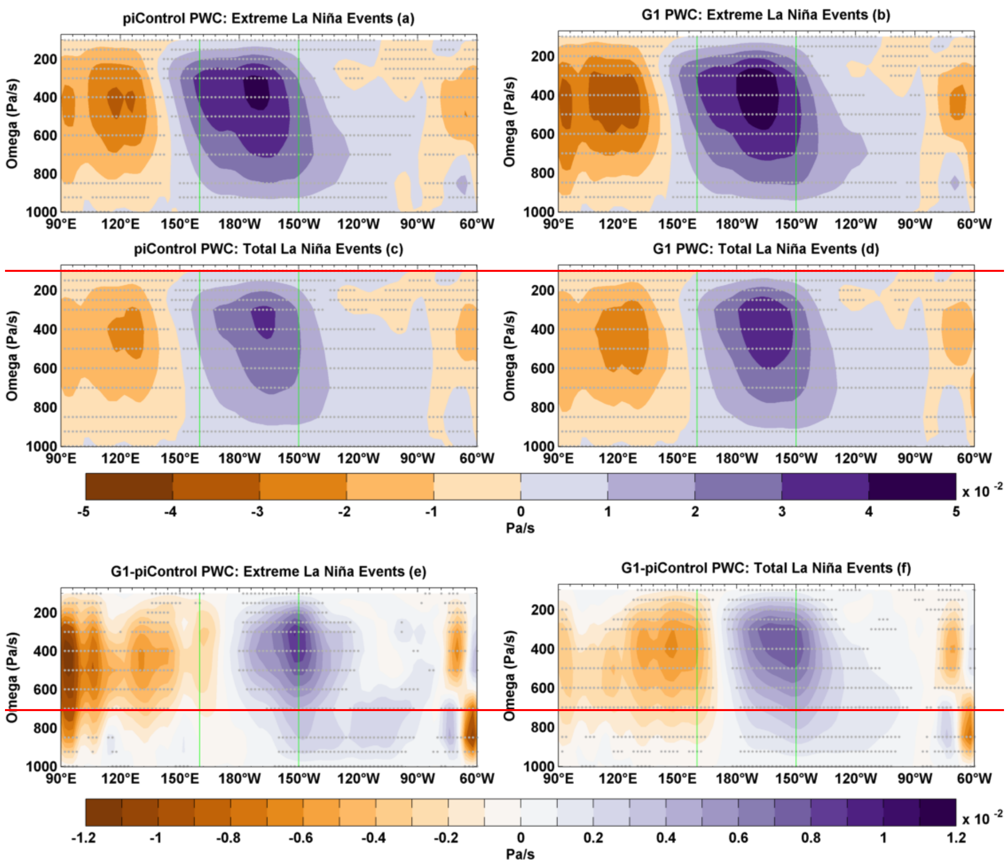

piControl PWC: Extreme La Niña Events (a)
G1 PWC: Extreme La Niña Events (b)
piControl PWC: Total La Niña Events (c)
G1 PWC: Total La Niña Events (d)
G1-piControl PWC: Extreme La Niña Events (e)
G1-piControl PWC: Total La Niña Events (f)
Omega (Pa/s)
200
400
600
800
1000
90°E
120°E
150°E
180°W
150°W
120°W
90°W
60°W
-5
-4
-3
-2
-1
0
1
2
3
4
5
x 10 -2
Pa/s
-1.2
-1
-0.8
-0.6
-0.4
-0.2
0
0.2
0.4
0.6
0.8
1
1.2
x 10 -2
Pa/s

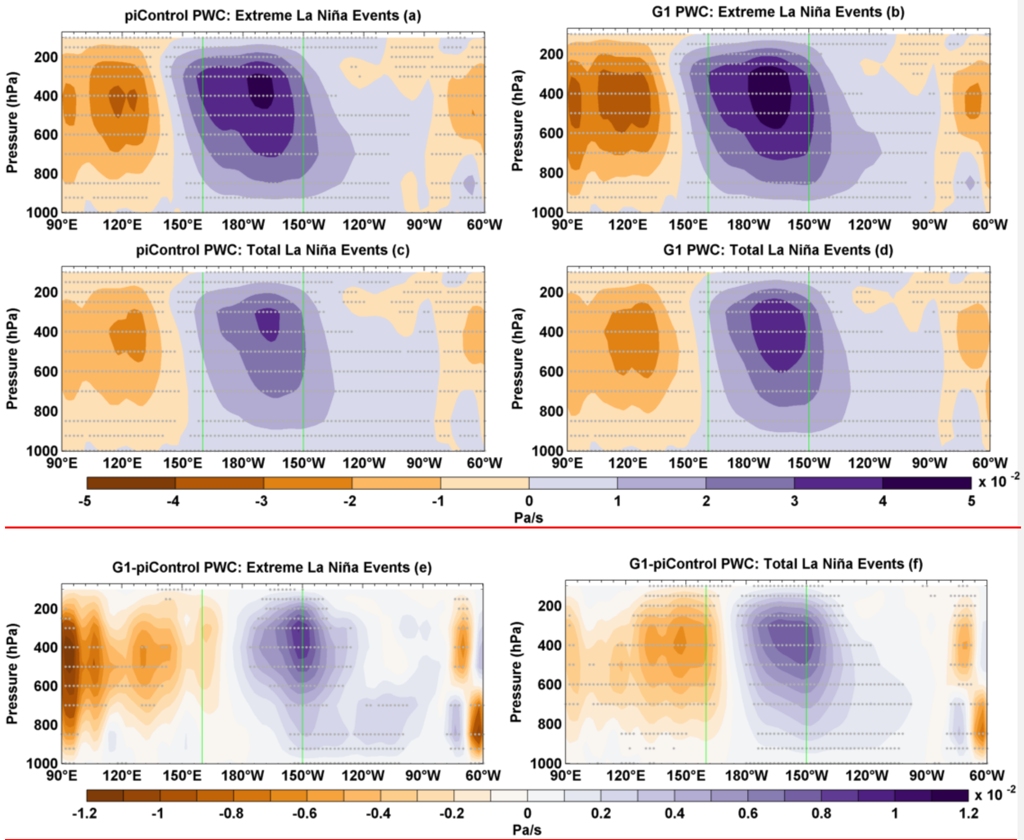

Figure ~~13~~14. Composites of PWC anomalies for extreme La Niña events in (a) piControl and (b) G1. Composites of PWC for the total number of La Niña events in (c) piControl and (d) G1. Composite differences (G1-piControl) of PWC anomalies for (e) extreme La Niña events and (f) the total number of La Niña events. Stipples indicate grid points with statistical significance at ~~90~~99 % cl using a non-parametric Wilcoxon rank~~-~~-sum test. The green vertical lines indicate the Niño4 region.

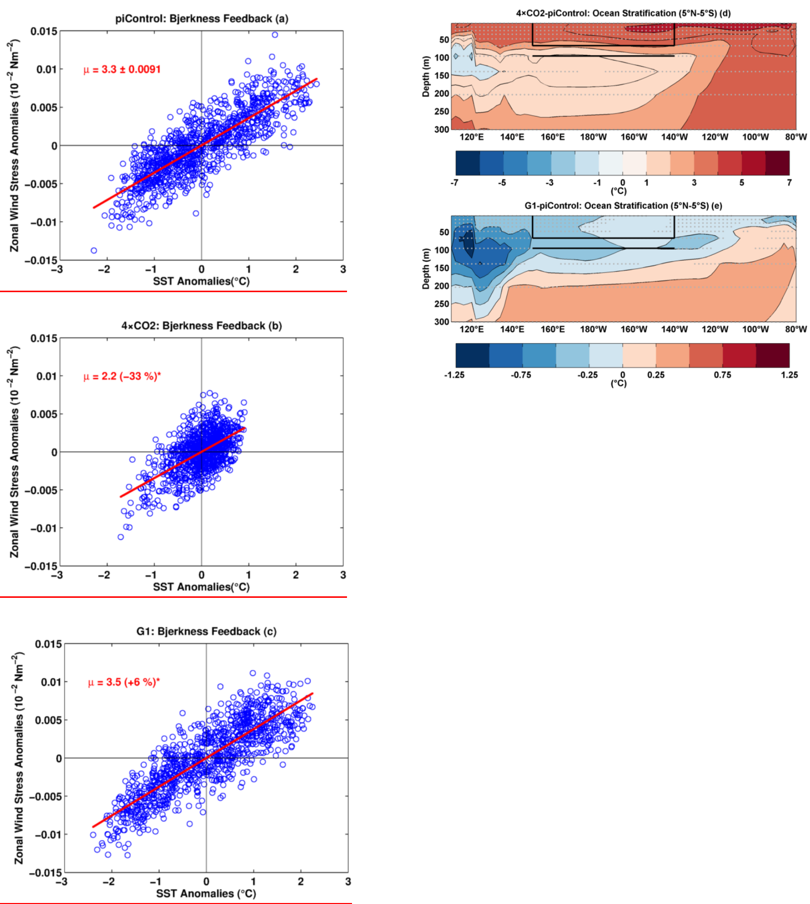

Figure 15. BJ feedback (μ; 10^{-2} $Nm^{-2}/^{o}C$) for (a) piControl (b) 4×CO_2, and (c) G1. The value with ± sign indicates s.d. of μ after 10,000 bootstrap realizations. An asterisk indicates statistical significance at 99 % cl. Mean change in ocean temperature, (d) 4×CO_2-piControl, and (e) G1-piControl. The black box shows the area averaging region for upper ocean temperature, and the black line shows the lower layer used for calculation of stratification as a difference of upper and lower layer. Stipples indicate grid points with statistical significance at 99 % cl using a non-parametric Wilcoxon rank-sum test.

Tables and Table Captions

Table 1. Eastern Pacific ENSO amplitude

Experiment	**Amplitude (°C)**	**Difference w.r.t. piControl (°C)**	**Std. Dev. 10,000 Realizations (°C)**	**~ Change w.r.t. piControl (%)**
piControl	1.04 ~~(0.78)~~ [1.~~04~~03]		0.0213 ~~(~~[0.~~0132)~~ ~~[0.0176~~03]	
4×CO_2	0.55 ~~(~~ [0.~~28)~~ ~~[0.49~~85]	-0.49 ~~(-~~ [-0.~~50) [-~~ ~~0.55~~18]		-47* ~~(-64*) [-55~~ [-17*]
G1	1.13 ~~(0.79)~~ [1.~~09~~13]	0.09 ~~(~~ [0.~~01)~~ ~~[0.05~~1]		+~~8* (+1) [+59*~~ [+10**]

Key: Niño3 ~~(Niño4) [Niño3.4~~ [E-Index]; *99 % cl; **95 % cl

Table 2. Central Pacific ENSO amplitude

Experiment	**Amplitude (°C)**	**Difference w.r.t. piControl (°C)**	**Std. Dev. 10,000 Realizations (°C)**	**~ Change w.r.t. piControl (%)**
piControl	(0.78) [0.85]		(0.0132) [0.0167]	
4×CO_2	(0.28) [0.53]	(-0.50) [-0.32]		(-64*) [-38*]
G1	(0.79) [0.83]	(0.01) [0.03]		(+1) [-3]

Key: (Niño4) [C-Index]; *99 % cl; **95 % cl

Table 3. Maximum amplitude of warm events

Experiment	**Amplitude (°C)**	**Difference w.r.t. piControl (°C)**	**Std. Dev. 10,000 Realizations (°C)**	**~ Change w.r.t. piControl (%)**
piControl	2.97 ~~(1.32) [2.34~~ [4.59]		0.0687 ~~(~~ [0.~~0159)~~ ~~[0.03672~~342]	
4×CO_2	1.29 ~~(0.92)~~ ~~[1.08~~[3.65]	-1.68 ~~(-~~ [-0.~~40) [-~~ ~~1.26~~94]		-57* ~~(-30*) [-54~~ [-21*]
G1	2.85 ~~(1.17) [2.18~~ [4.33]	-0.12 ~~(-~~ [-0.~~15) [-~~ ~~0.16~~26]		-4 ~~(-11*) [-7*]~~ [-6]

Key: Niño3 ~~(Niño4) [Niño3.4~~ [E-Index]; *99 % cl; **95 % cl

Table ~~3~~4. Maximum amplitude of cold events

Experiment	**Amplitude (°C)**	**Difference w.r.t. piControl (°C)**	**Std. Dev. 10,000 Realizations (°C)**	**~ Change w.r.t. piControl (%)**
piControl	~~-2.31~~ (-2.13) [-2.~~42~~47]		~~0.1439~~ (0.0459) [0.1452]	
4×CO_2	~~-1.86~~ (-1.37) [-~~1.91~~2.17]	~~0.45 (~~(-0.76) ~~[~~[-0.~~51~~30]		~~-19*~~ (-36*) [-~~21~~12*]
G1	~~-2.26~~ (-2.55) [-2.~~62~~90]	~~0.05 (-~~ (0.42) ~~[-~~ [0.~~20~~43]		~~-2~~ (+20*) [+~~8]~~17*]

Key: ~~Niño3~~ (Niño4) ~~[Niño3.4~~ [C-Index]; *99 % cl; **95 % cl

Formatted: Line spacing: single

Formatted: Line spacing: single

Formatted: Line spacing: single

Formatted: Line spacing: single

Formatted: Line spacing: single

Formatted: Font: 10 pt, Not Bold

Table 45. Niño3 SST skewness

Experiment	Skewness	Difference w.r.t. piControl	Std. Dev. 10,000 Realizations	~ Change w.r.t. piControl (%)
piControl	0.52*		0.0542	
4×CO_2	-0.47*	-0.99		-190*
G1	0.18*	-0.34		-65*

Key: *99 % cl; **95 % cl

Point-by-Point Listing of Response to Referee Comments

The authors thank the referees for their comments and suggestions, which have greatly helped us to improve our manuscript. Below, we reply point-by-point, highlighting the changes we have implemented. The primary concern of the referees was the evaluation of the climate model capability to simulate ENSO variability, and the lack of detailed explanations on possible mechanisms responsible for changes in ENSO both under $4{\times}CO_2$ and solar geoengineering (G1). In the revised manuscript, we therefore put a strong emphasis on model evaluation and are able to confirm the necessary model skill (section 2.4). We also provide an entirely new section (section 4) on possible mechanisms behind the changes in ENSO extremes and ENSO amplitudes.

Referee #1

Major Points

1)

It is not clear exactly why the modeled ENSO changed from 4xCO2 to G1 in this model? Is it because of the air-sea heat fluxes act more less as a damping in the eastern equatorial Pacific associated with the mean state change in G1? More interestingly, why G1 does not recover many of the climatic states of piControl? Initial thought would be the ocean state never fully recovers. But as stated in the paper the change in thermocline depth is not statistically different between G1 and piControl. I don't think I came across a plot of subsurface temperature, e.g., depth-longitude differences between 4xCO2 and G1 vs piControl. Perhaps while the thermocline depth statistics do not change, there are still changes in the subsurface ocean temperatures in certain areas.

In the revised manuscript, we have calculated ENSO feedbacks, Bjerknes and heat flux, and ocean stratification to explain the mechanisms for change in ENSO. We have added Section 4 elaborating on the mechanism for change in ENSO under both 4xCO_2 and G1. (See section 4, from page 17 and line 1 to page 18 and line 29). Specifically we write:

4 Mechanisms behind the changes in ENSO variability

4.1 Under greenhouse gas forcing

The reduced ENSO amplitude under 4×CO_2 is mainly caused by stronger hf and weaker BJ feedback relative to piControl (Fig. 15a-b, and Table S5-6). More rapid warming over the eastern than western equatorial Pacific regions reduces the SST asymmetry between western and eastern Pacific (Fig. 1d), resulting in the weakening of ZSSTG (Fig. 4b) that significantly weakens the zonal winds stress (Fig. 4a) and hence PWC (Fig. 6b, d, see Bayr et al., 2014). The overall reduction of zonal wind stress reduces the BJ feedback, which, in turn, can weaken the ENSO amplitude. Climate models show an inverse relationship between hf feedback and ENSO amplitude (Lloyd et al., 2009, 2011; Kim and Jin 2011b). The increased hf feedback might be the result of enhanced clouds due to strengthened convection (Fig. 5b, d) and stronger evaporative cooling in response to enhanced SSTs under 4×CO_2 (Knutson and Manabe 1994; Kim and Jin 2011b). Kim and Jin (2011a, b) found intermodel consensus on the strengthening of hf feedback in CMIP3 models under enhanced GHG warming scenario (Ferret and Collins 2019). Further, we see increased ocean stratification under 4×CO_2 (Fig. 15d and Table S7). A more stratified ocean is associated with an increase in both the El Niño events and amplitude in the eastern Pacific (Wang et al. 2020). It can also modify the balance between feedback processes (Dewitte et al., 2013). Enhanced stratification may also cause negative temperature anomalies in the central to the western Pacific through changes in thermocline tilt (Dewitte et al., 2013). Since the overall ENSO amplitude decreases in our 4xCO_2 simulation, we, thus, conclude that the ocean stratification mechanisms cannot be the dominant factor here, but that hf and BJ feedbacks must more than cancel out the effect of ocean stratification on ENSO amplitude.

The increased frequency of extreme El Niño events under 4×CO_2 is due to change in the mean position of the ITCZ (Fig. S2), causing frequent reversals of MSSTG (Fig. S3), and eastward extension of the western branch of PWC (Fig. 6), which both result in increased rainfall over the eastern Pacific (see Wang et al. 2020). This is due to greater east equatorial than off-equatorial Pacific warming (see Cai et al. 2020), which shifts the mean position of ITCZ towards the equator (Fig. S2). Simultaneously more rapid warming of the eastern than western equatorial Pacific reduces the ZSSTG, and hence zonal wind stress, as also evident from the weakening and shift of the PWC (Fig. 6) and increased instances of negative ZSSTG anomalies (Fig. S9). Ultimately, this leads to more frequent vigorous convection over the Niño3 region (Fig. 5d), and enhanced rainfall (Fig. 2d, S8). Therefore, despite the weakening of the ENSO amplitude under 4×CO_2, rapid warming of the eastern equatorial Pacific causes frequent reversals of meridional and zonal SST gradients, resulting in an increased frequency of extreme El Niño events (see also Cai et al., 2014; Wang et al., 2020).

We note that under GHG forcing, HadCM3L does not simulate an increase in the frequency of extreme La Niña events as found by Cai et al. (2015b) using CMIP5 models. However, it does show an increase in the total number of La Niña events (Table S4). In a multimodel ensemble mean, Cai et al. (2015b) found that the western Pacific warms more rapidly than the central Pacific under increased GHG forcing, resulting in strengthening of the zonal SST gradient between these two regions. Strengthening of this zonal SST gradient and increased vertical upper ocean stratification provide conducive conditions for increased frequency of extreme La Niña events (Cai et al., 2015b). One reason why we do not see an increase in the frequency of central Pacific extreme La Niña events might be that HadCM3L does not simulate more rapid warming of the western Pacific compared to the central Pacific as noticed by Cai et al. (2015b) (compare our Fig. 1d with Fig. 3b in Cai et al., 2015b), hence, as stronger zonal SST gradient does not develop, across the equatorial Pacific, as needed for extreme La Niña events to occur (see Fig. S9a, c and S10).

4.2 Under solar geoengineering

G1 over cools the upper ocean layers, whereas the GHG-induced warming in the lower ocean layers is not entirely offset, thus increasing ocean stratification (Fig. 15). The increased stratification boosts atmosphere-ocean coupling (see Cai et al., 2018), which favours enhanced westerly wind bursts (Fig. 4a) (e.g., Capotondi et al., 2018) to generate stronger SST anomalies over the eastern Pacific (Wang et al. 2020). The larger cooling of the western Pacific than the eastern Pacific can also enhance westerly wind bursts reinforcing the BJ feedback and hence SST anomalies in the eastern Pacific. We conclude that increased ocean stratification, along with stronger BJ feedback, is the most likely mechanism behind the overall strengthening of ENSO amplitude under G1.

The increased frequency of extreme El Niño events under G1 can be linked to the changes in MSSTG and ZSSTG (see Cai et al., 2014, and Fig. S3, S9). The eastern off-equatorial Pacific cools more than the eastern equatorial regions, providing relatively more conducive conditions for convection to occur through a shift of ITCZ over to the Niño3 region (Fig. 1e). At the same time, the larger cooling of the western equatorial Pacific than of the eastern equatorial Pacific reduces the ZSSTG and convective activity over the western Pacific, which leads to a weakening of the western branch of PWC (Fig. 6e). Hence we see reduced rainfall over the western Pacific and enhanced rainfall from the Niño3 to the central Pacific region (Fig 2e). These mean state changes, strengthening of convection between ~140^o W and ~150^o E, and more reversals of the MSSTG and ZSSTG (Fig. S3) result in an increased number of extreme El Niño events in G1 than in piControl (Fig. 7).

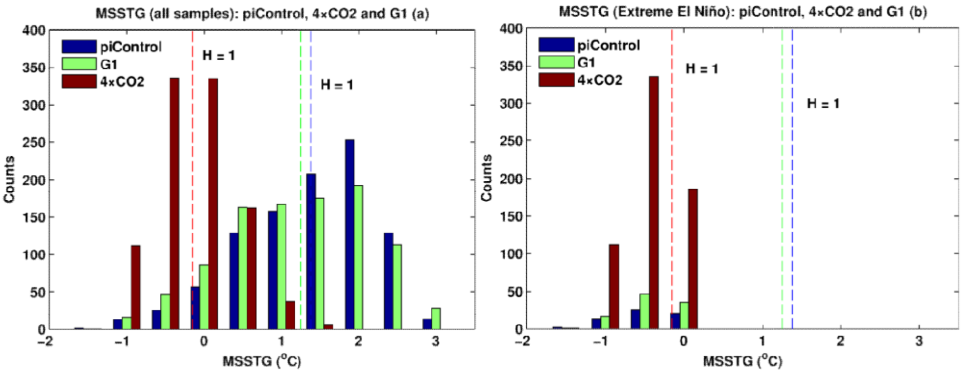

Figure S3. Histogram of MSSTG for piControl, 4×CO_2, and G1 for all samples (a) and for extreme El Niño events. The values are plotted at the centre of each bin with an interval of 0.5 ^{o}C. Blue, red, and green vertical lines indicate climatological mean values of MSSTG under piControl (1.38 ^{o}C), 4×CO_2 (-0.15 ^{o}C), and G1 (1.25 ^{o}C), respectively. H = 1 indicates that the shift in the mean is statistically significant at 99 % cl using a non-parametric Wilcoxon rank-sum test.

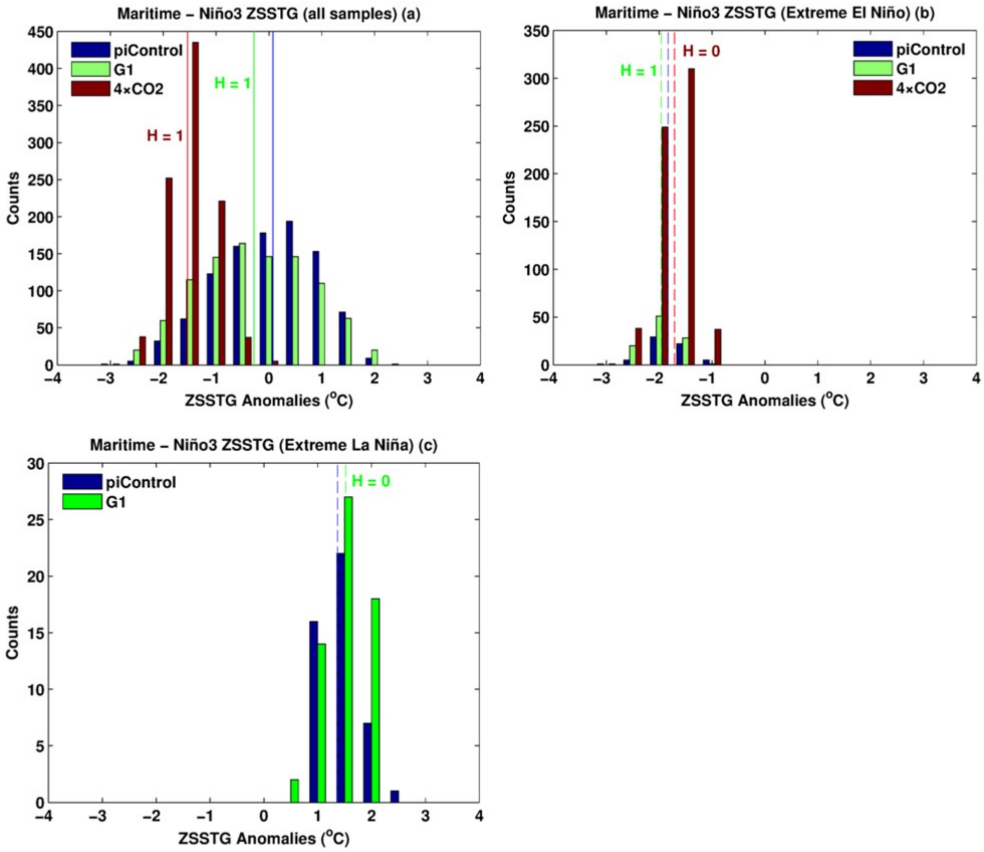

Figure S9. *Histogram of ZSSTG anomalies for (a) all samples, (b) extreme El Niño events only, and (c) extreme La Niña events only. The values are plotted at the centre of each bin with an interval of 0.5 ^oC. In a blue, red, and green solid vertical lines indicate climatological median ZSSTG under piControl (0.07 ^oC), 4×CO_2 (-1.54 ^oC), and G1 (-0.28 ^oC), respectively, for all samples. In b, blue, red, and green dashed vertical lines indicate climatological median ZSSTG under piControl (-1.83 ^oC), 4×CO_2 (-1.71 ^oC), and G1 (-1.96 ^oC), respectively, for extreme El Niño events. In c, blue, and green dashed vertical lines indicate climatological median ZSSTG under piControl (1.37 ^oC) and G1 (1.52 ^oC), respectively, for extreme La Niña events. H = 1 indicates that using a non-parametric Wilcoxon rank-sum test, the shift in the median is statistically significant at 99 (95) % cl in a (b). H = 0 means that the shift in the median is not statistically significant. The ZSSTG is defined as the difference between SST in the Maritime continent (5^o N-5^o S; 100^o E-126^o E) and eastern equatorial Pacific (Niño3 region: 5^o N-5^o S, 150^o W-90^{o}W). The anomalies are calculated relative to piControl.*

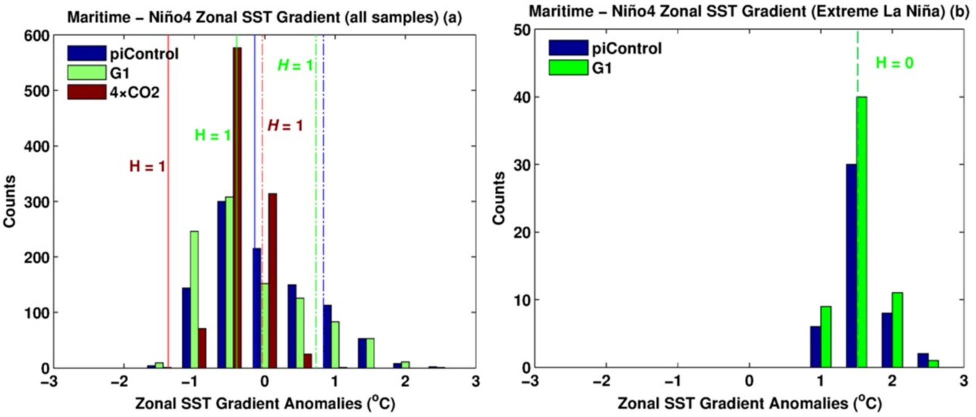

Figure S10. *Histogram of ZSSTG anomalies for (a) all samples and (b) extreme La Niña events only. The values are plotted at the centre of each bin with an interval of 0.5 °C. Blue, red, and solid green lines indicate climatological median ZSSTG under piControl (-0.14 °C), 4×CO_2 (-1.37 °C), and G1 (-0.40 °C), respectively, for all samples. Blue, red, and green dash-dotted lines indicate climatological median ZSSTG under piControl (0.84 °C), 4×CO_2 (-0.03 °C), and G1 (0.72 °C), respectively, for all La Niña events. In b, blue, red, and green dashed lines indicate climatological median ZSSTG under piControl (1.52 °C) and G1 (3.35 °C), respectively, for extreme La Niña events. H = 1 indicates that the shift in the median is statistically significant at 99 % cl using the non-parametric Wilcoxon rank-sum test. The ZSSTG is defined as the difference between SST in the Maritime continent (5° N-5° S; 100° E-126° E) and central equatorial Pacific (Niño4 region: 5° N-5° S, 160° E-150° W) (Cai et al., 2015). The anomalies are calculated relative to piControl.*

Table S5. Mean DJF Heat Flux (hf) Feedback

Experiment	hf feedback or Damping Coefficient ($Wm^{-2}/^{o}C$)	Difference w.r.t. piControl ($Wm^{-2}/^{o}C$)	Std. Dev. 10,000 Realizations ($Wm^{-2}/^{o}C$)	~ Change w.r.t. piControl (%)
ERA5	-14.59			
piControl	-14.70		0.52	
4×CO_2	-21.90	+7.19		+48*
G1	-14.85	+0.15		+1.0

*99% cl; **95% cl; Calculation period: ERA5 (41-yrs); HadCM3L (990-yrs)

Table S6. Mean DJF Bjerknes (BJ) Feedback

Experiment	BJ feedback (10^{-2} $Nm^{-2}/^{o}C$)	Difference w.r.t. piControl (10^{-2} $Nm^{-2}/^{o}C$)	Std. Dev. 10,000 Realizations ($Wm^{-2}/^{o}C$)	~ Change w.r.t. piControl (%)
ERA5	3.3			
piControl	3.3		0.0091	
4×CO_2	2.2	-1.1		-33*
G1	3.5	+0.2		+6*

*99% cl; **95% cl; Calculation period: ERA5 (41-yrs); HadCM3L (990-yrs)

Table S7. Mean DJF Ocean Stratification

Experiment	Stratification (°C)	Difference w.r.t. piControl (°C)	Std. Dev. 10,000 Realizations (°C)	~ Change w.r.t. piControl (%)
piControl	2.28*		0.0331	
4×CO_2	5.06*	+2.78		+122*
G1	2.37*	+0.09		+4**

*99% cl; **95% cl

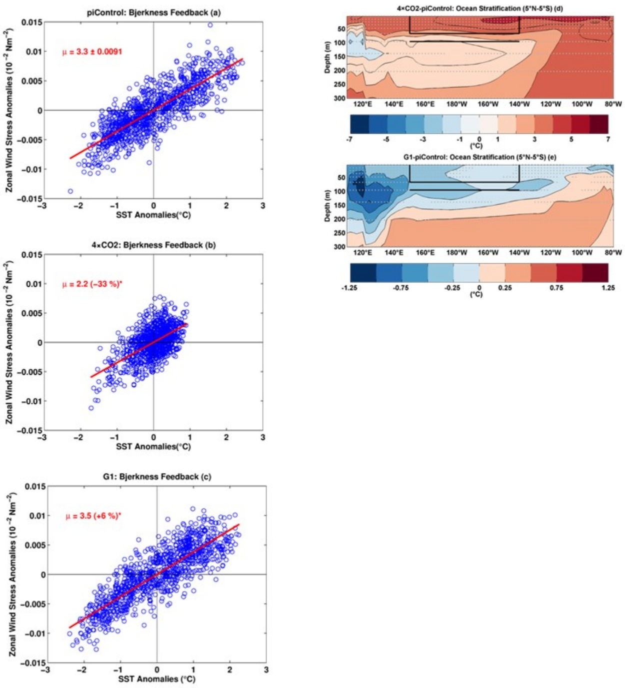

Figure 15. BJ feedback (μ; 10^{-2} $Nm^{-2}/^{o}C$) for (a) piControl (b) 4×CO_2, and (c) G1. The value with ± sign indicates s.d. of μ after 10,000 bootstrap realizations. An asterisk indicates statistical significance at 99 % cl. Mean change in ocean temperature, (d) 4×CO_2-piControl, and (e) G1-piControl. The black box shows the area averaging region for upper ocean temperature, and the black line shows the lower layer used for calculation of stratification as a difference of upper and lower layer. Stipples indicate grid points with statistical significance at 99 % cl using a non-parametric Wilcoxon rank-sum test.

In the Discussion and conclusion (section 5, page 19, lines 1-14), we have added the following paragraph:

To conclude, solar geoengineering can compensate many of the GHG-induced changes in the tropical Pacific, but, importantly, not all of them. In particular, controlling the downward shortwave flux cannot correct one of the climate system's most dominant modes of variability, i.e., ENSO, wholly back to preindustrial conditions. The ENSO feedbacks (Bjerkness and heat flux) and more stratified ocean temperatures may induce ENSO to behave differently under G1 than under piControl and 4×CO_2. Different meridional distributions of shortwave and longwave forcings (e.g., Nowack et al., 2016) resulting in the surface ocean overcooling, and residual warming of the deep ocean are the plausible reasons for the solar geoengineered climate not reverting entirely to the preindustrial state. However, we note that this is a single model study, and more studies are needed to show the robustness and model-dependence of any results discussed here, e.g. using long-term multimodel ensembles from GeoMIP6 (Kravitz et al., 2015), once the data are released. The long-term Stratospheric Aerosol Geoengineering Large Ensemble (GLENS; Tilmes et al., 2018) data can also be explored to investigate ENSO variability under geoengineering.

2)

Nonetheless this leads to the question: How large are the differences in mean state and ENSO statistics between G1 and piControl state in comparison to the internal variability in piControl? For example P9, L20-21: the reduction in MSSTG is 9% in G1, is this substantial compared internal variability in piControl and to that seen during an El Nino?

We have shown that the 9 % change in MSSTG under G1 is statistically significant (99 % confidence level) relative to piControl using both Bootstrap resampling and a non-parametric Wilcoxon rank-sum test. The increase in the frequency of extreme El Niño events is due to more frequent reversals of MSSTG (Fig. S3 and Table S2). In the revised manuscript, we have tested the change in frequency under both 4×CO_2 and G1, relative to piControl, first by using rainfall > 5 mm day^{-1} as a threshold for extreme El Niño events and then selecting only those events for which rainfall > 5 mm day^{-1} and MSSTG < 0. Both methods show a statistically significant increase in extreme El Niño events. Choosing extreme events having MSSTG < 0 assures that strong convection has established over the Niño3 region during the extreme. Further, we have shown the histograms of MSSTG for all samples and exclusively for extreme El Niño events, which indicate more frequent reversals of MSSTG both under 4×CO_2 and G1 relative to piControl. In the revised manuscript, we have incorporated the following changes:

Overall there is a change in sign and reduction of MSSTG in 4×CO_2 (~-111 %, 99 % cl) and only decrease in G1 (~-9 %, 99 % cl) (Fig. S3, and Table S2). (Section 3.1.4, page11, lines 17-19)

A threshold of detrended Niño3 total rainfall of 5 mm day^{-1} recognizes events as extremes even when the MSSTG is positive and stronger, especially under 4×CO_2, which plausibly means that ITCZ might not shift over the equator for strong convection to occur during such extremes. The El Niño event of 2015 is a typical example of such events. We test our results with a more strict criterion by choosing only those events as extremes, which have characteristics similar to that of 1982 and 1997 El Niño events (i.e., Niño3 rainfall > 5 mm day^{-1} and MSSTG < 0). We declare events having characteristics similar to that of the 2015 event as moderate El Niño events (Fig. S5). Based on this method, we find a robust increase in the number of extreme El Niño events both in 4×CO_2 (924 %) and G1 (61 %) at 99 % cl. (Section 3.2.2, page14, lines 26-34)

Table S2. Meridional SST Gradient (MSSTG)

Experiment	Mean (°C)	Difference w.r.t. piControl (°C)	Std. Dev. 10,000 Realizations (°C)	~ Change w.r.t. piControl (%)
piControl	1.38*		0.0265	
4×CO_2	-0.15*	-1.53		-111*
G1	1.25*	-0.13		-9*

Key: *99 % cl; **95 % cl

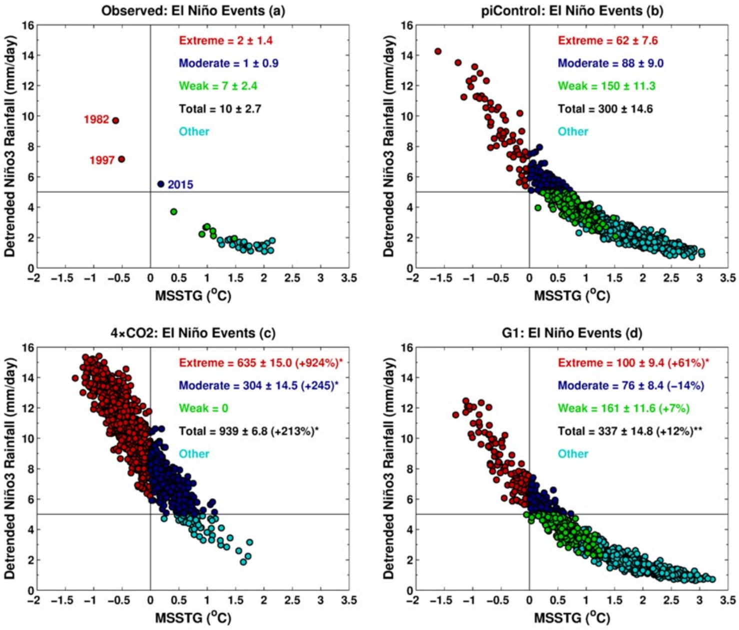

Figure S5. Relationship between MSSTG and quadratically detrended Niño3 rainfall for (a) observations (b) piControl (c) 4×CO_2, and (d) G1. The solid black horizontal line indicates a threshold of 5 mm day^{-1}. A single (double) asterisk indicates that the change in frequency, relative to piControl, is statistically significant at 99 % (95 %) cl. Numbers with a ± symbol indicate s.d. calculated with 10,000 bootstrap realizations. Following Cai et al. (2014), a non-ENSO related trend has been removed from the rainfall time series. Events are classified as: Extreme (Niño3 rainfall > 5 mm day^{-1} and MSSTG < 0), moderate (Niño3 rainfall > 5 mm day^{-1} and MSSTG > 0), weak (Standardized Niño3 SSTs > 0.5 °C and Niño3 rainfall < 5 mm day^{-1}), total is sum of extreme, moderate, and weak events.

3)

In many of the plots showing differences between experiments and piControl, the confidence level was set to 90%. Given the long time series of the model output, it should be increased to 95% or even 99%. This would perhaps show more regions in G1 where the differences are not significantly different from piControl.

All statistics have been recalculated either with a 95 % or 99 % confidence level. See the manuscript with tracked changes.

4)

The conclusion section could provide the reader with a little perspective on whether it is worth it to do the geoengineering solution in the context of projected increase in extreme ENSO activity. A relevant paper to help the discussion: Trenberth KE, Dai A 2007). Geophys Res Lett 34:L15702. doi: 10.1029/2007GL030524

In the revised manuscript (section 5, page 19, lines 1-14), we have included the following paragraphs/statements:

To conclude, solar geoengineering can compensate many of the GHG-induced changes in the tropical Pacific, but, importantly, not all of them. In particular, controlling the downward shortwave flux cannot correct one of the climate system's most dominant modes of variability, i.e., ENSO, wholly back to preindustrial conditions.

The ENSO feedbacks (Bjerkness and heat flux) and more stratified ocean temperatures may induce ENSO to behave differently under G1 than under piControl and $4\times CO_2$. Different meridional distributions of shortwave and longwave forcings (e.g., Nowack et al., 2016) resulting in the surface ocean overcooling, and residual warming of the deep ocean are the plausible reasons for the solar geoengineered climate not reverting entirely to the preindustrial state. However, we note that this is a single model study, and more studies are needed to show the robustness and model-dependence of any results discussed here, e.g. using long-term multimodel ensembles from GeoMIP6 (Kravitz et al., 2015), once the data are released. The long-term Stratospheric Aerosol Geoengineering Large Ensemble (GLENS; Tilmes et al., 2018) data can also be explored to investigate ENSO variability under geoengineering.

5)

P11, L36: Picking a result on one model sounds rather odd as we know that the change in ENSO amplitude varies widely across models (e.g., Collins et al. 2010). In a recent study by Cai et al. (2018, Nature, https://www.nature.com/articles/s41586-018-0776-9), however, there seems to be a stronger inter-model agreement on the increase in ENSO amplitude in models that are able to simulate ENSO flavors (see their Extended Data Fig. 8b), as implied in the PC1-PC2 space. So does the HadCM3L model capture the nonlinear relationship between PC1 and PC2 as observed? Here PC1 and PC2 refer to the first and second eigenmodes of tropical Pacific SST (see their Fig. 1). Also, it is relevant to discuss the results of Cai et al. (2018) in 1st paragraph of Page 3.

Regarding the change in amplitude, we refer to other studies in the revised manuscript and include the following paragraphs/statements:

Previous studies found that climate models produced mixed responses (both increases and decreases in amplitude) in terms of how ENSO amplitude change with global warming (see Latif et al. 2009; Collins et al. 2010; Vega-Westhoff and Sriver 2017). However, Cai et al. (2018) found an intermodel consensus, for models capable of reproducing ENSO diversity, for strengthening of ENSO amplitude under A2, RCP4.5, and RPC8.5 transient scenarios. (see section 3.2.1, page 13, lines 6-11)

We have included a separate section (2.4) under the title "ENSO representation in HadCM3L" which discusses the HadCM3L capability to simulate ENSO diversity as described by Cai et al. (2018). We have incorporated the following paragraphs/statements in the revised manuscript:

Before employing HadCM3L for studying ENSO variability under $4\times CO_2$, and G1, we evaluate its piControl simulation against present-day observational data. (see section 2.4, page 6, lines 40-41)

Further, we have included the following paragraphs (section 2.4, page 7, and line 14 to next page line 21):

In addition, we evaluate the ENSO modelled by HadCM3L following a principal component (PC) approach suggested by Cai et al. (2018). Considering distinct eastern and central Pacific ENSO regimes based on Empirical Orthogonal Function (EOF) analysis, they found that climate models capable of reproducing present-day ENSO diversity show a robust increase in eastern Pacific ENSO amplitude in a greenhouse warming scenario. Specifically, the approach assumes that any ENSO event can be represented by performing EOF analysis on monthly SST anomalies and combining the first two principal patterns (Cai et al., 2018). The first two PCs time series, PC1 and PC2, show a non-linear relationship in observational datasets (Fig. S1m). Climate models that do not show such a non-linear relationship cannot satisfactorily reproduce ENSO diversity, and hence are not sufficiently skilful for studying ENSO properties (Cai et al., 2018). Here, we perform EOF analysis on quadratically detrended monthly SST and wind stress anomalies of ERA5 and piControl over a consistent period of 41-year. We evaluate HadCM3L's ability to simulate two distinct ENSO regimes and the non-linear relationship between the first two PCs, i.e., $PC2(t) = \alpha[PC1(t)]^2 + \beta[PC1(t)]^2 + \gamma$ (Fig. S1). From ERA5, $\alpha = -0.36$ (statistically significant at 99 % confidence level, hereafter "cl") whereas in piControl $\alpha = -0.31$ (99 % cl), which is same as the mean $\alpha = -0.31$ value calculated by Cai et al. (2018) averaged over five reanalysis datasets. The 1st and 2nd EOF patterns of monthly SST and wind stress anomalies of piControl (Fig. S1 b, e) are comparable with that of ERA5 (Fig. S1 a, d). EOF1 of piControl shows slightly stronger warm *anomalies in the eastern equatorial Pacific, whereas negative anomalies over the western Pacific are slightly weaker compared to ERA5. In EOF1, the stronger wind stress anomalies occur to the west of the Niño3 region, which is a characteristic feature during the eastern Pacific El Niño events (see Kim and Jin 2011a). Compared to ERA5, the spatial pattern of warm eastern Pacific anomalies is slightly stretched westwards, and wind stress anomalies are relatively stronger over the equator and South Pacific Convergence Zone (SPCZ). The 2^{nd} EOF, in both ERA5 and piControl, shows warm SST anomalies over the equatorial central Pacific Niño4 region. The variance distributions for ERA5 and HadCM3L match well for EOF1 (ERA5: 82 %, piContol: 90 %) whereas a large difference exist for EOF2 (ERA5: 18 %, piControl: 10 %).*

The PCA is also useful for evaluating how well HadCM3L represents certain types of ENSO events. Eastern and central Pacific ENSO events can be described by an E-Index (PC1-PC2)/√2), which emphasizes maximum warm anomalies in the eastern Pacific region, and a C-Index (PC1+PC2)/√2) respectively, which focuses on maximum warm anomalies in the central Pacific (Cai et al., 2018). Here, we show the eastern Pacific (EP) Pattern (Fig. S1 g, h) and central Pacific (CP) pattern (Fig. S1 j, k) by linear regression of mean DJF E- and C-Index, respectively, onto mean DJF SST and wind stress anomalies. We find that model's EP and CP patterns agree reasonably well with that of ERA5. HadCM3L underestimates the E-index skewness (1.16) whereas overestimates the C-Index skewness (-0.89) compared to ERA5 (2.08 and -0.58 respectively) averaged over DJF. HadCM3L's performance averaged over the entire simulated period of piControl is also consistent with ERA5 (Fig. S1; α: -0.32, EOF1: 64 %, EOF2, 8%, E-index skewness: 1.30, C-index skewness: -0.42). In general, in HadCM3L, the contrast between the E- and C-index skewness over the entire simulated period is sufficient enough to differentiate relatively strong warm (cold) events in the eastern (central) equatorial Pacific compared to the central (eastern) equatorial Pacific. Finally, we also evaluated the hf and BJ feedbacks which, for piControl, are very similar to those of ERA5 (Table S5-6).

We conclude that HadCM3L has a reasonable skill for studying long-term ENSO variability and its response to solar geoengineering. However, we also highlight the need for and hope to motivate future modelling studies that will help identify model dependencies in the ENSO response.

We discuss the results of Cai et al. (2018) as follows:

As diagnosed from Sea Surface Temperature (SST) indices in state-of-the-art AOGCMs, there was no intermodel consensus about change in frequency of ENSO events and amplitude in a warming climate (Vega-Westhoff and Sriver 2017; Yang et al., 2018) until Cai et al. (2018) used SST indices based on Principal Component Analysis (PCA). (see section 1, page 2, and line 41 to next page line 4)

However, Cai et al. (2018) later found robust evidence of a consistent increase in El Niño amplitude in the subset of CMIP5 climate models, which were capable of reproducing both eastern and central Pacific ENSO modes. (see section 1, page 3, line 11-14)

See Supplementary Fig. S1 and Tables S5-S6

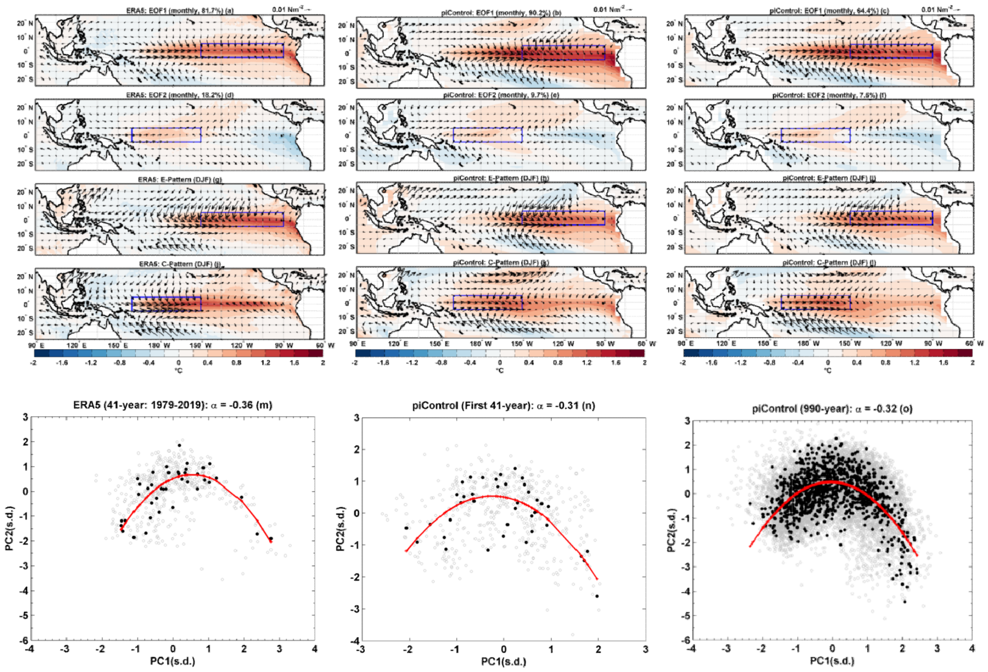

Figure S1. *ENSO diversity and nonlinear relationship between PCs. First monthly principal pattern, EOF1, for (a) ERA5 and (b, c) piControl. Second monthly principal pattern, EOF2, for (d) ERA5 and (e, f) piControl. DJF EP pattern for (g) ERA5 and (h, i) piControl. DJF CP pattern for (j) ERA5 and (k, l) piControl. The nonlinear relationship between PC1 and PC2 for (m) ERA5 and (n, o) piControl. The blue box indicates the Niño3 (Niño4) region in a-c, and g-I (d-f and j-l). The left and the middle panel shows EOF analysis over the 41 years of ER5 (1979-2019) and piControl. The right panel shows EOF analysis over 990-year of piControl.*

Table S5. Mean DJF Heat Flux (hf) Feedback

Experiment	**hf feedback or Damping Coefficient ($Wm^{-2}/^oC$)**	**Difference w.r.t. piControl ($Wm^{-2}/^oC$)**	**Std. Dev. 10,000 Realizations ($Wm^{-2}/^oC$)**	**~ Change w.r.t. piControl (%)**
ERA5	-14.59			
piControl	-14.70		0.52	
4×CO_2	-21.90	+7.19		+48*
G1	-14.85	+0.15		+1.0

*99% cl; **95% cl; Calculation period: ERA5 (41-yrs); HadCM3L (990-yrs)

Table S6. Mean DJF Bjerknes (BJ) Feedback

Experiment	**BJ feedback (10^{-2} $Nm^{-2}/^oC$)**	**Difference w.r.t. piControl (10^{-2} $Nm^{-2}/^oC$)**	**Std. Dev. 10,000 Realizations ($Wm^{-2}/^oC$)**	**~ Change w.r.t. piControl (%)**
ERA5	3.3			
piControl	3.3		0.0091	
4×CO_2	2.2	-1.1		-33*
G1	3.5	+0.2		+6*

*99% cl; **95% cl; Calculation period: ERA5 (41-yrs); HadCM3L (990-yrs)

6)

P7, L10: make clear the results are in *qualitative* agreement with previous studies. Not all of the cited studies are based on 4xCO2.

We check our results and categorically mention that our results qualitatively agree with previous studies. Thus we add the following change:

Our SST results under 4xCO_2 qualitatively agree with previous studies (Liu et al., 2005; van Oldenborgh et al., 2005; Collins et al., 2010; Vecchi and Wittenberg et al., 2010; Cai et al., 2015a; Huang and Ying et al., 2015; Luo et al., 2015; Kohyama et al., 2017; Nowack et al., 2017). (see section 3.1.1, page 9, line 9-12)

7)

P.7, L13: some studies argue against the use of "El Nino-like" term in describing the mean-state change under greenhouse forcing (e.g., Collins et al. 2010; see also Xie et al. 2010 https://journals.ametsoc.org/doi/10.1175/2009JCLI3329.1). Cautionary is needed to avoid confusions. A relevant reference on the mean state change: diNezio et al https://journals.ametsoc.org/doi/full/10.1175/2009JCLI2982.1.

We have deleted the term "El Nino-like" from the revised manuscript and have replaced it with appropriate words like *"a significant mean warming"* or *"a warming state"* (see section 1, page 3, lines 18-19; and section 3.1.1 page 8, line 37)

8)

Fig. 2d, e: title of the figure states +0.21 mm/day, -0.23 mm/day. Please explain in the caption that those numbers correspond to the area average difference between experiment and piControl in the tropical Pacific (state domain).

The following change is made in the caption of Fig. 1:

The numbers in a-c represent a mean temperature in the corresponding simulation, and numbers in d-e represent an area-averaged difference of piControl with 4×CO_2 and G1, respectively, in the tropical Pacific region (25^o N-25^o S; 90^o E-60^o W). (page 28, lines 8-11)

The following change is made in the caption of Fig. 2:

The numbers in a-c represent mean rainfall in the corresponding simulation, and numbers in d-e represent an area-averaged difference of piControl with 4×CO_2 and G1, respectively, in the tropical Pacific region (25^o N-25^o S; 90^o E-60^o W). (page 29, lines 7-10)

9)

P9, L22-24: This sentence needs a rework. Avoid the word "observe" on model analysis (models are not observations). I think Wang et al. (2017) was referring to zonal temperature gradient between the maritime continent and central Pacific, not eastern Pacific. The difference is not significant in RCP2.6, but should be significant in RCP8.5 (Cai et al. 2015, Nature Climate Change on extreme La Nina).

The use of word "observed" for modelled data has been replaced with appropriate words in the revised manuscript. The reference of Wang et al. (2017) for weakening of ZSSTG has also been removed from the revised manuscript. Instead we add the following statements:

Our results under 4xCO_2 are in agreement with Coats and Karnauskas (2017), who using several climate models found a weakening of the ZSSTG under the RCP8.5 scenario.(see section 3.1.4, page 11, line 11-13)

The weakening of the MSSTG is qualitatively in agreement with previous studies under increased GHG forcings (e.g., Cai et al., 2014; Wang et al., 2017). (see section 3.1.4, page 11, lines 21-22)

10)

Fig. 7: Please indicate clearly in the caption that the timeseries have been detrended with non ENSO related trend removed following Cai et al. (2017). Otherwise it would create confusion as other studies show that the 2015/16 Nino3 rainfall is close to the 5 mm/day threshold and is thus classified as an extreme El Nino (Santoso et al. 2017). In panel c, d, it must be rainfall anomalies that are shown because there are negative rainfall values, so wouldn't the 4 or 3 mm/day threshold be applied here? Panel a and b also have negative rainfall values. Please double check.

In the captions, we have added the following text:

Following Cai et al. (2014), a non-ENSO related trend has been removed from the rainfall time series. (see Fig. 7, page 32, lines 8-9; and Fig.S5-S6)

In Fig. 7 and Fig. S5-6, revised manuscript, we have shown total rainfall after subtracting the non-ENSO related trend as described by Cai et al. (2017). In the previous manuscript, we subtracted the non-ENSO related trend, including the intercept term; therefore, negative values were present, and it's been corrected now.

11)

P12, L28-31: under 4xCO2 the rainfall skewness is dramatically reduced. Does that mean there are less extreme El Nino based on the rainfall definition? If so, this does not seem consistent with the PPE results of Cai et al. (2014) using the same model.

In the revised manuscript, we have included the analysis for 4×CO_2. We show that extreme El Niño events increase under 4×CO_2 using metrics based on rainfall and E-index (See section 3.2.2). The climate regime under 4×CO_2 is substantially different from that of piControl (See Fig. S8). The comparison of piControl and 4×CO_2 is not simple as mean rainfall, despite zero skewness, significantly shifts to a higher value (9.8 mm day^{-1}) under 4×CO_2. We have added the following text in the revised manuscript:

With detrended Niño3 total rainfall exceeding 5 mm day^{-1} as an extreme, three extreme and seven moderate El Niño events can be identified from the historical record between 1979 and 2017 (Fig. 7a). A statistically significant increase of 526 % (99 % cl) in extreme El Niño events can be seen under 4×CO_2 (939 events) relative to piControl (150 events) (Fig. 7b-c). The geoengineering of climate (G1) largely offsets the increase in extreme El Niño frequency under 4×CO_2 (Fig. 7d), however, compared to piControl, still a 17 % increase in extremes and a 12 % increase in the total number of El Niño events (moderate plus extreme) can be seen at 95 % cl. Thus, an El Niño event occurring every ~3.3-yr under preindustrial conditions occurs every ~2.9-yr under solar geoengineered conditions. (see section 3.2.2, page 14, line 17-25)

A threshold of detrended Niño3 total rainfall of 5 mm day^{-1} recognizes events as extremes even when the MSSTG is positive and stronger, especially under 4×CO_2, which plausibly means that ITCZ might not shift over the equator for strong convection to occur during such extremes. The El Niño event of 2015 is a typical example of such events. We test our results with a more strict criterion by choosing only those events as extremes, which have characteristics similar to that of 1982 and 1997 El Niño events (i.e., Niño3 rainfall > 5 mm day^{-1} and MSSTG < 0). We declare events having characteristics similar to that of the 2015 event as moderate El Niño events (Fig. S5). Based on this method, we find a robust increase in the number of extreme El Niño events both in 4×CO_2 (924 %) and G1 (61 %) at 99 % cl. We also performed the same analysis by linearly detrending the rainfall time series and find similar results (Fig. S6). (see section 3.2.2, page 14, line 26-36)

An alternative approach to quantifying extreme El Niño events is based on Niño3 SST index > 1.75 s.d. as an extreme event threshold (Cai et al., 2014). We note that using this definition, no statistically significant change in the number of extreme El Niño events is detected in G1 (61 events), whereas they reduced from 57 in piControl to zero events in 4×CO_2 highlighting the dependency of specific results on the precise definition of El Niño events used. However, relative to piControl, Niño3 SST index indicates a statistically significant increase (decrease) of 12 % (46 %) in the frequency of the total number of El Niño events (Niño3 SST index > 0.5 s.d.) (Table S3) in G1 (4×CO_2). Further, we examine the change in extreme El Niño events using E-Index > 1.5 s.d. (see Cai et al., 2018) as threshold. The SST based E-Index identifies 79, 147, and 93 extreme El Niño events in *piControl, 4×CO_2, and G1, respectively. Thus using E-Index, extreme El Niño events increase by 86 % (99 % cl) and 17 % (missing 95 % cl by three events) in 4×CO_2 and G1, respectively. Based on the E-index definition, we also see a statistically significant increase in the total number of El Niño events in 4×CO_2 (88 %) and G1 (12 %) (Table S3). Note that Wang et al. (2020) showed that extreme convective events can still happen even if the E-index is not greater than 5 mm day^{-1} (cf. Figure 2 in Wang et al. 2020).* (see section 3.2.2, from page 14, and line 37 to next page line 12)

The increased frequency of extreme El Niño events under 4×CO_2 is due to change in the mean position of the ITCZ (Fig. S2), causing frequent reversals of MSSTG (Fig. S3), and eastward extension of the western branch of PWC (Fig. 6), which both result in increased rainfall over the eastern Pacific (see Wang et al. 2020). This is due to greater east equatorial than off-equatorial Pacific warming (see Cai et al. 2020), which shifts the mean position of ITCZ towards the equator (Fig. S2). Simultaneously more rapid warming of the eastern than western equatorial Pacific reduces the ZSSTG, and hence zonal wind stress, as also evident from the weakening and shift of the PWC (Fig. 6) and increased instances of negative ZSSTG anomalies (Fig. S9). Ultimately, this leads to more frequent vigorous convection over the Niño3 region (Fig. 5d), and enhanced rainfall (Fig. 2d, S8). Therefore, despite the weakening of the ENSO amplitude under 4×CO_2, rapid warming of the eastern equatorial Pacific causes frequent reversals of meridional and zonal SST gradients, resulting in an increased frequency of extreme El Niño events (see also Cai et al., 2014; Wang et al., 2020). (see section 4.1, page 17, line 24-36)

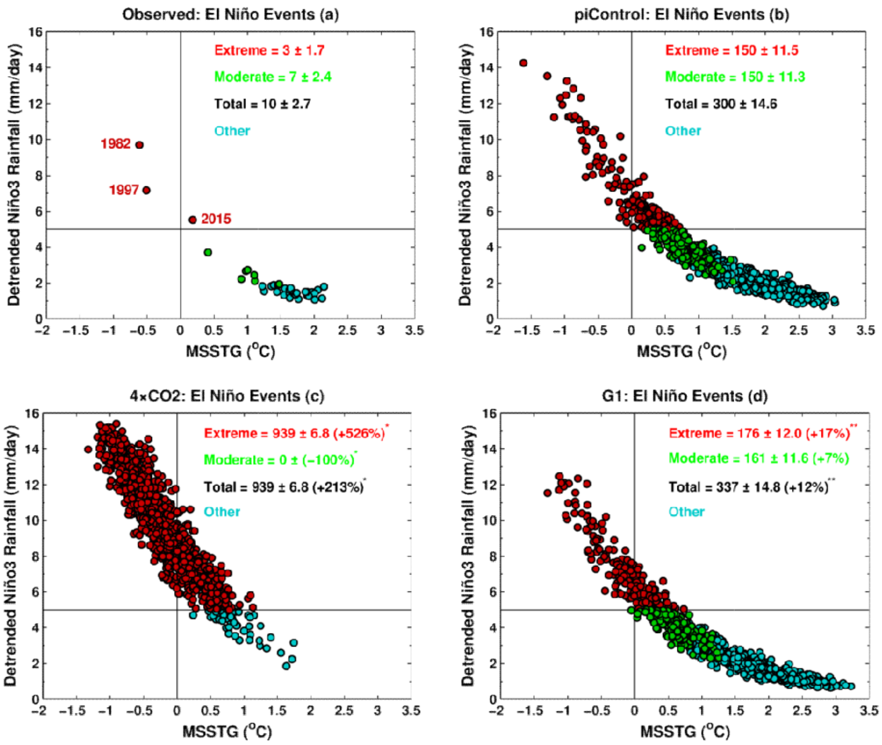

Figure 7. *Relationship between MSSTG and Niño3 rainfall for (a) observations (b) piControl (c) 4×CO_2, and (d) G1. A solid black horizontal line indicates a threshold value of 5 mm day^{-1}. See text for the definition of extreme, moderate, and total El Niño events. A single (double) asterisk indicates that the change in frequency, relative to piControl, is statistically significant at 99 % (95 %) cl. Numbers with a ± symbol indicate s.d. calculated with 10,000 bootstrap realizations. Following Cai et al. (2014), a non-ENSO related trend has been removed from the rainfall time series.*

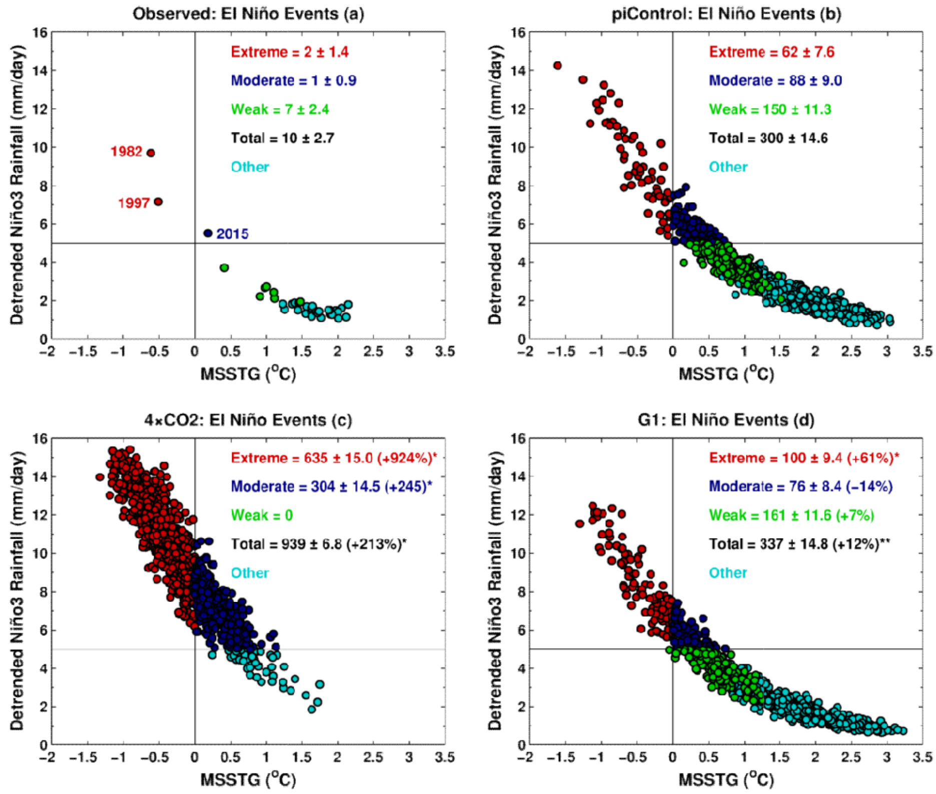

Figure S5. *Relationship between MSSTG and quadratically detrended Niño3 rainfall for (a) observations (b) piControl (c) 4×CO_2, and (d) G1. The solid black horizontal line indicates a threshold of 5 mm day^{-1}. A single (double) asterisk indicates that the change in frequency, relative to piControl, is statistically significant at 99 % (95 %) cl. Numbers with a ± symbol indicate s.d. calculated with 10,000 bootstrap realizations. Following Cai et al. (2014), a non-ENSO related trend has been removed from the rainfall time series. Events are classified as: Extreme (Niño3 rainfall > 5 mm day^{-1} and MSSTG < 0), moderate (Niño3 rainfall > 5 mm day^{-1} and MSSTG > 0), weak (Standardized Niño3 SSTs > 0.5 °C and Niño3 rainfall < 5 mm day^{-1}), total is sum of extreme, moderate, and weak events.*

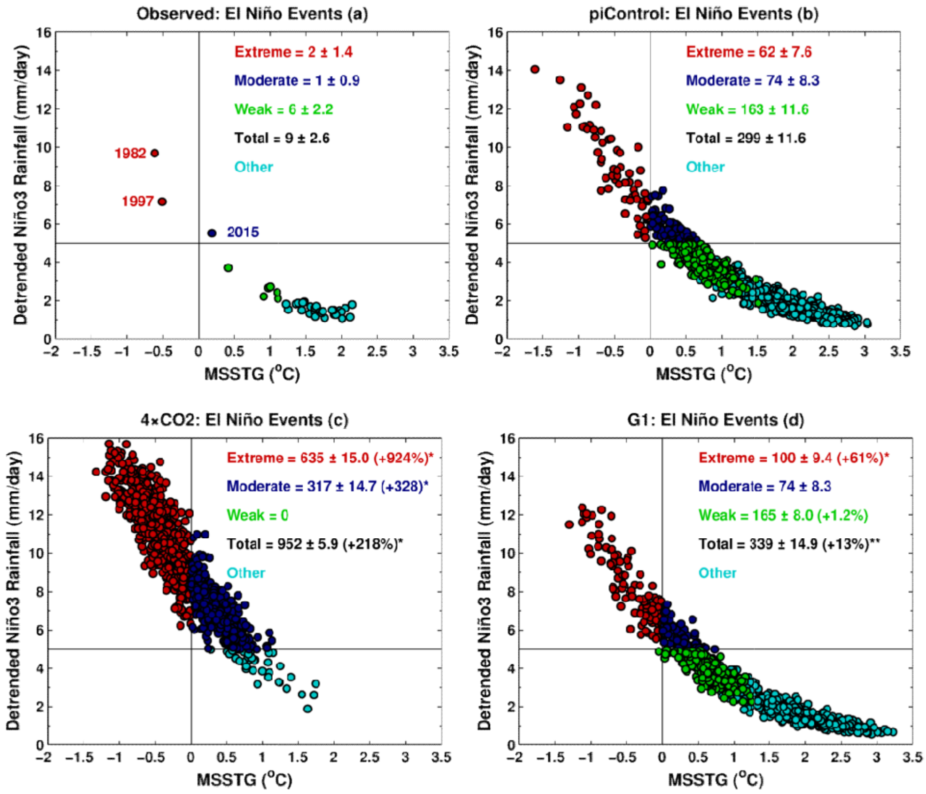

Figure S6. *Relationship between MSSTG and linearly detrended Niño3 rainfall for (a) observations (b) piControl (c) 4×CO_2, and (d) G1. The solid black horizontal line indicates a threshold of 5 mm day^{-1}. A single (double) asterisk indicates that the change in frequency, relative to piControl, is statistically significant at 99 % (95 %) cl. Numbers with a ± symbol indicate s.d. calculated with 10,000 bootstrap realizations. Following Cai et al. (2014), a non-ENSO related trend has been removed from the rainfall time series. Events are classified as: Extreme (Niño3 rainfall > 5 mm day^{-1} and MSSTG < 0), moderate (Niño3 rainfall > 5 mm day^{-1} and MSSTG > 0), weak (Standardized Niño3 SSTs > 0.5 °C and Niño3 rainfall < 5 mm day^{-1}), total is sum of extreme, moderate, and weak events.*

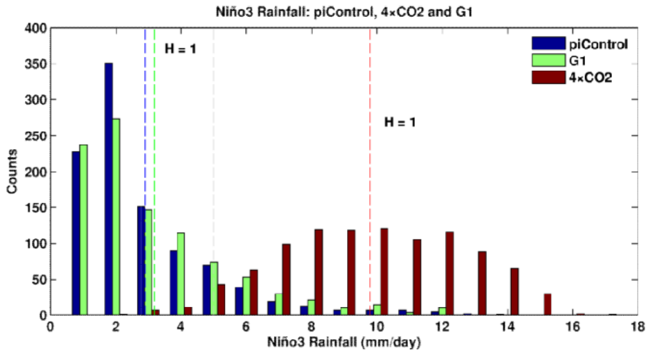

Figure S8. *Histogram of Niño3 rainfall for piControl, 4×CO_2, and G1. The values are plotted at the centre of each bin with an interval of 1 mm day^{-1}. Blue, red, and green vertical lines indicate climatological mean values of Niño3 rainfall under piControl (2.9 mm day^{-1}), 4×CO_2 (9.8 mm day^{-1}), and G1 (3.2 mm day^{-1}), respectively. H = 1 indicates that the shift in the mean is statistically significant at 99 (95) % cl for 4×CO_2 (G1) using the non-parametric Wilcoxon rank-sum test. The grey vertical line show threshold of 5 mm day^{-1}.*

Table S3. Total number of El Niño events (SST > 0.5 s.d.)

Experiment	No. of Events	Difference w.r.t. piControl	Std. Dev. 10,000 Realizations	~ Change w.r.t. piControl (%)
piControl	300 [300]		14.6 [14.6]	
4×CO_2	161 [565]	139 [265]		-46* [+88*]
G1	337 [337]	37 [37]		+12** [+12**]

Key: Niño3 [E-Index]; *99 % cl; **95 % cl

12)

P13, L28-39: The characterization of extreme La Nina is based on Nino4 (Cai et al. 2015), so it is not clear how Nino3 and Nino3.4 indices are used here to infer changes in extreme La Nina.

We have deleted inferences based on Nino3 and Nino3.4 in section 3.2.3 of the revised manuscript.

<u>Figure presentation</u>

13)

Fig. 1e, some areas look white (e.g., eastern equatorial Pacific which is supposed to be approx. -0.2C p7, L9) while the colorbar does not have white on it.

We have reproduced Fig. 1e with a different color bar, and visibility of colors has improved in the revised manuscript.

14)

Figure 10: the color limit does not seem correct, which shows much larger values in e, f G1-piControl than the composite anomalies themselves in panels a-d.

We have corrected the color limits in Fig. 10.

15)

The colorbar of Fig. 2, right panel especially is not ideal. It is hard to immediately see which are positive or negative without referring to the colorbar.

In the revised manuscript, we have reproduced Fig. 2 with a diverging color bar.

16)

Might be best to have the same color scale for comparing the results of 4xCO2 – piControl vs G1 – piControl. This is to convey the message the difference is much smaller for G1 – piControl than for 4xCO2.

The differences under G1-piControl are small; if we use the same color bar for $4xCO_2$-piControl and G1-piControl, most of the information is suppressed for G1-piControl. Therefore we have used two different color bars.

<u>**Minor points**</u>

17)

Page 4, L34: that sentence is due to Cai et al. (2014).

We have cited Cai et al. (2014) in the revised manuscript. (see section 2.4, page 7, line 2)

18)

P4, L35: delete "the northern part of" – the ITCZ is located north of equator, and that rainfall band moves equatorward during strong El Nino events.

We have deleted "the northern part of" in the revised manuscript.

19)

P5, L23: "ggradients"

Corrected in the revised manuscript. (see section 2.3, page 5, line 24)

20)

P6, L2: extreme El Ninos are not resulting in just "anomalous rainfall" but unusually large rainfall in the eastern equatorial Pacific.

We have deleted the word anomalous and modified the text as follows:

.... Niño3 region resulting in rainfall higher than 5mm day^{-1} (Cai et al., 2014). (see section 2.3, page 6, lines 1-2)

21)

P6, L 35: "depicts this SSTasymmetry between the western and eastern equatorial Pacific well (Fig. 1a)." – not clear since the observed counterpart is not presented.

In the text, we have cited a reference for comparing the piControl SST asymmetry with an observational dataset. We have modified the version as follows:

The piControl simulation (Fig. 1a) reproduces the SST asymmetry between the western and eastern equatorial Pacific well (cf. Fig 1a in Vecchi and Wittenberg 2010). (see section 3.1.1, page 8, lines 34-36)

22)

P8, L10: "problem" – not clear, in what way it is a problem?

The word "problem" has been deleted in the revised manuscript. We have modified the text as follows:

That is, while the relative additional rainfall asymmetry between the western and eastern Pacific in 4×CO_2 is mostly resolved in G1, the tropical Pacific is overall wetter under 4×CO_2 but drier in G1. (see section 3.1.2, page 10, lines 13-15)

23)

P9, L19: repetitive: El Nino being stronger than La Nina already implies asymmetric amplitude.

In the revised manuscript, we have modified text as follows:

However, the use of standard deviations to define ENSO amplitude is suboptimal, because amplitudes of El Niño and La Niña events are asymmetric, i.e., in general, El Niño events are stronger than La Niña events (An and Jin 2004; Schopf and Burgman 2006; Ohba and Ueda 2009; Ham 2017). (see section 3.2.1, page 13, lines 22-25)

24)

P9, L29: the shoaling of thermocline is also due to increased stratification associated with surface intensified warming in response to greenhouse forcing.

We have added the following text in the revised manuscript:

In 4xCO_2, most likely the weakened easterlies (as noticed in Sect. 3.1.3; e.g., Yeh et al., 2009, Wang et al., 2017) and greater ocean temperature stratification due to increased surface warming (see Sect. 4 and Cai et al., 2018) lead to a significant shoaling of the thermocline across the western and central equatorial Pacific. In contrast, relatively little change takes place between 130° W and 90° W. In a CMIP3 multimodel (SRESA1B scenario) ensemble, Yeh et al. (2009) found a more profound deepening of the thermocline in this part of the eastern equatorial Pacific; however, for example, Nowack et al. (2017) did not find such changes under 4xCO_2 (cf. their Fig. S9). One possible explanation for this behaviour is the competing effects of upper-ocean warming (which deepens the thermocline) and the weakening of westerly zonal wind stress, causing thermocline shoaling (see Kim et al. 2011a). (see section 3.1.5, from page 11 and line 37 to next page line 8)

25)

P9, L32-36: why not use the maximum of vertical temperature gradient as a proxy of thermocline depth for all scenarios?

In the revised manuscript, we have included a map for ocean stratification; we think it can provide some details on this. Further, model ocean vertical resolution (13 levels) is not very high to calculate maximum vertical temperature gradient.

26)

P14, L6-7: for extreme El Nino events, are the PWC, SST, and rainfall anomalies strengthened as well?

For extreme El Niño events, the PWC, SST, and rainfall anomalies are weakened. We have rectified the text as follows:

These composites provide process-based evidence for the strengthening (weakening) of extreme La Niña (El Niño) events in G1. We show that the PWC, SST, and composite rainfall anomalies are strengthened for extreme La Niña events, while they are weakened for extreme El Niño events under G1. (see section 3.3, page, 16, lines 5-8)

27)

P14, L23-25: this must be referring to the difference between G1 and piControl. Please make that clear.

In the revised manuscript, we have modified text as follows:

During extreme El Niño events, in G1, we find reduced SST (Fig. 9e) and rainfall anomalies (Fig. 10e) over the eastern and western equatorial Pacific with a consistent weakening of the eastern and western branch of PWC (Fig. 11e). (see section 3.3.1, page 16, lines 15-17)

Referee #2

Major Points

1)

To study the ENSO changes under solar geoengineering, the results are all based on one single model HadCM3L. In Cai et al. (2014) and Collins et al. (2001), the model they used is HadCM3. I admit that HadCM3L and HadCM3 are identical in most aspects, but there are still differences between these two simulations. The differences should be mentioned in this study because the HadCM3L may not be skillful in reproducing ENSO variabilities, and thus the sentence in P4 L32-33 may not be completely correct. I suggest that the ENSO simulated in HadCM3L should be addressed first, regarding its magnitude and pattern. For instance, the EOF analyses can be carried out on the piControl simulations. It will help us to have a general idea of how capable the HadCM3L is in simulating the ENSO and its diversity, and what's the biases compared with observations. As pointed out in Cai et al. (2018), the magnitude and location of ENSO events are inconsistent among models. The averaged SSTA in a fixed box to measure the intensity of ENSO can be tricky. A look at the ENSO pattern in HadCM3L can also facilitate a better ENSO extreme definition, i.e. the Nino indices may not be best to define ENSO intensity. At least, a glimpse of the Figure 8 reveals that ENSO simulation is not good enough, especially the shape, maximum location and horseshoe-shaped cold SSTA in the western Pacific during El Nino events.

We have deleted the text referring to P4 and L32-33 in the revised manuscript. In the revised manuscript we have evaluated the model skill for reproducing ENSO diversity following Cai et al. (2018). The HadCM3L belongs to the family of HadCM3 models; the only difference between HadCM3 and HadCM3L is lower ocean resolution. We have included a separate section on model evaluation. We have also mentioned the apparent biases in HadCM3L compared to observations. We find that HadCM3L has a reasonable skill to simulate ENSO and can be employed for the current study. The HadCM3L simulates the sea surface temperature maximum anomaly pattern over the Niño3 region. In the revised manuscript, we have made the following additions:

HadCM3L stems from the family of HadCM3 climate models; the only difference is lower ocean resolution (HadCM3: $1.25^o \times 1.25^o$; Valdes et al., 2017). (see section 2.1, page 4, lines 25-27)

Before employing HadCM3L for studying ENSO variability under $4\times CO_2$, and G1, we evaluate its piControl simulation against present-day observational data. (see section 2.4, page 6, lines 40-41)

Further, we have included the following paragraphs (section 2.4, page 7, and line 14 to next page line 21):

In addition, we evaluate the ENSO modelled by HadCM3L following a principal component (PC) approach suggested by Cai et al. (2018). Considering distinct eastern and central Pacific ENSO regimes based on Empirical Orthogonal Function (EOF) analysis, they found that climate models capable of reproducing present-day ENSO diversity show a robust increase in eastern Pacific ENSO amplitude in a greenhouse warming scenario. Specifically, the approach assumes that any ENSO event can be represented by performing EOF analysis on monthly SST anomalies and combining the first two principal patterns (Cai et al., 2018). The first two PCs time series, PC1 and PC2, show a non-linear relationship in observational datasets (Fig. S1m). Climate models that do not show such a non-linear relationship cannot satisfactorily reproduce ENSO diversity, and hence are not sufficiently skilful for studying ENSO properties (Cai et al., 2018). Here, we perform EOF analysis on quadratically detrended monthly SST and wind stress anomalies of ERA5 and piControl over a consistent period of 41-year. We evaluate HadCM3L's ability to simulate two distinct ENSO regimes and the non-linear relationship between the first two PCs, i.e., $PC2(t) = \alpha[PC1(t)]^2 + \beta[PC1(t)]^2 + \gamma$ (Fig. S1). From ERA5, $\alpha = -0.36$ (statistically significant at 99 % confidence level, hereafter "cl") whereas in piControl $\alpha = -0.31$ (99 % cl), which is same as the mean $\alpha = -0.31$ value calculated by Cai et al (2018) averaged over five reanalysis datasets. The 1st and 2nd EOF patterns of monthly SST and wind stress anomalies of piControl (Fig. S1 b, e) are comparable with that of ERA5 (Fig. S1 a, d). EOF1 of piControl shows slightly stronger warm anomalies in the eastern equatorial Pacific, whereas negative anomalies over the western Pacific are slightly weaker compared to ERA5. In EOF1, the stronger wind stress anomalies occur to the west of the Niño3 region, which is a characteristic feature during the eastern Pacific El Niño events (see Kim and Jin 2011a). Compared *to ERA5, the spatial pattern of warm eastern Pacific anomalies is slightly stretched westwards, and wind stress anomalies are relatively stronger over the equator and South Pacific Convergence Zone (SPCZ). The 2^{nd} EOF, in both ERA5 and piControl, shows warm SST anomalies over the equatorial central Pacific Niño4 region. The variance distributions for ERA5 and HadCM3L match well for EOF1 (ERA5: 82 %, piContol: 90 %) whereas a large difference exist for EOF2 (ERA5: 18 %, piControl: 10 %).*

The PCA is also useful for evaluating how well HadCM3L represents certain types of ENSO events. Eastern and central Pacific ENSO events can be described by an E-Index (PC1-PC2)/√2), which emphasizes maximum warm anomalies in the eastern Pacific region, and a C-Index (PC1+PC2)/√2) respectively, which focuses on maximum warm anomalies in the central Pacific (Cai et al., 2018). Here, we show the eastern Pacific (EP) Pattern (Fig. S1 g, h) and central Pacific (CP) pattern (Fig. S1 j, k) by linear regression of mean DJF E- and C-Index, respectively, onto mean DJF SST and wind stress anomalies. We find that model's EP and CP patterns agree reasonably well with that of ERA5. HadCM3L underestimates the E-index skewness (1.16) whereas overestimates the C-Index skewness (-0.89) compared to ERA5 (2.08 and -0.58 respectively) averaged over DJF. HadCM3L's performance averaged over the entire simulated period of piControl is also consistent with ERA5 (Fig. S1; α: -0.32, EOF1: 64 %, EOF2, 8%, E-index skewness: 1.30, C-index skewness: -0.42). In general, in HadCM3L, the contrast between the E- and C-index skewness over the entire simulated period is sufficient enough to differentiate relatively strong warm (cold) events in the eastern (central) equatorial Pacific compared to the central (eastern) equatorial Pacific. Finally, we also evaluated the hf and BJ feedbacks which, for piControl, are very similar to those of ERA5 (Table S5-6).

We conclude that HadCM3L has a reasonable skill for studying long-term ENSO variability and its response to solar geoengineering. However, we also highlight the need for and hope to motivate future modelling studies that will help identify model dependencies in the ENSO response.

See Supplementary Fig. S1 and Tables S5-S6

Table S5. Mean DJF Heat Flux (hf) Feedback

Experiment	**hf feedback or Damping Coefficient ($Wm^{-2}/^oC$)**	**Difference w.r.t. piControl ($Wm^{-2}/^oC$)**	**Std. Dev. 10,000 Realizations ($Wm^{-2}/^oC$)**	**~ Change w.r.t. piControl (%)**
ERA5	-14.59			
piControl	-14.70		0.52	
4×CO_2	-21.90	+7.19		+48*
G1	-14.85	+0.15		+1.0

*99% cl; **95% cl; Calculation period: ERA5 (41-yrs); HadCM3L (990-yrs)

Table S6. Mean DJF Bjerknes (BJ) Feedback

Experiment	**BJ feedback (10^{-2} $Nm^{-2}/^oC$)**	**Difference w.r.t. piControl (10^{-2} $Nm^{-2}/^oC$)**	**Std. Dev. 10,000 Realizations ($Wm^{-2}/^oC$)**	**~ Change w.r.t. piControl (%)**
ERA5	3.3			
piControl	3.3		0.0091	
4×CO_2	2.2	-1.1		-33*
G1	3.5	+0.2		+6*

*99% cl; **95% cl; Calculation period: ERA5 (41-yrs); HadCM3L (990-yrs)

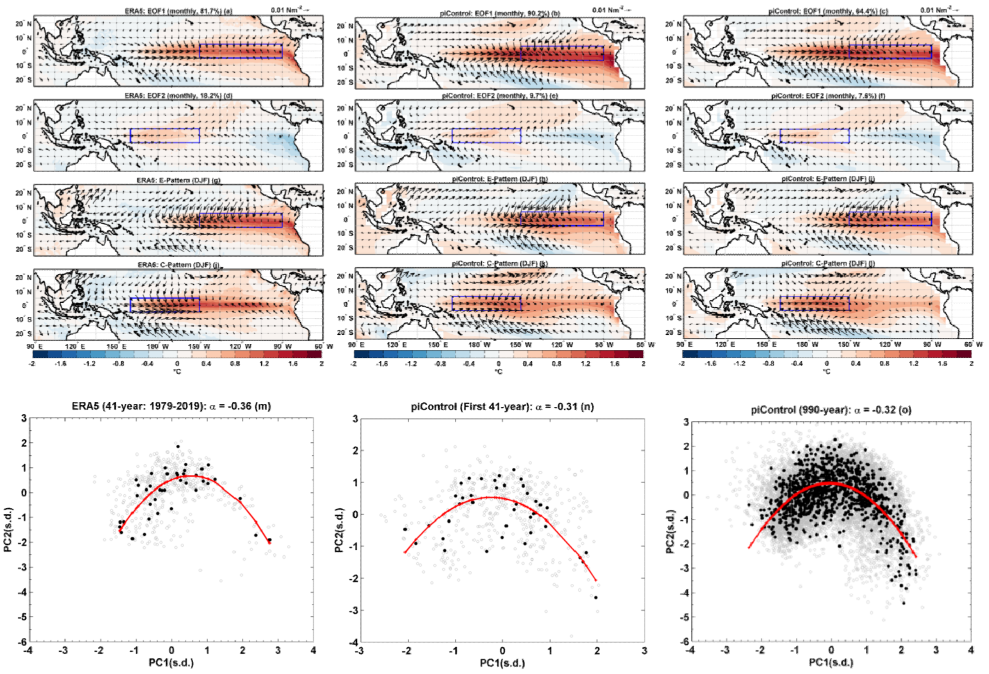

Figure S1. *ENSO diversity and nonlinear relationship between PCs. First monthly principal pattern, EOF1, for (a) ERA5 and (b, c) piControl. Second monthly principal pattern, EOF2, for (d) ERA5 and (e, f) piControl. DJF EP pattern for (g) ERA5 and (h, i) piControl. DJF CP pattern for (j) ERA5 and (k, l) piControl. The nonlinear relationship between PC1 and PC2 for (m) ERA5 and (n, o) piControl. The blue box indicates the Niño3 (Niño4) region in a-c, and g-I (d-f and j-l). The left and the middle panel shows EOF analysis over the 41 years of ER5 (1979-2019) and piControl. The right panel shows EOF analysis over 990-year of piControl.*

2)

The change of extreme ENSO under solar geoengineering is a major concern in this study. This paper shows adequate results to uncovering the phenomenon that may happen but lacks the investigations on underlying mechanisms. The magnitude of ENSO is mainly driven by the positive and negative feedbacks involving air-sea interactions. In the manuscript, the major atmospheric and oceanic components are depicted, such as the thermocline, zonal wind stress and zonal SST gradient. A clear physical process is needed to understand how ENSO can be modified in G1 and 4_CO2. The Bjerknes feedback, thermocline feedback and heat flux feedback can be evaluated under different scenarios. This may be helpful to illustrate why ENSO in G1 can be modified even though the thermocline, zonal SST gradient and zonal wind stress are not well separated in G1 and piControl. Also, it's necessary to go deeper into the reason why the responses of El Nino and La Nina are different for magnitude change and same for frequency change.

In the revised manuscript, we have calculated ENSO feedbacks, Bjerknes and heat flux, and ocean stratification to explain the mechanisms for change in ENSO. We have added Section 4 elaborating on the mechanism for change in ENSO under both 4xCO_2 and G1. (See section 4, from page 17 and line 1 to page 18 and line 29). Specifically we write:

4 Mechanisms behind the changes in ENSO variability

4.1 Under greenhouse gas forcing

The reduced ENSO amplitude under 4×CO_2 is mainly caused by stronger hf and weaker BJ feedback relative to piControl (Fig. 15a-b, and Table S5-6). More rapid warming over the eastern than western equatorial Pacific *regions reduces the SST asymmetry between western and eastern Pacific (Fig. 1d), resulting in the weakening of ZSSTG (Fig. 4b) that significantly weakens the zonal winds stress (Fig. 4a) and hence PWC (Fig. 6b, d, see Bayr et al., 2014). The overall reduction of zonal wind stress reduces the BJ feedback, which, in turn, can weaken the ENSO amplitude. Climate models show an inverse relationship between hf feedback and ENSO amplitude (Lloyd et al., 2009, 2011; Kim and Jin 2011b). The increased hf feedback might be the result of enhanced clouds due to strengthened convection (Fig. 5b, d) and stronger evaporative cooling in response to enhanced SSTs under 4×CO_2 (Knutson and Manabe 1994; Kim and Jin 2011b). Kim and Jin (2011a, b) found intermodel consensus on the strengthening of hf feedback in CMIP3 models under enhanced GHG warming scenario (Ferret and Collins 2019). Further, we see increased ocean stratification under 4×CO_2 (Fig. 15d and Table S7). A more stratified ocean is associated with an increase in both the El Niño events and amplitude in the eastern Pacific (Wang et al. 2020). It can also modify the balance between feedback processes (Dewitte et al., 2013). Enhanced stratification may also cause negative temperature anomalies in the central to the western Pacific through changes in thermocline tilt (Dewitte et al., 2013). Since the overall ENSO amplitude decreases in our 4xCO_2 simulation, we, thus, conclude that the ocean stratification mechanisms cannot be the dominant factor here, but that hf and BJ feedbacks must more than cancel out the effect of ocean stratification on ENSO amplitude.*

The increased frequency of extreme El Niño events under 4×CO_2 is due to change in the mean position of the ITCZ (Fig. S2), causing frequent reversals of MSSTG (Fig. S3), and eastward extension of the western branch of PWC (Fig. 6), which both result in increased rainfall over the eastern Pacific (see Wang et al. 2020). This is due to greater east equatorial than off-equatorial Pacific warming (see Cai et al. 2020), which shifts the mean position of ITCZ towards the equator (Fig. S2). Simultaneously more rapid warming of the eastern than western equatorial Pacific reduces the ZSSTG, and hence zonal wind stress, as also evident from the weakening and shift of the PWC (Fig. 6) and increased instances of negative ZSSTG anomalies (Fig. S9). Ultimately, this leads to more frequent vigorous convection over the Niño3 region (Fig. 5d), and enhanced rainfall (Fig. 2d, S8). Therefore, despite the weakening of the ENSO amplitude under 4×CO_2, rapid warming of the eastern equatorial Pacific causes frequent reversals of meridional and zonal SST gradients, resulting in an increased frequency of extreme El Niño events (see also Cai et al., 2014; Wang et al., 2020).

We note that under GHG forcing, HadCM3L does not simulate an increase in the frequency of extreme La Niña events as found by Cai et al. (2015b) using CMIP5 models. However, it does show an increase in the total number of La Niña events (Table S4). In a multimodel ensemble mean, Cai et al. (2015b) found that the western Pacific warms more rapidly than the central Pacific under increased GHG forcing, resulting in strengthening of the zonal SST gradient between these two regions. Strengthening of this zonal SST gradient and increased vertical upper ocean stratification provide conducive conditions for increased frequency of extreme La Niña events (Cai et al., 2015b). One reason why we do not see an increase in the frequency of central Pacific extreme La Niña events might be that HadCM3L does not simulate more rapid warming of the western Pacific compared to the central Pacific as noticed by Cai et al. (2015b) (compare our Fig. 1d with Fig. 3b in Cai et al., 2015b), hence, as stronger zonal SST gradient does not develop, across the equatorial Pacific, as needed for extreme La Niña events to occur (see Fig. S9a, c and S10).

4.2 Under solar geoengineering

G1 over cools the upper ocean layers, whereas the GHG-induced warming in the lower ocean layers is not entirely offset, thus increasing ocean stratification (Fig. 15). The increased stratification boosts atmosphere-ocean coupling (see Cai et al., 2018), which favours enhanced westerly wind bursts (Fig. 4a) (e.g., Capotondi et al., 2018) to generate stronger SST anomalies over the eastern Pacific (Wang et al. 2020). The larger cooling of the western Pacific than the eastern Pacific can also enhance westerly wind bursts reinforcing the BJ feedback and hence SST anomalies in the eastern Pacific. We conclude that increased ocean stratification, along with stronger BJ feedback, is the most likely mechanism behind the overall strengthening of ENSO amplitude under G1.

The increased frequency of extreme El Niño events under G1 can be linked to the changes in MSSTG and ZSSTG (see Cai et al., 2014, and Fig. S3, S9). The eastern off-equatorial Pacific cools more than the eastern *equatorial regions, providing relatively more conducive conditions for convection to occur through a shift of ITCZ over to the Niño3 region (Fig. 1e). At the same time, the larger cooling of the western equatorial Pacific than of the eastern equatorial Pacific reduces the ZSSTG and convective activity over the western Pacific, which leads to a weakening of the western branch of PWC (Fig. 6e). Hence we see reduced rainfall over the western Pacific and enhanced rainfall from the Niño3 to the central Pacific region (Fig 2e). These mean state changes, strengthening of convection between ~140° W and ~150° E, and more reversals of the MSSTG and ZSSTG (Fig. S3) result in an increased number of extreme El Niño events in G1 than in piControl (Fig. 7).*

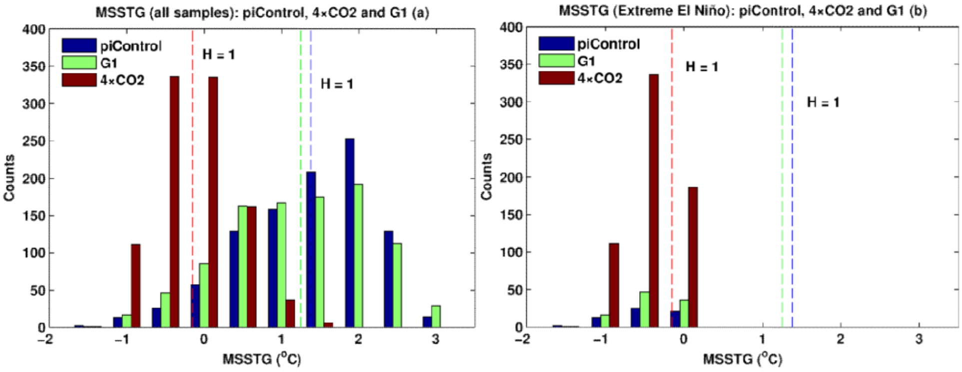

Figure S3. Histogram of MSSTG for piControl, 4×CO_2, and G1 for all samples (a) and for extreme El Niño events. The values are plotted at the centre of each bin with an interval of 0.5 °C. Blue, red, and green vertical lines indicate climatological mean values of MSSTG under piControl (1.38 °C), 4×CO_2 (-0.15 °C), and G1 (1.25 °C), respectively. H = 1 indicates that the shift in the mean is statistically significant at 99 % cl using a non-parametric Wilcoxon rank-sum test.

Table S5. Mean DJF Heat Flux (hf) Feedback

Experiment	hf feedback or Damping Coefficient ($Wm^{-2}/°C$)	Difference w.r.t. piControl ($Wm^{-2}/°C$)	Std. Dev. 10,000 Realizations ($Wm^{-2}/°C$)	~ Change w.r.t. piControl (%)
ERA5	-14.59			
piControl	-14.70		0.52	
4×CO_2	-21.90	+7.19		+48*
G1	-14.85	+0.15		+1.0

*99% cl; **95% cl; Calculation period: ERA5 (41-yrs); HadCM3L (990-yrs)

Table S6. Mean DJF Bjerknes (BJ) Feedback

Experiment	BJ feedback (10^{-2} $Nm^{-2}/°C$)	Difference w.r.t. piControl (10^{-2} $Nm^{-2}/°C$)	Std. Dev. 10,000 Realizations ($Wm^{-2}/°C$)	~ Change w.r.t. piControl (%)
ERA5	3.3			
piControl	3.3		0.0091	
4×CO_2	2.2	-1.1		-33*
G1	3.5	+0.2		+6*

*99% cl; **95% cl; Calculation period: ERA5 (41-yrs); HadCM3L (990-yrs)

Table S7. Mean DJF Ocean Stratification

Experiment	Stratification (°C)	Difference w.r.t. piControl (°C)	Std. Dev. 10,000 Realizations (°C)	~ Change w.r.t. piControl (%)
piControl	2.28*		0.0331	
4×CO_2	5.06*	+2.78		+122*
G1	2.37*	+0.09		+4**

*99% cl; **95% cl

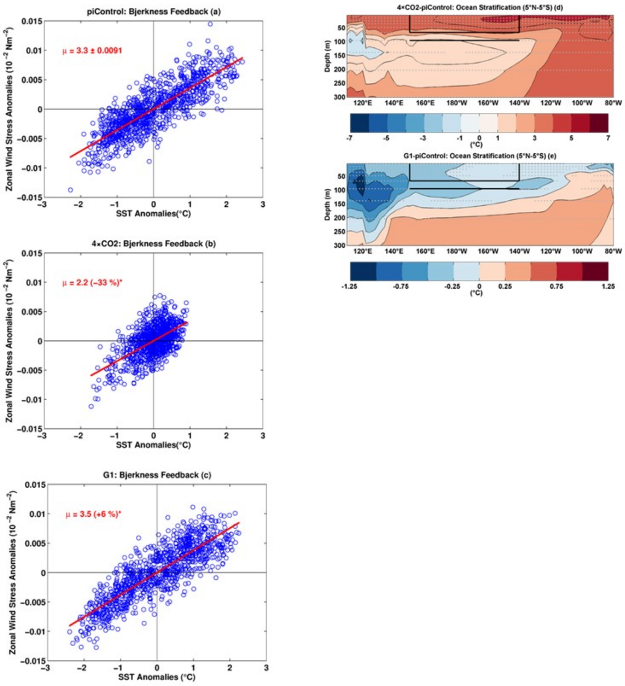

Figure 15. BJ feedback (μ; 10^{-2} $Nm^{-2}/^{o}C$) for (a) piControl (b) 4×CO_2, and (c) G1. The value with ± sign indicates s.d. of μ after 10,000 bootstrap realizations. An asterisk indicates statistical significance at 99 % cl. Mean change in ocean temperature, (d) 4×CO_2-piControl, and (e) G1-piControl. The black box shows the area averaging region for upper ocean temperature, and the black line shows the lower layer used for calculation of stratification as a difference of upper and lower layer. Stipples indicate grid points with statistical significance at 99 % cl using a non-parametric Wilcoxon rank-sum test.

In the Discussion and conclusion (section 5, page 19, lines 1-14), we have added the following paragraph:

To conclude, solar geoengineering can compensate many of the GHG-induced changes in the tropical Pacific, but, importantly, not all of them. In particular, controlling the downward shortwave flux cannot correct one of the climate system's most dominant modes of variability, i.e., ENSO, wholly back to preindustrial conditions. The ENSO feedbacks (Bjerkness and heat flux) and more stratified ocean temperatures may induce ENSO to behave differently under G1 than under piControl and 4×CO_2. Different meridional distributions of shortwave and longwave forcings (e.g., Nowack et al., 2016) resulting in the surface ocean overcooling, and residual warming of the deep ocean are the plausible reasons for the solar geoengineered climate not reverting entirely to the preindustrial state. However, we note that this is a single model study, and more studies are needed to show the robustness and model-dependence of any results discussed here, e.g. using long-term multimodel ensembles from GeoMIP6 (Kravitz et al., 2015), once the data are released. The long-term Stratospheric Aerosol Geoengineering Large Ensemble (GLENS; Tilmes et al., 2018) data can also be explored to investigate ENSO variability under geoengineering.

3)

This manuscript pays a lot of efforts on how mean state of tropical Pacific might be modified under 4_CO2 and G1. A connection between mean state change and ENSO change is simply built by using the previously proposed conclusions, i.e. the reduction of MSSTG in both 4_CO2 and G1 indicate increase of extreme El Nino. However, more detailed explanations should be reviewed before applying this theory.

In the revised manuscript, we have tested the change in frequency under both 4×CO_2 and G1, relative to piControl, first by using rainfall > 5 mm day^{-1} as a threshold for extreme El Niño events and then selecting only those events for which rainfall > 5 mm day^{-1} and MSSTG < 0. Both methods show a statistically significant increase in extreme El Niño events. Choosing extreme events having MSSTG < 0 assures that strong convection has established over the Niño3 region during the extreme. Further, we have shown the histograms of MSSTG for all samples and exclusively for extreme El Niño events, which indicate more frequent reversals of MSSTG both under 4×CO_2 and G1 relative to piControl. See also the discussion on mechanism now presented in Sect. 4 and included in a response above. In the revised manuscript, we have further incorporated the following changes:

A threshold of detrended Niño3 total rainfall of 5 mm day^{-1} recognizes events as extremes even when the MSSTG is positive and stronger, especially under 4×CO_2, which plausibly means that ITCZ might not shift over the equator for strong convection to occur during such extremes. The El Niño event of 2015 is a typical example of such events. We test our results with a more strict criterion by choosing only those events as extremes, which have characteristics similar to that of 1982 and 1997 El Niño events (i.e., Niño3 rainfall > 5 mm day^{-1} and MSSTG < 0). We declare events having characteristics similar to that of the 2015 event as moderate El Niño events (Fig. S5). Based on this method, we find a robust increase in the number of extreme El Niño events both in 4×CO_2 (924 %) and G1 (61 %) at 99 % cl. (Section 3.2.2, page14, lines 26-34)

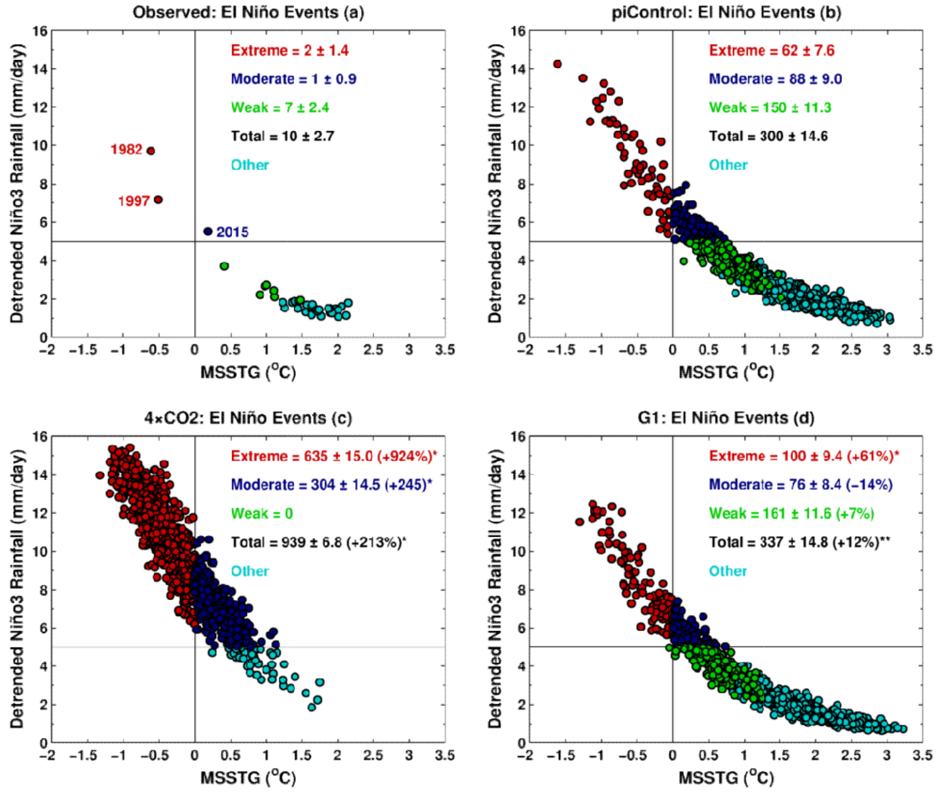

Figure S5. *Relationship between MSSTG and quadratically detrended Niño3 rainfall for (a) observations (b) piControl (c) 4×CO_2, and (d) G1. The solid black horizontal line indicates a threshold of 5 mm day^{-1}. A single (double) asterisk indicates that the change in frequency, relative to piControl, is statistically significant at 99 % (95 %) cl. Numbers with a ± symbol indicate s.d. calculated with 10,000 bootstrap realizations. Following Cai et al. (2014), a non-ENSO related trend has been removed from the rainfall time series. Events are classified as: Extreme (Niño3 rainfall > 5 mm day^{-1} and MSSTG < 0), moderate (Niño3 rainfall > 5 mm day^{-1} and MSSTG >*

0), weak (Standardized Niño3 SSTs > 0.5 °C and Niño3 rainfall < 5 mm day^{-1}), total is sum of extreme, moderate, and weak events.

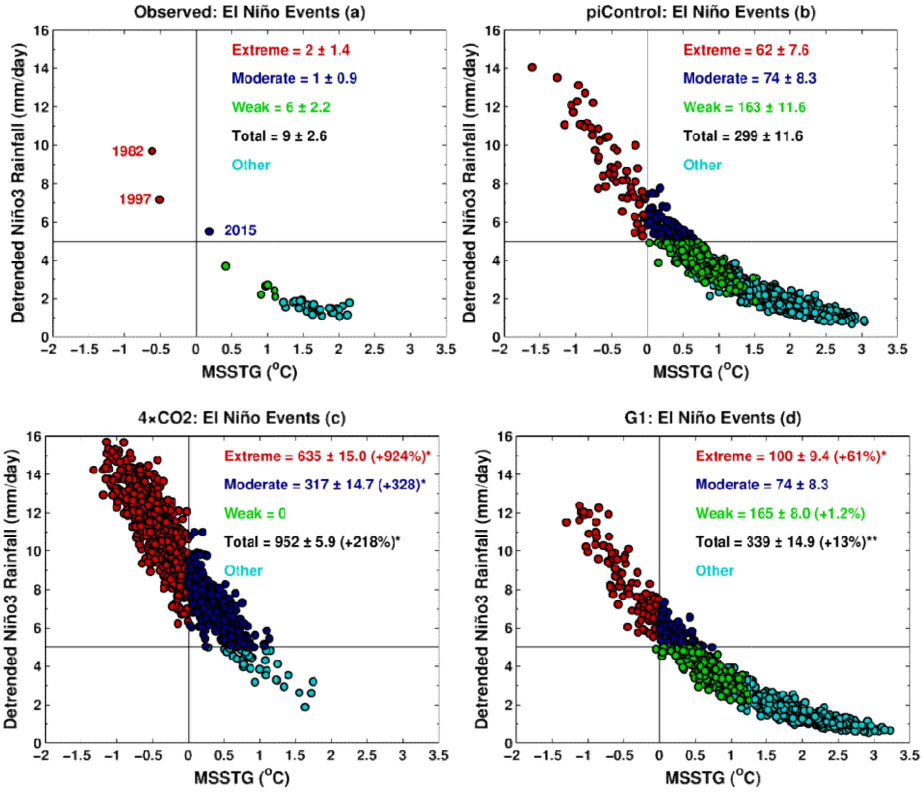

***Figure S6.** Relationship between MSSTG and linearly detrended Niño3 rainfall for (a) observations (b) piControl (c) 4×CO_2, and (d) G1. The solid black horizontal line indicates a threshold of 5 mm day^{-1}. A single (double) asterisk indicates that the change in frequency, relative to piControl, is statistically significant at 99 % (95 %) cl. Numbers with a ± symbol indicate s.d. calculated with 10,000 bootstrap realizations. Following Cai et al. (2014), a non-ENSO related trend has been removed from the rainfall time series. Events are classified as: Extreme (Niño3 rainfall > 5 mm day^{-1} and MSSTG < 0), moderate (Niño3 rainfall > 5 mm day^{-1} and MSSTG > 0), weak (Standardized Niño3 SSTs > 0.5 °C and Niño3 rainfall < 5 mm day^{-1}), total is sum of extreme, moderate, and weak events.*

Minor Points

1)

In P11, L24, the calculation of skewness of SST should be clarified in the context.

In the revised manuscript we have made the following changes:

Skewness is a measure of asymmetry around the mean of the distribution (see eq. S1). Positive skewness means that in given data distribution, the tail of the distribution is spread out towards high positive values, and vice versa (Ghandi et al., 2016). (See section 2.4, page 7, lines 2-5)

(See Supplementary, page 13)

$$S = \left[\frac{1}{n-1}\right]\frac{\sum_i^n (X_i-\bar{X})^3}{\sigma^3} \quad \ldots\ldots\ldots\ldots\ldots\ldots\ldots\ldots\ldots\ldots\ldots \text{(S1; Ghandi et al., 2016)}$$

Where

S = skewness
n = sample size
X_i *= sample ith observation*
$\bar{X}$ *= sample mean*
σ^3 *= sample standard deviation*

2)

In P9, L22-24 and P11, L36-39, the independent paragraphs seem abrupt for the context. Better to immerse in the other paragraphs.

We have edited and merged the text with other paragraphs as follows:

The weakening of the MSSTG is qualitatively in agreement with previous studies under increased GHG forcings (e.g., Cai et al., 2014; Wang et al., 2017). (see section 3.1.4, page 11, lines 21-22)

Previous studies found that climate models produced mixed responses (both increases and decreases in amplitude) in terms of how ENSO amplitude change with global warming (see Latif et al. 2009; Collins et al. 2010; Vega-Westhoff and Sriver 2017). However, Cai et al. (2018) found an intermodel consensus, for models capable of reproducing ENSO diversity, for strengthening of ENSO amplitude under A2, RCP4.5, and RPC8.5 transient scenarios. (see section 3.2.1, page 13, lines 6-11)

3)

In P12, L6-10, please clarify why quadratic trend to the time series of rainfall data should be excluded.

In the revised manuscript, the text has been edited as follows:

To study changes in El Niño frequency, we first need to define what constitutes an El Niño event. We here define extreme El Niño events as episodes when monthly-mean DJF Niño3 total rainfall exceeds 5 mm day^{-1}*, following the threshold definition by Cai et al. (2014). However, as pointed out by Cai et al. (2017), trends in Niño3 rainfall are mainly driven by two factors: (1) the change in the mean state of the tropical Pacific and (2) the change in frequency of extreme El Niño events. Therefore, since we want to focus on the changes in the extremes, we need to remove contribution (1) from the raw Niño3 time series. We, therefore, fit a quadratic polynomial to the time series of rainfall data from which all extreme El Niño events (DJF total rainfall > 5 mm day*$^{-1}$*) have been excluded and then subtract this trend from the raw Niño3 rainfall time series. Linearly detrending the rainfall time series produces similar results.* (See section 3.2.2, page 14, lines 4-14)

4)

In P13, L13-15, the central Pacific El Nino is not mentioned in the introduction. Also, the question backs to the major comment 1. The HadCM3L may not be able to capture ENSO diversity.

We have deleted the referred text from the revised manuscript.

5)

In Figure 4c, why the thermocline depth is not significantly changed over the eastern Pacific. If this is the case, is it due to the choice of 24 isotherms?

In a CMIP3 multimodel (SRESA1B scenario) ensemble, Yeh et al. (2009) showed a deepening of the thermocline in the eastern equatorial Pacific; however, Nowack et al. (2017) did not find any change under 4xCO_2. Both studies defined thermocline using a maximum vertical temperature gradient. Thus, we believe that no-significant-change in the eastern Pacific is not due to the choice of 24 °C isotherm, but rather due to a cancellation of competing effects on thermocline depth. In the revised manuscript, we have therefore added the following text:

In $4xCO_2$, most likely the weakened easterlies (as noticed in Sect. 3.1.3; e.g., Yeh et al., 2009, Wang et al., 2017) and greater ocean temperature stratification due to increased surface warming (see Sect. 4 and Cai et al., 2018) lead to a significant shoaling of the thermocline across the western and central equatorial Pacific. In contrast, relatively little change takes place between 130° W and 90° W. In a CMIP3 multimodel (SRESA1B scenario) ensemble, Yeh et al. (2009) found a more profound deepening of the thermocline in this part of the eastern equatorial Pacific; however, for example, Nowack et al. (2017) did not find such changes under $4xCO_2$ (cf. their Fig. S9). One possible explanation for this behaviour is the competing effects of upper-ocean warming (which deepens the thermocline) and the weakening of westerly zonal wind stress, causing thermocline shoaling (see Kim et al. 2011a). (see section 3.1.5, from page 11 and line 37 to next page line 8)

6)

The significance level is 90% for differences between G1, 4_CO2 and piControl. How about 95% or even 99%? Will the significant regions be much less?

All statistics have been recalculated either with a 95 % or 99 % confidence level. See the manuscript with track changes.

7)

In P23, the height of color bars for figures can be smaller to enlarge the main part of figures. In Figure 2 d & e, symmetric colors are better to represent the negative and positive shadings.

In the revised manuscript, all figures have been re-plotted with relatively small and diverging color bars.

8)

In Figure 6 d & e, it's better to set the color bar range with the same ratio as in Figure 5 d & e.

In the revised manuscript, both figures are re-plotted with the same color range.